RESEARCH ACTIVITIES

Theoretical and Computational Molecular Science

It is our goal to develop new theoretical and computational methods based on quantum mechanics and statistical mechanics to predict and understand the structures, chemical reactions, and functions of molecules in gas and condensed phases including nano- and bio-systems.

Theoretical Studies on Heterogeneous Correlated Dynamics in Condensed Phases

Department of Theoretical and Computational Molecular Science
Division of Theoretical Molecular Science I

SAITO, Shinji
Professor

KIM, Kang
Assistant Professor

ONO, Junichi	IMS Fellow	KONDO, Naoko	Secretary
HIGASHI, Masahiro	Post-Doctoral Fellow		
IMOTO, Sho	Graduate Student		

Liquids and biological systems show complicated dynamics because of their structural flexibility and dynamical hierarchy. Understanding these complicated dynamics is indispensable to elucidate chemical reactions, thermodynamical and dynamical properties in solutions, and functions of proteins. We have been investigating ultrafast fluctuations and relaxation dynamics in liquid water and solution by using linear and nonlinear spectroscopy.[1–4] In addition, we have been studying heterogeneous dynamics in supercooled liquids in terms of multi-time correlation function[5] and the molecular origin of anomalous thermodynamic properties of supercooled water.[6]

1. Fluctuations and Relaxation Dynamics of Liquid Water Revealed by Linear and Nonlinear Spectroscopy[1]

Many efforts have been devoted to elucidating the intra- and intermolecular dynamics of liquid water because of their important roles in many fields of science and engineering. Nonlinear spectroscopy is a powerful tool to investigate the dynamics. Because nonlinear response functions are described by more than one time variable, it is possible to analyze static and dynamic mode couplings. Here we review the intra- and intermolecular dynamics of liquid water revealed by recent linear and nonlinear spectroscopic experiments and computer simulations. In particular, we discuss the population relaxation, anisotropy decay, and spectral diffusion of the intra- and intermolecular motions of water and their temperature dependence, which play important roles in ultrafast dynamics and relaxations in water.

2. Molecular Origin of the Difference in the HOH Bend of the IR Spectra between Liquid Water and Ice[2]

The intensity of the HOH bend in the infrared (IR) spectrum of ice is significantly smaller than the corresponding one in liquid water. This difference in the IR intensities of the HOH bend in the two systems is investigated using Molecular Dynamics (MD) simulations with the flexible, polarizable, *ab intio* based TTM3-F model for water, a potential that correctly reproduces the experimentally observed increase of the HOH angle in liquid water and ice from the water monomer value. We have identified two factors that are responsible for the difference in the intensity of the HOH bend in liquid water and ice: (i) the decrease of the intensity of the HOH bend in ice caused by the strong anti-correlation between the permanent dipole moment of a molecule and the induced dipole moment of neighboring hydrogen bond acceptor molecules, and (ii) the weakening of this anti-correlation by the disordered hydrogen bond network in liquid water. The presence of the anti-correlation in ice is further confirmed by *ab intio* electronic structure calculations of water pentamer clusters extracted from the trajectories of the MD simulations with the TTM3-F potential for ice and liquid water.

3. Ultrafast Dynamics of Liquid Water: Frequency Fluctuations of the OH Stretch and the HOH Bend[3)]

Frequency fluctuations of the OH stretch and the HOH bend in liquid water are reported from the third-order response function evaluated using the TTM3-F potential for water. The simulated two dimensional infrared spectra of the OH stretch are similar to previously reported theoretical results. The present study suggests that the frequency fluctuation of the HOH bend is faster than that of the OH stretch. The ultrafast loss of the frequency correlation of the HOH bend is due to the strong couplings with the OH stretch as well as the intermolecular hydrogen bond bend.

4. Multiple Length and Time Scales of Dynamic Heterogeneities in Model Glass-Forming Liquids: A Systematic Analysis of Multi-Point and Multi-Time Correlations[5)]

We report an extensive and systematic investigation of the multi-point and multi-time correlation functions to reveal the spatio-temporal structures of dynamic heterogeneities in glass-forming liquids. Molecular dynamics simulations are carried out for the supercooled states of various prototype models of glass-forming liquids such as binary Kob–Andersen, Wahnström, soft-sphere, and network-forming liquids. While the first three models act as fragile liquids exhibiting super-Arrhenius temperature dependence in their relaxation times, the last is a strong glass-former exhibiting Arrhenius behavior. First, we quantify the length scale of the dynamic heterogeneities utilizing the four-point correlation function. The growth of the dynamic length scale with decreasing temperature is characterized by various scaling relations that are analogous to the critical phenomena. We also examine how the growth of the length scale depends upon the model employed. Second, the four-point correlation function is extended to a three-time correlation function to characterize the temporal structures of the dynamic heterogeneities based on our previous studies [K. Kim and S. Saito, *Phys. Rev. E* **79**, 060501(R) (2009); *J. Chem. Phys.* **133**, 044511 (2010)]. We provide comprehensive numerical results obtained from the three-time correlation function for the above models. From these calculations, we examine the time scale of the dynamic heterogeneities and determine the associated lifetime in a consistent and systematic way. Our results indicate that the lifetime of the dynamical heterogeneities becomes much longer than the α-relaxation time determined from a two-point correlation function in fragile liquids. The decoupling between the two time scales is remarkable, particularly in supercooled states, and the time scales differ by more than an order of magnitude in a more fragile liquid. In contrast, the lifetime is shorter than the α-relaxation time in tetrahedral network-forming strong liquid, even at lower temperatures.

5. Frequency Dependence of Specific Heat in Supercooled Liquid Water and Emergence of Correlated Dynamics[6)]

Molecular origin of the well-known specific heat anomaly in supercooled liquid water is investigated here by using extensive computer simulations and theoretical analyses. A rather sharp increase in the values of isobaric specific heat with lowering temperature and the weak temperature dependence of isochoric specific heat in the same range are reproduced in simulations. We calculated the spatio-temporal correlation among temperature fluctuations and examined the frequency dependent specific heat. The latter shows a rapid growth in the low frequency regime as temperature is cooled below 270 K. In order to understand the microscopic basis of this increase, we have performed a shell wise decomposition of contributions of distant molecules to the temperature fluctuations in a central molecule. This decomposition reveals the emergence, at low temperatures, of temporally slow, spatially long ranged large temperature fluctuations. The temperature fluctuation time correlation function (TFCF) can be fitted to a William-Watts stretched exponential form with the stretching parameter close to 0.6 at low temperatures, indicating highly non-exponential relaxation. Temperature dependence of the relaxation time of the correlation function can be fitted to Vogel-Fulcher-Tamermann expression which provides a quantitative measure of the fragility of the liquid. Interestingly, we find that the rapid growth in the relaxation time of TFCF with lowering temperature undergoes a sharp crossover from a markedly fragile state to a weakly fragile state around 220 K.

References

1) T. Yagasaki and S. Saito, *Annu. Rev. Phys. Chem.* **64**, 55–75 (2013).
2) S. Imoto, S. Xantheas and S. Saito, *J. Chem. Phys.* **138**, 054506 (2013).
3) S. Imoto, S. Xantheas and S. Saito, *J. Chem. Phys.* **139**, 044503 (2013).
4) M. Higashi, S. Hirai, M. Banno, K. Ohta, S. Saito and K. Tominaga, *J. Phys. Chem. B* **117**, 4723–4731 (2013).
5) K. Kim and S. Saito, *J. Chem. Phys. (Special Topic: Glass Transition)* **138**, 12A506 (2013).
6) S. Saito, I. Ohmine and B. Bagchi, *J. Chem. Phys.* **138**, 094503 (2013).

Photoinduced Electron Dynamics in Nanostructures

Department of Theoretical and Computational Molecular Science
Division of Theoretical Molecular Science I

NOBUSADA, Katsuyuki
Associate Professor

YASUIKE, Tomokazu
Assistant Professor

IIDA, Kenji	JSPS Post-Doctoral Fellow
NODA, Masashi	Post-Doctoral Fellow
YAMADA, Mariko	Secretary

We have developed theoretical methods to calculate photo-induced electron dynamics in nanoclusters. Furthermore, a highly efficient computational program of massively parallel calculations for electron dynamics has been developed to investigate optical response of nanostructures of more than ten-nanometers in size. More specifically, we have achieved electron dynamics simulations with the maximum size of 82,944 nodes (663,552 cores) on the K computer at RIKEN. We have also presented a theoretical method to investigate electrochemical processes on the basis of a finite temperature density functional theory (FT-DFT) approach combined with our recently developed open-boundary cluster model (OCM). In addition, structural and electronic properties of gold-thiolate clusters have been elucidated in collaboration with an experimental group.

1. Raman Enhancement by Plasmonic Excitation of Structurally-Characterized Metal Clusters: Au_8, Ag_8, and Cu_8

We have investigated the plasmonic excitations in small group-11element (Au, Ag, and Cu) clusters on the basis of ab initio electronic structure theory.[1)] Unlike alkali metal clusters,[2)] the plasmonic excitations mainly formed with (s,p) orbitals are affected by the inner d-electron excitations. The energy splitting between d and (s,p) levels is the largest for the silver atom among Au, Ag, and Cu, and thus the most intense plasmon in the BOCT M_8 cluster is formed for Ag_8. However, the structural modification to the linear isomer was found to give potential abilities as an optical sensitizer even for gold and copper clusters having nearly degenerate (d,s,p) energy levels. The linear cluster is highly anisotropic and gives multiple plasmonic modes along the molecular axis in the low excitation energy corresponding to the visible light. By utilizing the multiple excitations in the visible region, one can use this material as a universal optical sensitizer available for incident lights with various wavelengths.

As an example of sensitizing, we demonstrated the Raman enhancement of a pyrazine molecule by the linear and BOCT Au_8 clusters. The linear Au_8 cluster has a higher potential for both an enhancement intrinsic to the details of its electronic structures and an enhancement due to its robustness to altering the pyrazine–Au_8 intermolecular distance. It should be emphasized that recent development in experiments allows us to construct such an artificial linear structure on surfaces. We conclude that the structured nanoclusters are a promising strategy for designing effective optical sensitizers.

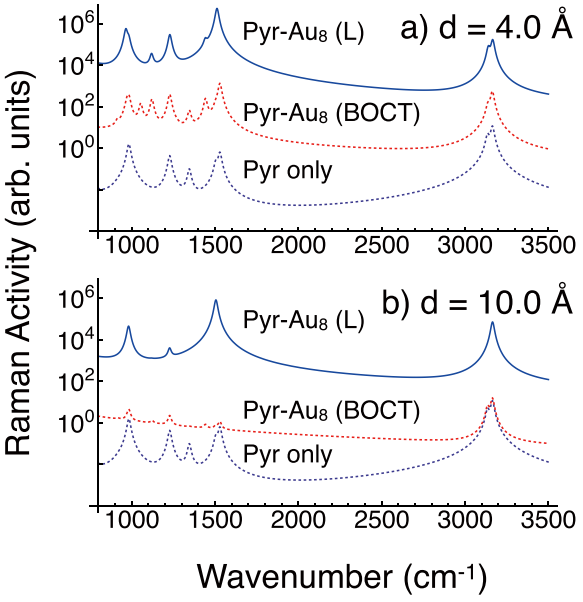

Figure 1. Raman vibrational activity spectra of the pyrazine–Au_8 complex under the pre-resonance conditions with the plasmonic excitations of Au_8. The adsorption distance is set to be (a) 4.0 and (b) 10.0 Å. In each figure, the uppermost solid, middle-dotted, and downmost-dotted curves are for the pyrazine-linear Au_8, pyrazine–BOCT Au_8, and the isolated pyrazine, respectively.

2. Massively-Parallel TDDFT Calculations Based on Finite Difference Method in Real-Time and Real-Space

A highly efficient computational program of massively parallel calculations for electron dynamics has been developed in an effort to apply the method to optical response of nanostructures of more than ten-nanometers in size. The approach is based on time-dependent density functional theory calculations in real-time and real-space. The computational code is implemented by using simple algorithms with a finite-difference method in space derivative and Taylor expansion in time-propagation. Since the computational program is free from the algorithms of eigenvalue problems and fast-fourier-transformation, which are usually implemented in conventional quantum chemistry or band structure calculations, the program is highly suitable for massively parallel calculations. Computational performance is severely affected by both increase in network communications and imbalance of CPU time due to waiting for synchronization. These computational bottlenecks are significantly alleviated by utilizing optimal orbital and space hybrid-parallelization procedures. We have achieved electron dynamics simulations with the maximum size of 82,944 nodes (663,552 cores) on the K computer at RIKEN. The peak performance is ~13% with 5,656 nodes and ~10.0% with 22,624 nodes. The method is applied to optical response of arrays of C_{60} orderly nanostructures of more than 10 nm in size. The computed absorption spectrum is in good agreement with the experimental observation.

3. Development of Open-Boundary Cluster Model Approach for Electrochemical Systems and Its Application to Ag^+ Adsorption on Au(111) and Ag(111) Electrodes

We have developed the theoretical method to investigate electrochemical processes by combining OCM with FT-DFT.[3] Introducing OBC rationalized by OCM allows us to well mimic a semi-infinite electrode by using a finite-sized cluster. FT-DFT describes electronic properties in an equilibrium state at a constant μ. The developed method is therefore capable of reproducing the smooth μ dependence intrinsic to semi-infinite systems having the continuous DOS. The conductor-like polarized continuum model named C-PCM is also employed to take account of a solvation effect.

The method is applied to the electrochemical processes of Ag^+ adsorption on the Au(111) and Ag(111) electrodes. The present constant μ approach qualitatively reproduces the experimental evidence that Ag^+ adsorbs more on the Au electrode than the Ag one while the constant *N* approach gives the opposite result. This result proves that the constant μ condition is absolutely necessary to understand the adsorption. By investigating the relationship between *N* and μ, it is found that the Au electrode is more negatively charged than the Ag one at any electrode potential because of the difference in their work functions. This is the physicochemical reason for the electrode dependence of the Ag^+ adsorption. The present first-principles method clearly describes such an electrochemical system.

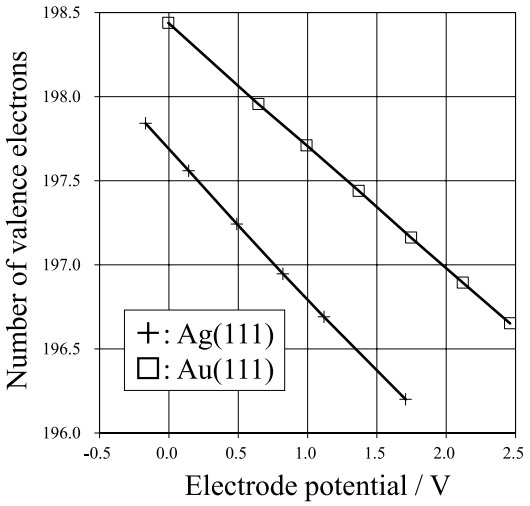

Figure 2. Electrode potential dependence of the number of valence electrons of the Ag(111) (+) and Au(111) (□) electrodes.

4. Total Structure and Optical Properties of a Phosphine/Thiolate-Protected Au_{24} Nanocluster

This work reports the synthesis and crystal structure determination of a new $[Au_{24}(PPh_3)_{10}(SC_2H_4Ph)_5X_2]^+$ (counter-ion: X = halide) nanocluster protected by phosphine/ thiolate ligands.[4] This Au_{24} nanocluster exhibits distinct differences from the previously reported Au_{25} nanocluster in the structure and optical properties. DFT calculations reproduced the optical absorption spectrum and interpreted the optical features, which can be divided into high-energy electronic transitions within individual Au_{12} units and a low-energy unique transition due to interactions between two Au_{12} units. The mechanism of preferential growth of $[Au_{24}(PPh_3)_{10}(SC_2H_4Ph)_5X_2]^+$ over $[Au_{25}(PPh_3)_{10}(SC_2H_4Ph)_5X_2]^{2+}$ remains to be unraveled in future work.

References

1) T. Yasuike and K. Nobusada, *Phys. Chem. Chem. Phys.* **15**, 5424–5429 (2013).
2) T. Yasuike, K. Nobusada and M. Hayashi, *Phys. Rev. A* **83**, 013201 (7 pages) (2011).
3) K. Iida, T. Yasuike and K. Nobusada, *J. Chem. Phys.* **139**, 104101 (2013).
4) A. Das, T. Li, K. Nobusada, Q. Zeng, N. L. Rosi and R. Jin, *J. Am. Chem. Soc.* **134**, 20286–20289 (2012).

Advanced Electronic Structure Theory in Quantum Chemistry

Department of Theoretical and Computational Molecular Science
Division of Theoretical Molecular Science I

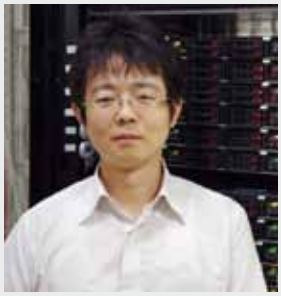

KURASHIGE, Yuki
Assistant Professor

YANAI, Takeshi
Associate Professor

CHALUPSKÝ, Jakub	IMS Fellow	YAMADA, Mariko	Secretary
TRAN, Lan Nguyen	Graduate Student		
SAITOW, Masaaki	Graduate Student		

Quantum chemistry is a subdiscipline of physical chemistry, and practicing its theory by computer is a powerful approach to chemical theory problems that are rather realistic in terms of size and behaviors. We focus on development of the electronic structure theory that is capable of supplying analytic interpretation of chemical phenomena and is being advanced so that it provides accurate information of experiments a priori. The research is aimed at establishing much better ab initio quantum chemistry methodologies that allow one to describe a wide range of complex electronic structures, which can be found in challenging chemical systems, to a predictive chemical accuracy by exploiting cutting-edge many-body theory and sophisticated computing techniques. The resultant methods are applied for studying molecular science.

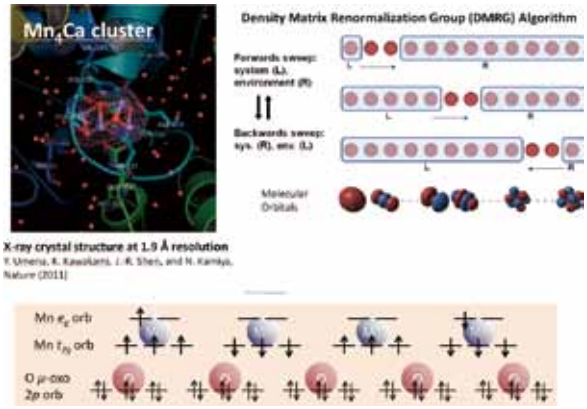

Figure 1. Determination of oxidation state of Mn_4CaO_5 cluster in photosystem II from a multireference wavefunction theory based on Denisty Matrix Renormalization Group method.

1. Entangled Quantum Electronic Wave Functions of the Mn_4CaO_5 Cluster in Photosystem II

It is a long-standing goal to understand the reaction mechanisms of catalytic metalloenzymes at an entangled many-electron level, but this is hampered by the exponential complexity of quantum mechanics. Here, by exploiting the special structure of physical quantum states and using the density matrix renormalization group, we compute near-exact many-electron wavefunctions of the Mn_4CaO_5 cluster of photosystem II, with more than 10^{18} quantum degrees of freedom.[1)] This is the first treatment of photosystem II beyond the single-electron picture of density functional theory. Our calculations support recent modifications to the structure determined by X-ray crystallography. We further identify multiple low-lying energy surfaces associated with the structural distortion seen using X-ray crystallography, highlighting multistate reactivity in the chemistry of the cluster. Direct determination of Mn spin-projections from our wavefunctions suggests that current candidates that have been recently distinguished using parameterized spin models should be reassessed. Through entanglement maps, we reveal rich information contained in the wavefunctions on bonding changes in the cycle (**Figure 1**).

The capability to obtain a more controlled description of the electronic structure in this complex problem enabled us to more rigorously address structural and electronic questions for the S1 and S2 states. In the S1 case our work confirms the most recent interpretations, and in the S2 state, our direct access to spin states and spin projections suggests that existing candidates, determined on the basis of agreement with EPR data, must be reassessed. The completeness of the many-electron formulation also allowed us to investigate new phenomenology, for example by computing multiple potential-energy surfaces near the S1 state, which highlight non-adiabaticity and multistate reactivity in the OEC. In addition, we

have shown how the information in the many-electron wavefunction can be interpreted through its orbital entanglement map, which graphically illustrates the different kinds of chemical bonding and their changes during the Kok cycle. The detailed mechanistic implications of these changes are intriguing and remain an eventual target of study for the future. More broadly, the theoretical methodology we have established is very generally applicable, and opens up the possibility of understanding the electronic structure and, eventually, the chemical mechanism of biological processes at the entangled quantum many-electron level.

2. Correlated One-Body Potential from Second-Order Møller-Plesset Perturbation Theory: Alternative to Orbital-Optimized MP2 Method

The molecular orbitals (MOs) are a key concept in quantum chemistry to interpret the role of electrons in chemical bondings and reactions. They represent the behavior of one electron moving in the effective potential to which Coulomb interactions with many other electrons are averaged out. The effective mean field description is formulated in the Hartree-Fock (HF) theory as a result of using a single determinant as the model wave function in which electron correlation is dismissed in the solution of many-electron Schrödinger equation. In addition to the shapes of MOs, the orbital energies play a central role to characterize molecular electronic structures. The energy levels and associated canonical MOs are determined as eigenspectrum of the one-electron effective Hamiltonian or the so-called Fock operator that includes the mean field interaction potential.

We have reported the development of a mean-field (or one-particle) theory to represent electron correlation at the level of the second-order Møller-Plesset perturbation (MP2) theory.[2] Orbitals and associated energy levels are given as eigenfunctions and eigenvalues of the resulting one-body (or Fock-like) MP2 Hamiltonian, respectively. They are optimized in the presence of MP2-level correlation with the self-consistent field procedure and used to update the MP1 amplitudes including their denominators. Numerical performance is illustrated in molecular applications for computing reaction energies, applying Koopmans' theorem, and examining the effects of dynamic correlation on energy levels of metal complexes.

3. Multireference Configuration Interaction Theory Using Cumulant Reconstruction with Internal Contraction of Density Matrix Renormalization Group Wave Function

We report development of the multireference configuration interaction (MRCI) method that can use active space scalable to much larger size references than has previously been possible[3] (**Figure 1**).The recent development of the density matrix renormalization group (DMRG) method in multi-reference quantum chemistry offers the ability to describe static correlation in a large active space. The present MRCI method provides a critical correction to the DMRG reference by including high-level dynamic correlation through the CI treatment. When the DMRG and MRCI theories are combined (DMRG-MRCI), the full internal contraction of the reference in the MRCI ansatz, including contraction of semi-internal states, plays a central role. However, it is thought to involve formidable complexity because of the presence of the five-particle rank reduced-density matrix (RDM) in the Hamiltonian matrix elements. To address this complexity, we express the Hamiltonian matrix using commutators, which allows the five-particle rank RDM to be canceled out without any approximation. Then we introduce an approximation to the four-particle rank RDM by using a cumulant reconstruction from lower-particle rank RDMs. A computer-aided approach is employed to derive the exceedingly complex equations of the MRCI in tensor-contracted form and to implement them into an efficient parallel computer code. This approach extends to the size-consistency-corrected variants of MRCI, such as the MRCI+Q, MR-ACPF, and MR-AQCC methods. We demonstrate the capability of the DMRG-MRCI method in several benchmark applications, including the evaluation of single-triplet gap of free-base porphyrin using 24 active orbitals.

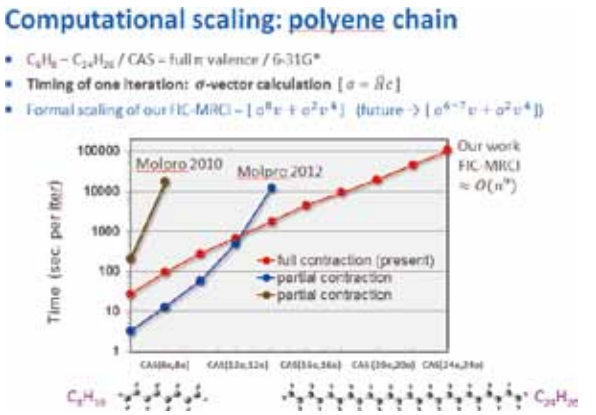

Figure 2. Calculation times (in seconds) of a single iteration including the construction of a σ vector in FIC-cu(4)-, CW-, WK-MRCI calculations for polyene molecules from C_6H_8 to $C_{24}H_{26}$ with the CAS(*ne*,*no*) reference.

References

1) Y. Kurashige, G. K.-L. Chan and T. Yanai, *Nat. Chem.* **5**, 660–666 (2013).
2) T. N. Lan and T. Yanai, *J. Chem. Phys.* **138**, 224108 (12 pages) (2013).
3) M. Saitow, Y. Kurashige and T. Yanai, *J. Chem. Phys.* **139**, 044118 (15 pages) (2013).

Award

YANAI, Takeshi; The 2013 International Academy of Quantum Molecular Science Medal.

Theoretical Study on Photochemistry and Catalysis

Department of Theoretical and Computational Molecular Science
Division of Computational Molecular Science

EHARA, Masahiro
Professor

FUKUDA, Ryoichi
Assistant Professor

TASHIRO, Motomichi
IMS Research Assistant Professor

BOBUATONG, Karan	Post-Doctral Fellow	HIRUNSIT, Pussana	Visiting Scientist
BOEKFA, Bundet	Post-Doctral Fellow	KAWAGUCHI, Ritsuko	Secretary
MEEPRASERT, Jittima	Visiting Scientist	SUGIMOTO, Yukari	Secretary

We investigate the photochemistry or photophysical properties of molecules based on the accurate coupled cluster methodologies, that are of interest in view of fundamental chemistry or material chemistry. We also focus on the mechanism and theoretical design of the various types of catalytic reactions on nanoparticles or bulk surface by developing the theoretical approaches of hetero junction. In this report, we present our recent studies on the mechanism for solvatochromic shifts of free-base porphine,[1] electronic excitations of C_{60} fullerene,[2] theoretical design of dye-sensitized solar cells,[3] and interatomic relaxation effects of double core hole states.

1. Mechanism for Solvatochromic Shifts of Free-Base Porphine

It has been known that π–π* excitation energies of nonpolar conjugated molecules generally exhibit a bathochromic shift (redshift) in solution. The origin of this bathochromic shift is considered to be the dispersive interaction between solute and solvent molecules. Several studies have been conducted on the mechanisms of the solvatichrimic shift for nonpolar molecules, and many models have been proposed. However, different approximations lead different conclusions. The dispersive interaction in excited electronic states has not yet been well understood.

The solvatochromic shifts of free-base porphine in the Q- and B-bands were studied using the polarizable continuum model (PCM) and explicit solvent molecules employing TDDFT and the SAC-CI method. The state-specific and linear-response methods were examined in the PCM calculations. These methods involve different types of solute–solvent interactions. The SAC-CI calculation with explicit solvent molecules includes all types of microscopic solute–solvent interactions including dispersive interaction. Based on our calculations the experimental trends in the solvatochromic shifts of free-base porphine can be explained as follows.

1. The observed bathochromic shift of the B-band in solution is attributed to the interaction of transition dipole with the solvent reaction field.
2. The dispersive interaction caused by the polarizability difference between the ground and excited states is an origin of the observed decrease in the Q-band splitting in nonpolar solvents.
3. The observed refractive index-dependence of the solvent shift in n-alkane can be explained by the dispersive interaction, which relate to the optical dielectric constants of bulk solvent
4. The remarkable decrease in the Q-band splitting in dipolar and quadrupolar solvents cannot be explained by the dispersive interaction alone. Specific solute–solvent interactions are important. Anisotropic interactions are more important than the geometry relaxation for the decrease in the Q-band splitting in solution.

2. Electronic Excitations of C_{60} Fullerene

Because of its unique photo-electronic properties, C_{60} fullerene well known as buckyball, is receiving an extensive interest in terms of scientific and practical purposes. Derivatives of C_{60} are expected to be practical materials for organic thin-film solar cells. Their electronic structure is, however,

quite complicated; it is highly-degenerated and delocalized. Therefore, it has been difficult to perform quantum chemical calculations for excited states of C_{60} fullerene using highly accurate theories. We successfully applied the direct SAC-CI method to C_{60} fullerene. The excited states of C_{60} were accurately calculated by the direct SAC-CI method in the visible to near UV region (below 6.2 eV, 200 nm).

Figure 1 shows the comparison between the SAC-CI results and experimental spectrum of C_{60}, where circles and x-marks denote optically-forbidden states by the selection rule. The absorption in 500–600 nm corresponds to optically-forbidden states, and therefore, very weak absorption peaks are observed induced by vibronic couplings.

The assignments of photoabsorption spectrum based on the direct SAC-CI results are partially different from the previous assignments based on the semi-empirical molecular orbital calculations. In the previous study, the band A observed around 400 nm has been assigned to the optically-allowed 1^1T_{1u} state; based on the direct SAC-CI calculations, however, this peak should be assigned to the optically-forbidden 1^1T_{2u} state. The present assignment based on the direct SAC-CI results can explain the experimental findings more consistently than the previous study.

To understand the electronic excited states of fullerenes and to predict their energetics are essentially important for the development of molecular electronics such as organic thin-film solar cells. For such purpose, semi-empirical molecular orbital method and density functional theory are insufficient. It is necessary to use highly accurate wavefunction theories that are applicable to large systems such as the direct SAC-CI method.

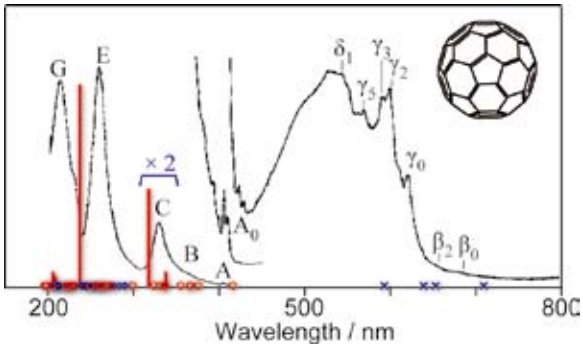

Figure 1. The SAC-CI results and experimental absorption spectrum of C_{60} fullerene.

3. Theoretical Study on Dye-Sensitized Solar Cells (DSSCs)

Dye-sensitized solar cell (DSSC) is a solar battery using cheap metal oxides like titanium oxide (TiO_2). It is expected as a low-cost solar battery without using the silicon semiconductor. Because TiO_2 does not have photoabsorption in the visible region, the organic dyes adsorbed on the titanium oxide is used as a sensitizer and the electromotive force and electric current are achieved by the electron transfer from the electronically excited dyes to TiO_2. Because many factors concern to the efficiency and durability of the cells, the design based on the quantum chemical calculations is necessary. The D-D-π-type organic dyes with two electron donors (D), π-spacer (π), and acceptor (A) suggested by experiment show relatively high energy conversion efficiency. We obtained detailed assignments of the excited states, stability, and assembly of these dyes by theoretical calculations. In addition, the electronic injection process to TiO_2 conduction band was calculated using a cluster model. "Direct" mechanism where the electron injection from dyes to TiO_2 occurs directly was suggested by calculations and the high efficiency of electron injection was supported theoretically.

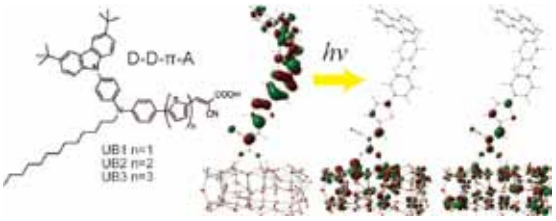

Figure 2. Structure of the D-D-π-type DSSC and direct mechanism. Electronic transition occurs from the dye MO to TiO_2 conduction band.

4. Polarization and Site Dependence of Interatomic Relaxation Effects in Double Dore Hole States

The interatomic relaxation (IR) effects of two-site double core hole (tsDCH) states in selected molecules with a polarizable unit have been systematically investigated using *ab initio* calculations. The IR effects are analyzed by varying size of this polarizable unit and its position relative to the DCHs. The systems with the DCHs located at the opposite sides of the polarizable unit show large negative IR energies, while those at the same side of the polarizable unit have smaller negative IR effects. Here, the IR energies can even be positive if the polarizable unit is large enough. The generalized Wagner plots of tsDCH states are used to visualize the trend of the IR effects in the molecules studied.

References

1) R. Fukuda and M. Ehara, *J. Chem. Theory Comput.* **9**, 470–480 (2013).
2) R. Fukuda and M. Ehara, *J. Chem. Phys.* **137**, 134304 (7 pages) (2012).
3) S. Namuangruk, R. Fukuda, M. Ehara, J. Meeprasert, T. Khanasa, S. Morada, T. Kaewin, S. Jungsuttiwong, T. Sudyoadsuk and V. Promarak, *J. Phys. Chem. C* **116**, 25653–25663 (2012).
4) M. Tashiro, N. V. Kryzhevoi, L. S. Cederbaum and M. Ehara, *J. Phys. B* **46**, 164012 (6 pages) (2013).

Development of New Algorithms for Molecular Dynamics Simulation and Its Application to Biomolecular Systems

Department of Theoretical and Computational Molecular Science
Division of Computational Molecular Science

OKUMURA, Hisashi
Associate Professor

ITOH, G. Satoru
Assistant Professor

MORI, Yoshiharu
IMS Research Assistant Professor

NOMURA, Hitomi	Graduate Student
KHUNTAWEE, Wasinee	Graduate Student
KAWAGUCHI, Ritsuko	Secretary

Biomolecules such as proteins and peptides have complicated free-energy landscape with many local minima. In the conventional canonical-ensemble simulations, it is difficult to realize efficient samplings in such systems because the simulations tend to get trapped in a few of the local- minimum states. To overcome these difficulties, we have proposed new generalized-ensemble algorithms, such as helix-strand replica-exchange method and replica- permutation method. It is important to realize efficient samplings in the conformational space and to predict the native structures of proteins. We apply these methods to proteins and peptides.

1. Transformation of a Design Peptide between the α-Helix and β-Hairpin Structures by a Helix-Strand Replica-Exchange Molecular Dynamics Simulation

We investigated the transformation between the α-helix and β-hairpin structures of an 18-residue design peptide, whose sequence is INYWLAHAKAGYIVHWTA.[1] This peptide has both α-helix and β-hairpin structures in aqueous solution. For this purpose, we proposed the helix-strand replica-exchange method. This is one of the Hamiltonian replica-exchange methods in which we exchange parameters for umbrella potentials to enhance the α-helix or β-strand structure formation, as in Figure 1. We performed an all-atom helix-strand replica-exchange molecular dynamics (MD) simulation of this peptide in explicit water solvent with five replicas. Because the suitable umbrella potential was applied, the helix-strand replica-exchange MD simulation reproduced conformations closer to experimental conformations than a temperature replica-exchange MD simulation when the same numbers of the replicas were used, while the temperature replica-exchange MD simulation does not require bias along any specific order parameter. We calculated its free-energy landscape and revealed the transformation pathways between the α-helix and β-hairpin structures and the folding pathways from an extended structure. The free-energy difference between the two structures is calculated to be almost zero, which agrees with the experimental results.

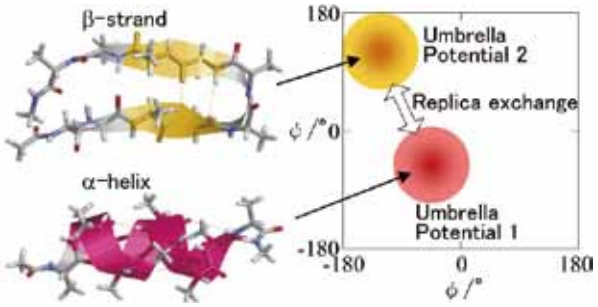

Figure 1. Schematic illustration of the helix-strand replica-exchange method.

2. Replica-Permutation Method with the Suwa-Todo Algorithm beyond the Replica-Exchange Method

We proposed a new method for MD and Monte Carlo simulations, which is referred to as the replica-permutation method, to realize more efficient sampling than the replica-exchange method.[2] In replica-permutation method, not only exchanges between two replicas but also permutations among more than two replicas are performed, as in Figure 2. Furthe-

rmore, instead of the Metropolis algorithm, the Suwa–Todo algorithm is employed for replica-permutation trials to minimize its rejection ratio. We applied RPM to particles in a double-well potential energy, Met-enkephalin in a vacuum, and a C-peptide analog of ribonuclease A in explicit water. For comparison purposes, replica-exchange molecular dynamics simulations were also performed. As a result, replica-permutation method sampled not only the temperature space but also the conformational space more efficiently than REM for all systems. From our simulations of C-peptide, we obtained the α-helix structure with salt bridges between Gly2 and Arg10, which is known in experiments. Calculating its free-energy landscape, the folding pathway was revealed from an extended structure to the α-helix structure with the salt bridges.

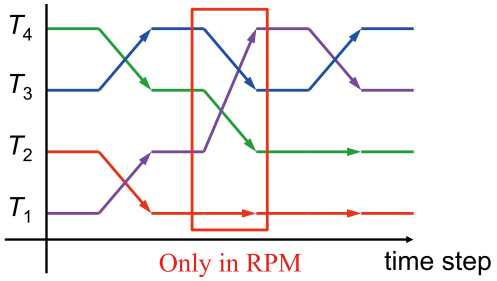

Figure 2. An example of time series of temperatures in replica-permutation method (RPM). The transitions of replicas in the red square frame are not realized in replica-exchange method (REM).

3. Pressure-Induced Helical Structure of a Peptide Studied by Simulated Tempering Molecular Dynamics Simulations

It is known experimentally that an AK16 peptide forms more α-helix structures with increasing pressure while proteins unfold in general. In order to understand this abnormality, MD simulations with the simulated tempering method for the isobaric–isothermal ensemble were performed in a wide pressure range from 1.0×10^{-4} GPa to 1.4 GPa.[3] From the results of the simulations, it is found that the fraction of the folded state decreases once and increases after that with increasing pressure. The partial molar volume change from the folded state to unfolded state increases monotonically from a negative value to a positive value with pressure. The behavior under high pressure conditions is consistent with the experimental results. The radius of gyration of highly helical structures decreases with increasing pressure, which indicates that the helix structure shrinks with pressure. This is the reason why the fraction of the folded state increases as pressure increases.

4. Decomposition-Order Effects of Time-Integrator on Ensemble Averages for the Nosé-Hoover Thermostat

Decomposition-order dependence of time development integrator on ensemble averages for the Nosé-Hoover dynamics is discussed.[4] Six integrators were employed for comparison, which were extensions of the velocity-Verlet or position-Verlet algorithm. Molecular dynamics simulations by these integrators were performed for liquid-argon systems with several different time steps and system sizes. The obtained ensemble averages of temperature and potential energy were shifted from correct values depending on the integrators. These shifts increased in proportion to the square of the time step. Furthermore, the shifts could not be removed by increasing the number of argon atoms. We show the origin of these ensemble-average shifts analytically. Our discussion can be applied not only to the liquid-argon system but also to all MD simulations with the Nosé-Hoover thermostat. Our recommended integrators among the six integrators are presented to obtain correct ensemble averages.

5. Cutoff Effect in the Nosé-Poincaré and Nosé-Hoover Thermostats

We performed MD simulations of a Lennard-Jones system and investigated the effect of potential cutoff in the Nosé–Poincaré and Nosé–Hoover thermostats.[5] The Nosé–Poincaré thermostat is the symplectic algorithm of the Nosé thermostat, while the Nosé–Hoover thermostat is not a symplectic algorithm. If the potential energy is twice or more differentiable, the Hamiltonian was conserved well in the Nosé–Poincaré thermostat. If the potential energy is once or less differentiable, however, the Hamiltonian was not conserved, but increased because the continuity of potential energy is required in a symplectic MD simulation. The increase in the Hamiltonian caused the increase in instantaneous temperature, and physical quantities cannot be obtained correctly. It is because the difference in the Hamiltonian effectively increases the set temperature in the equations of motion. On the other hand, the Hamiltonian was not conserved for any cutoff method in the Nosé–Hoover thermostat because it is not a symplectic algorithm. However, temperature was controlled appropriately because the Hamiltonian deviation does not affect the set temperature.

References

1) H. Okumura and S. G. Itoh, *Phys. Chem. Chem. Phys.* **15**, 13852–13861 (2013).
2) S. G. Itoh and H. Okumura, *J. Chem. Theory Comput.* **9**, 570–581 (2013).
3) Y. Mori and H. Okumura, *J. Phys. Chem. Lett.* **4**, 2079–2083 (2013).
4) S. G. Itoh, T. Morishita and H. Okumura, *J. Chem. Phys.* **139**, 064103 (10 pages) (2013).
5) T. Sakaguchi and H. Okumura, *J. Phys. Soc. Jpn.* **82**, 034001 (7 pages) (2013).

Theory and Computation of Reactions and Properties in Solutions and Liquids

Department of Theoretical and Computational Molecular Science
Division of Computational Molecular Science

ISHIDA, Tateki
Assistant Professor

We focus on the projects both on ultrafast photoinduced electron energy transfer in the excited state in solution and on ionic liquids (ILs). The project on photoinduced electron energy transfer processes in the excited state in solution focuses on the development of a theoretical method to describe electron energy transfer including solvent motion and dynamics. On the other hand, ILs' projects concentrate the study of dynamical properties on ionic liquids with molecular dynamics simulation.

1. The Theoretical Study of Photoinduced Electron Energy Transfer Processes in the Excited State in Solution

We have developed a procedure for tracking the time-dependent evolution of the electronic structure of a solute molecule in solution, coupling an electronic structure theory with solvent motion. We have extended this prescription for studying electron energy transfer processes in the excited state in solution. It is revealed that the coupling between solvation dynamics and a fast intramolecular electron energy transfer is likely to play an important role in the emergence of photo-induced unique functionalities in biochemical and metal complex systems.

2. Investigations of Dynamical Properties on Ionic Liquids[1–2)]

We focus on the dynamical properties on ionic liquids (ILs). With molecular dynamics simulation, it have been found out that ILs indicate unique collective dynamics and distinctive ionic dynamics. We have studied interesting dynamical heterogeneity in ILs at room temperature. Also, we have investigated spatial heterogeneity.

References

1) T. Ishida, The Dynamical Properties on Ionic Liquids: Insights from Molecular Dynamics Study," in *Ionic Liquids—New Aspects for the Future*, J. Kadokawa, Ed., InTech; Rijeka, Croatia, pp. 3–29 (2013).
2) T. Ishida and H. Shirota, *J. Phys. Chem. B* **117**, 1136–1150 (2013).

Visiting Professors

Visiting Professor
HASEGAWA, Jun-ya *(from Hokkaido University)*

Quantum Chemistry for the Excited States of Functional Molecules in Proteins and Solutions

Molecular interactions between chromophore and environment are the essential to furnish a protein with the photo-functionality. I am interested in the machinery of the photo-functions such as photo-synthesis, vision, and bioluminescence. To understand the mechanism and to develop chemical concept behind the photo-functions, we develop electronic structure theories for excited state, analytical method for excitation-energy transfer pathway, and a hybrid quantum-mechanics/molecular mechanics method. In recent studies, we have clarified color-tuning mechanism of photo-functional proteins and excitation transfer mechanism of bridge-mediated donor-acceptor systems. We are also interested in developing a configuration interaction picture for the solvatochromic response of the molecular environment.

Visiting Associate Professor
ANDO, Koji *(from Kyoto University)*

Quantum Transfer Processes in Chemical and Biological Systems

At the core of chemistry, biochemistry, and materials sciences are reduction-oxidation and acid-base reactions, in which electron and proton transfers are the key elementary processes. Our research group has been working on theoretical and computational modeling of these inherently quantum dynamical processes in condensed matters. One recent achievement is a development of new quantum Monte Carlo simulation method with an account of induced-dipole corrections obtained from fragment molecular orbital calculations. It adequately described isotope mixing effect of dielectric phase transition temperature of hydrogen-bonding organic molecular crystal. Another is a development and numerical assessment of initial-value-represented propagator for semiquantal squeezed-state wave packet propagation, which extends our previous works of nuclear wave packet molecular dynamics simulation method.

Visiting Associate Professor
MORISHITA, Tetsuya *(from AIST)*

Development of *ab initio* Mean-Force Dynamics for Free-Energy Calculations

We have been developing a method for constructing free-energy profiles in the framework of *ab initio* molecular-dynamics. It is well known that the electronic state needs to be explicitly taken into account to describe bond formation or bond breaking in. *e.g.*, conformational transformations of biomolecules, which plays an important role in constructing their free-energy profiles. Developing force-fields that can describe such bond formations is, however, considered to be extremely difficult. It is therefore of great importance to develop a method that enables us to construct free-energy profiles without empirical force-fields.

Our interest particularly focuses on the incorporation of *ab initio* interatomic interactions into logarithmic mean-force dynamics (LogMFD), which is expected to enable us to efficiently construct free-energy profiles within the accuracy of *ab initio* force-fields. A preliminary result of "*ab initio*" LogMFD calculation for glycine dipeptide molecule has been recently obtained. We found that the free-energy landscape is sensitive to the description of the hydrogen bonding, which may not be appropriately handled with an empirical force-field only.

RESEARCH ACTIVITIES

RESEARCH ACTIVITIES

Photo-Molecular Science

We study the interaction between molecules and optical fields with its possible applications to active control of molecular functionality and reactivity. We also develop novel light sources to promote those studies. Two research facilities, the Laser Research Center for Molecular Science and the UVSOR, closely collaborate with the Department.

The core topics of the Department include ultrahigh-precision coherent control of gas- and condensed-phase molecules, high-resolution optical microscopy applied to nanomaterials, synchrotron-based spectroscopy of core-excited molecules and solid-state materials, vacuum-UV photochemistry, and the development of novel laser- and synchrotron-radiation sources.

Development of Advanced Near-Field Spectroscopy/Imaging and Application to Nanomaterials

Department of Photo-Molecular Science
Division of Photo-Molecular Science I

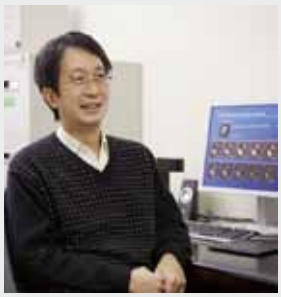

OKAMOTO, Hiromi
Professor

NARUSHIMA, Tetsuya
Assistant Professor

NISHIYAMA, Yoshio
IMS Research Assistant Professor

KOWAKA, Yasuyuki	Post-Doctoral Fellow	ISHIKAWA, Akiko	Technical Fellow
HASHIYADA, Shun	Graduate Student	NOMURA, Emiko	Secretary
WU, Huijun	Technical Fellow	YAMASAKI, Yumi	Secretary

There is much demand for the study of local optical properties of molecular assemblies and materials, to understand nanoscale physical and chemical phenomena and/or to construct nanoscale optoelectronic devices. Scanning near-field optical microscopy (SNOM) is an imaging method that enables spatial resolution beyond the diffraction limit of light. Combination of this technique with various advanced spectroscopic methods may provide direct probing methods for dynamics in nanomaterials and nanoscale functionalities. It may yield essential and basic knowledge to analyze origins of characteristic features of the nanomaterial systems. We have constructed apparatuses of near-field spectroscopy and microscopy for excited-state studies of nanomaterials, with the feasibilities of nonlinear and time-resolved measurements. The developed apparatuses enable near-field measurements of two-photon induced emission, femtosecond time-resolved signals, and circular dichroism, in addition to conventional transmission, emission, and Raman-scattering. Based on these methods, we are investigating the characteristic spatiotemporal behavior of various metal-nanostructure systems and molecular assemblies.

1. Visualization of Localized Optical Fields and Plasmon Wavefunctions in Metal Nanostructures

We reported that wavefunctions of localized plasmon resonances of chemically synthesized metal (Au and Ag) nanoparticles are visualized by near-field transmission or two-photon excitation measurements.[1,2] The same methods were also applied to Au nanoparticle assemblies to visualize confined optical fields.[1,2]

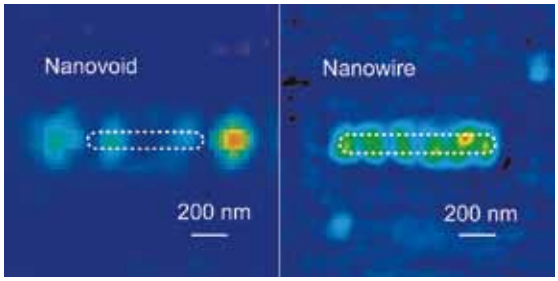

Figure 1. Near-field two-photon excitation images of an elongated rectangular nanoaperture on Au film (630 nm^l × 90 nm^w × 30 nm^t) observed at 810 nm (left) and a nanowire (860 nm^l × 100 nm^w × 30 nm^t) observed at 800 nm (right).

We have extended the studies to a variety of metal nanostructures including those manufactured by the electron-beam lithography technique, in part as collaboration with researchers of other institutions. For elongated rectangular apertures opened on thin Au film, we observed spatially oscillating features in the apertures that are arising from localized surface plasmon resonance of the nanostructures (Figure 1).[3] The elongated rectangular aperture corresponds to an inverted structure of a nanorod, and the oscillating structure observed may have a similar origin to that for nanorods.

For one-dimensional linear array of spherical Au nanoparticles, we revealed that enhanced fields (observed at ~800 nm) tend to localize near the ends of the arrays, when the number of particles exceeds 5 (Figure 2).[4] This observation is interpreted as a result of plasmon propagation among the particles and existence of localized modes near the boundaries

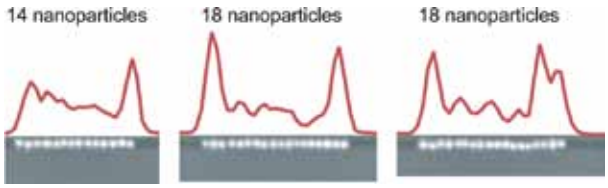

Figure 2. Plots of near-field two-photon excitation signals for the linear arrays of spherical Au nanoparticles (diameters ~100 nm) along the chain axis, observed at 785 nm. Images below the plot are corresponding scanning electron micrographs.

of the arrays.

We also tried to observe enhanced field characteristics for assemblies of particles with different shapes, specifically Ag nanowires joined with Ag nanospheres.[5] We have found that enhanced fields at the interstitial sites, polarized *perpendicular* to the long axis of the wire, are excited when the incident photons are polarized *along* the long axis of the wire. Such studies are essential as bases for designing unique optical properties and functions of metal nanostructures.

2. Near-Field Circular Dichroism Microscopy of Nanomaterials

Circular dichroism (CD) spectroscopy is widely used in the studies of chiral materials and magnetism. Some of nanomaterials composed of achiral molecules are reported to show CD activities arising from the nanoscale chirality. Two-dimensionally chiral metal nanostructures also show CD activities. Investigation of nanoscale local CD may provide valuable information on the origins of CD activities of such materials. For this purpose, we are developing an apparatus for near-field CD microscopy based on polarization modulation technique with a photoelastic modulator, and measuring CD images of nanoscale chiral materials.

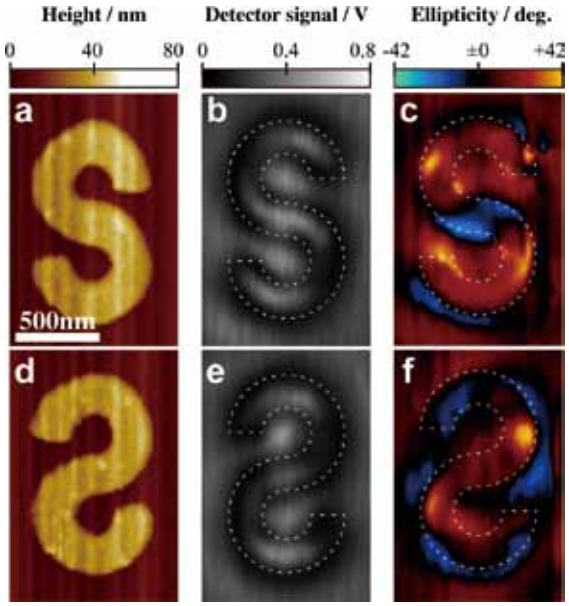

Figure 3. Topography (a, d), near-field transmission (b, e), and near-field CD (c, f) images of an S-shaped Au nanostructure (a, b, c) and its mirror-imaged structure (d, e, f) observed at 633 nm.

Here we report on a nanoscale CD imaging for a two-dimensional chiral pair of Au nanostructures to elucidate the relationship between nanoscale chirality and CD activity.[6] We adopted a two-dimensional "S"-shaped nanostructure (1200 nm × 700 nm, Au film thickness 40 nm) prepared with electron-beam lithography technique and its mirrored structure as the samples. The chiral pair exhibited very high local ellipticity at the center of the S-structure, and signals of both handedness coexisted in one nanostructure (Figure 3).

Based upon a model analysis for rotating dipole induced by the circular polarized light, we propose a mechanism of the strong CD signal at the center of the S-structure as mentioned in the following. If the rotational velocity of the induced polarization, in addition to the magnitude, changes reflecting the asymmetric structure of the sample, it produces perceivable difference between the optical response to the left-handed circular polarized light and that to the right-handed one, which yields a strong CD signal. This result indicates that it yields strong chiral field at the center of the structure, which may be potentially utilized for analysis of chiral molecules, chiral reaction fields, and so forth.

3. Construction of Apparatuses for Sub-20-fs Ultrafast Near-Field Spectroscopy

Surface plasmons of noble metal nanoparticles have very short lifetimes in the range of ~2-20 fs. To achieve a SNOM observation of such fast dynamics in the individual nanoparticles, we have to overcome serious dispersion effects arising from the optical components involved, especially from the optical fiber of the SNOM probe. We achieved that by combining the conventional dispersion compensation devices composed of prism and grating pairs with adaptive pulse shaping technique, and succeeded in delivering sub-20-fs pulses to the near-field aperture with a spatial resolution of ~100 nm.[1] At present we have obtained pulses of less than 15 fs FWHM at the near-field aperture. We are conducting position-dependence measurements for the dephasing time of localized plasmons for single gold nanorods.

References

1) H. Okamoto, *Bull. Chem. Soc. Jpn.* **86**, 397–413 (2013).
2) H. Okamoto and K. Imura, *J. Phys. Chem. Lett.* **4**, 2230–2241 (2013).
3) K. Imura, K. Ueno, H. Misawa and H. Okamoto, *J. Phys. Chem. C* **117**, 2449–2454 (2013).
4) T. Shimada, K. Imura, H. Okamoto and M. Kitajima, *Phys. Chem. Chem. Phys.* **15**, 4265–4269 (2013).
5) S. Kim, K. Imura, M. Lee, T. Narushima, H. Okamoto and D. H. Jeong, *Phys. Chem. Chem. Phys.* **15**, 4146–4153 (2013).
6) T. Narushima and H. Okamoto, *Phys. Chem. Chem. Phys.* **15**, 13805–13809 (2013).

Design and Reconstruction of Molecular Quantum States of Motion

Department of Photo-Molecular Science
Division of Photo-Molecular Science I

OHSHIMA, Yasuhiro
Professor

MIZUSE, Kenta
Assistant Professor

FUJIWARA, Masanori
IMS Research Assistant Professor

HAYASHI, Masato	Post-Doctoral Fellow
MIYAKE, Shinichiro	Post-Doctoral Fellow
INAGAKI, Itsuko	Secretary

Molecules are vital existence. In a gas-phase ensemble at room temperature, they are, in an average, flying away by a few hundred meters, making turns almost reaching to 10^{11} times, and shaking themselves more than 10^{13} times within the duration of only one second. The ultimate goal this research group has been aiming to is to capture the lively figures of molecules moving in such a dynamic manner and to have a perfect command over the molecular motions. Here lasers with ultimate resolution in time and energy domains are employed complementally and cooperatively for this purpose.

1. Nonadiabatic Excitation of Molecular Rotation Induced by Intense Ultrashort Laser Fields

When a gaseous molecular sample is irradiated by an intense nonresonant ultrashort laser pulse, the rotation of the molecules is coherently excited to create a rotational quantum wave packet (WP). We developed a method to explore the nonadiabatic excitation in a quantum-state resolved manner and applied it to diatomic and symmetric-top molecules.[1)] It has been shown that the state distribution is a useful experimental source for verifying the excitation process.[2,3)] When a pair of excitation pulses is implemented, partial control of rotational-state distribution has been achieved.[1,4)] In a favorable case, the double-pulse excitation has enabled us to reconstruct experimentally a rotational WP thus created.[5)] The sense of rotation can also be controlled, yielding to a rotational WP exhibiting angular-momentum orientation.[6,7)]

2. Coherent Excitation of Intermolecular Vibrations by Nonresonant Intense Ultrashort Laser Fields

Nonadiabatic interaction with an intense ultrashort laser field can also coherently excite vibration of molecule. We have succeeded in creating and observing WPs pertinent to intermolecular vibrations of several molecular clusters in their vibronic ground states.

3. Construction of an Ion-Imaging Apparatus for Wave Packet Imaging

We have constructed an ion-imaging apparatus for tracking the time-dependent molecular alignment by monitoring the 2D spatial distribution of Coulomb-exploded fragment ions. In the apparatus, ion clouds are repelled perpendicularly to hit a 2D detector, of which detection plate is set parallel along the initial flight direction of the ions. This unique arrangement allows us to record ion images for non-cylindrically symmetric fragment distribution. By using this experimental setup, we have monitored spatiotemporal propagation of the molecular alignment of jet-cooled N_2.

4. High-Resolution Laser Spectroscopy of Benzene Clusters with Atoms and Small Molecules[8,9)]

As prototypical systems for elucidating the intermolecular interaction pertinent to aromatic rings, we studied clusters of benzene with small numbers of atoms and molecules (such as He and H_2), by exploring via two-color resonant two-photon ionization in the vicinity of the monomer S_1–S_0 6_0^1 band. Extensive adiabatic cooling with the rotational temperature of < 0.5 K was conducted by the high-pressure pulsed expansion. Sub-Doppler resolution yielding the line width of 250 MHz was realized in a collimated molecular beam by employing Fourier-transform-limited ultraviolet pulses for the excitation.

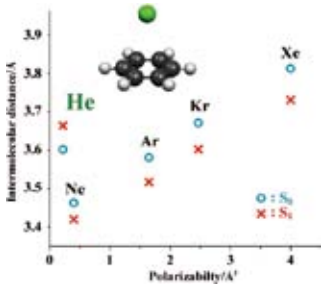

Figure 1. The effective intermolecular distances in the benzene–rare gas complexes.

The observed transition frequencies of benzene–$(He)_n$ with n = 1 and 2 were fitted to derive the molecular constants with accuracy improved by a factor of 50 than those reported previously.[10] The determined rotational constants for n = 1 set the distance of the He atom from the benzene ring, which is even larger than those of the analogous systems, *i.e.*, benzene–Ne and –Ar, as shown in Figure 1. This apparent anomaly is discussed with the recent theoretical results based on high-level quantum mechanical calculation coupled with the numerical solution of the 3D eigenvalue problem.[11] The electronic excitation induces the increase in the distance for benzene–He, as opposed to the contraction of other benzene–rare gas systems. The distance and the change for n = 2 are almost the same as those for n = 1. We also recorded the excitation spectrum of n = 1 with the mono ^{13}C-substituted benzene. The asymmetric substitution lifts the degeneracy of the S_1 6^1 state in the benzene molecule, and two vibronic bands located nearby to each other were observed.

For C_6H_6–$(H_2)_n$, two distinguished isomers, correlating to *para* and *ortho* H_2, are identified for n = 1 and 2. This finding is the manifestation of the internal rotation of the H_2 unit(s) located above (and below) the benzene molecular plane within the clusters. For the observation of the weaker binding *para* species, a gas sample of pure *para* H_2 was used. Rotationally resolved spectra allowed us to fix the cluster geometry unambiguously. Three vibronic bands involving vdW-mode excitation were observed for the *ortho* species with n = 1, yielding to probable sets of vibrational frequencies of all the three vdW modes. One of them correlates to the splitting between the m = 0 and ±1 sublevels in the j = 1 state of a freely rotating H_2 molecule, and the potential barrier for the hindered internal rotation has been evaluated from the values, as shown in Figure 2. Rotationally resolved spectrum of benzene–(*ortho* $H_2)_3$ is consistent with a (2 + 1) binding motif, where two H_2 molecules on one side of the benzene plane seem to scramble their positions and roles. All the clusters examined with rotational resolution exhibited homogeneous line broadening, which corresponds to the upper-state lifetimes in the sub-nanosecond regime, most probably due to vibrational predissociation in the S_1 6^1 manifold.

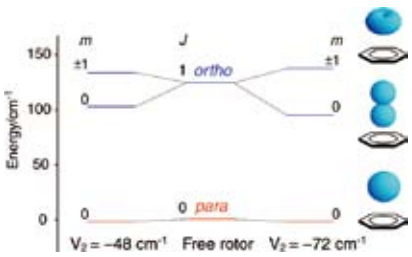

Figure 2. Schematic energy diagram for the internal rotation of H_2 inside benzene–H_2. Two probable values for the potential parameter, V_2, from the experimental results are adopted. On right, probability angular distributions of the H_2 molecular axis are schematically shown for the lowest three states.

5. Seeded Optical Parametric Amplifier for Generating Chirped Nanosecond Pulses[12]

To realize rapid adiabatic passage (RAP), which drives coherent population transfer from an initial quantum state to a target state with 100% efficiency, we constructed an optical parametric amplifier (OPA) with BiBO crystals, which was seeded by a phase-modulated cw beam in the 1,040–1,070 nm region. Two-stage pre-amplification by Yb-doped fibers were implemented for stable injection to the OPA. The frequency chirp in the OPA pulse was actively controlled, as shown in Figure 3. Down/up chirps with up to 500 MHz shift were demonstrated. The output pulse energy was ~40 mJ, which is sufficient for two-photon RAP.

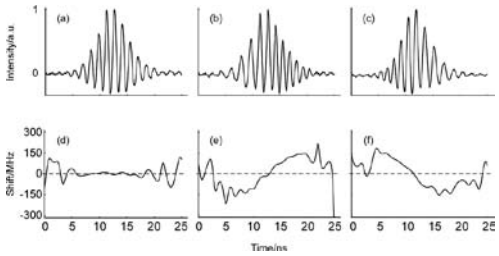

Figure 3. Observed heterodyne signals of the OPA pulses (a): without the phase modulation to the seeding beam, (b) and (c): with the phase modulation, and the time-dependent frequency shifts: (d), (e) and (f), corresponding to (a), (b) and (c), respectively.

References

1) Y. Ohshima and H. Hasegawa, *Int. Rev. Chem. Phys.* **29**, 619–663 (2010).
2) H. Hasegawa and Y. Ohshima, *Phys. Rev. A* **74**, 061401 (4 pages) (2006).
3) H. Hasegawa and Y. Ohshima, *Chem. Phys. Lett.* **454**, 148–152 (2008).
4) D. Baek, H. Hasegawa and Y. Ohshima, *J. Chem. Phys.* **134**, 224302 (10 pages) (2011).
5) H. Hasegawa and Y. Ohshima, *Phys. Rev. Lett.* **101**, 053002 (4 pages) (2008).
6) K. Kitano, H. Hasegawa and Y. Ohshima, *Phys. Rev. Lett.* **103**, 223002 (4 pages) (2009).
7) Y. Khodorkovsky, K. Kitano, H. Hasegawa, Y. Ohshima and I. Sh. Averbukh, *Phys. Rev. A* **83**, 023423 (10 pages) (2011).
8) M. Hayashi and Y. Ohshima, *Chem. Phys.* **419**, 131–137 (2013).
9) M. Hayashi and Y. Ohshima, *J. Chem. Phys. A*, in press (2013).
10) S, M. Beck, M. G. Liverman, D. L. Monts and R. E. Smalley, *J. Chem. Phys.* **70**, 232–237 (1979).
11) S. Lee, J. S. Chung, P. M. Felker, J. L. Cacheiro, B. Fernández, T. B. Pedersen and H. Koch, *J. Chem. Phys.* **119**, 12956–12964 (2003).
12) S. Miyake and Y. Ohshima, *Opt. Express* **21**, 5269–5274 (2013).

Development of High-Precision Coherent Control and Its Applications

Department of Photo-Molecular Science
Division of Photo-Molecular Science II

OHMORI, Kenji
Professor

TAKEI, Nobuyuki
Assistant Professor

GOTO, Haruka	Post-Doctoral Fellow	KOYASU, Kuniaki	Graduate Student
SOMMER, Christian	Post-Doctoral Fellow	INAGAKI, Itsuko	Secretary
NAKAGAWA, Yoshihiro	Graduate Student	YAMAGAMI, Yukiko	Secretary

Coherent control is based on manipulation of quantum phases of wave functions. It is a basic scheme of controlling a variety of quantum systems from simple atoms to nanostructures with possible applications to novel quantum technologies such as bond-selective chemistry and quantum computation. Coherent control is thus currently one of the principal subjects of various fields of science and technology such as atomic and molecular physics, solid-state physics, quantum electronics, and information science and technology. One promising strategy to carry out coherent control is to use coherent light to modulate a matter wave with its optical phase. We have so far developed a high-precision wave-packet interferometry by stabilizing the relative quantum phase of the two molecular wave packets generated by a pair of femtosecond laser pulses on the attosecond time scale. We will apply our high-precision quantum interferometry to gas, liquid, solid, and surface systems to explore and control various quantum phenomena.

1. Optically Engineered Quantum Interference of Delocalized Wavefunctions in a Bulk Solid: The Example of Solid Para-Hydrogen[1)]

Local excitations of indistinguishable particles in a solid are quantum-mechanically superposed to give delocalized wave functions. Their interference is often so short-lived that it eludes observation and manipulation. Here we have actively controlled interference of delocalized vibrational wave func-

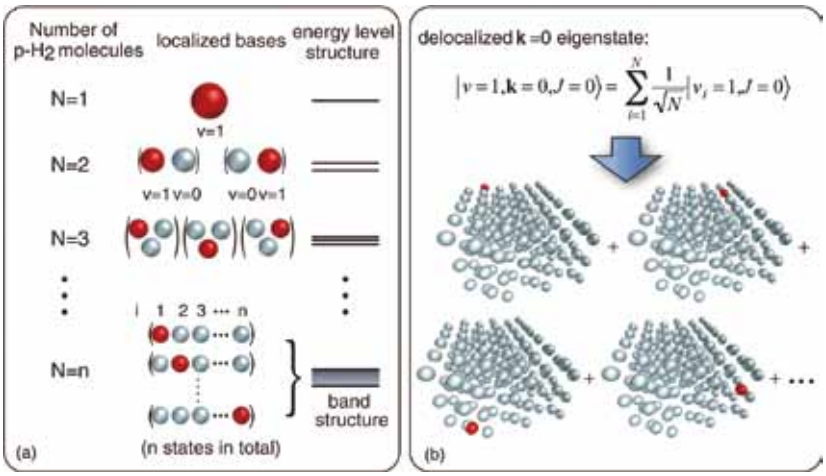

Figure 1. Formation of the delocalized vibron in solid p-H_2. (a) A band structure arises from the interaction among many indistinguishable p-H_2 molecules, one of which is vibrationally excited. The red and blue spheres stand for the vibrationally excited and ground-state p-H_2 molecules, respectively. (b) Every p-H_2 molecule within a single crystal has an equal probability to be vibrationally excited. These locally excited states $|v_i = 1\rangle$ (i = 1,...,N) are coherently superposed to give a delocalized vibron state $|v = 1, \mathbf{k} = 0\rangle$. This figure has been adopted from reference 1.

tions in solid *para*-hydrogen produced by a pair of ultrashort laser pulses. The ultrafast evolution of their interference changes from almost completely constructive (amplification by a factor of ~4) to destructive when we change the timing of those two laser pulses by only 4 fs. This active control serves as an experimental tool to investigate the spatiotemporal evolution of a wave function in a bulk solid.

2. Wavepacket Interferometry for Nuclear Densities and Flux Densities[2)]

The traditional wavepacket interferometry for nuclear densities is extended to nuclear flux densities. Accordingly, a molecule vibrating in an electronic excited state may be prepared such that at a given time, the nuclear densities correspond to a broad distribution of the molecular bond, from short to long distances, which is subdivided into a chain of lobes. We discover that neighbouring lobes, or groups of lobes, may flow towards alternating directions, implying alternating bond stretches and bond compressions. The corresponding nuclear flux densities may be controlled by appropriate parameters of the two laser pulses, which generate the underlying interferences. Similar patterns of the nuclear densities and flux densities may also be created by a single laser pulse, which may cause interferences of the overlapping tail and head of a wavepacket as they run towards or away from a turning point, respectively. The phenomena are demonstrated for the model system I_2(B).

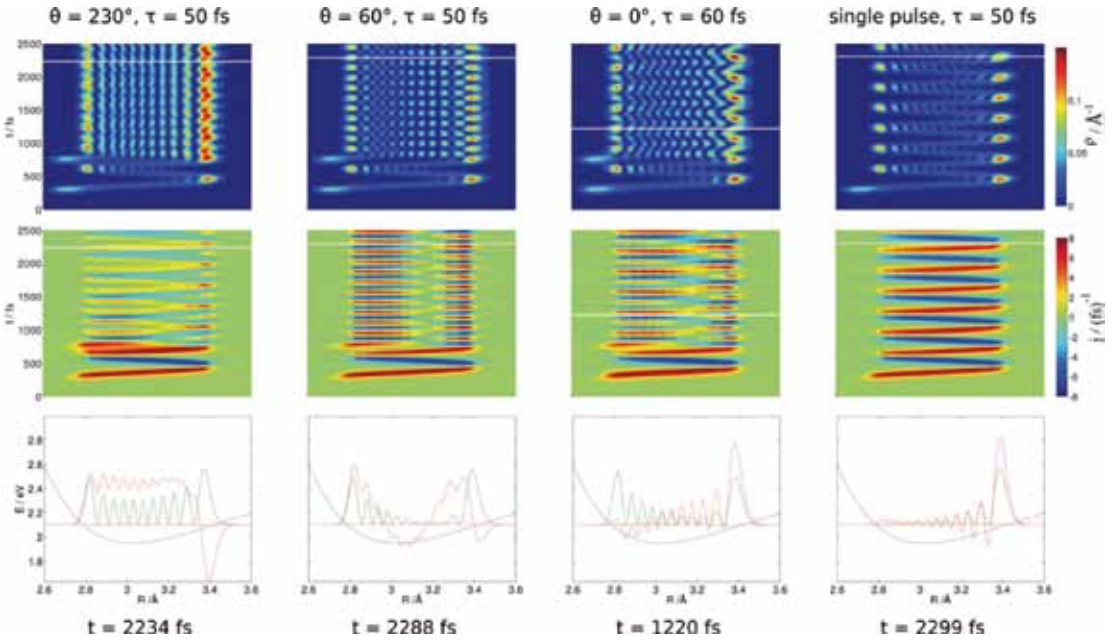

Figure 2. Wavepacket interferometry for the nuclear densities ρ(*R*, *t*) (top panels) and flux densities *j*(*R*, *t*) (middle panels) of the model I_2(B), after excitations by two sub-pulses (first three columns) or by a single pulse (last column) versus nuclear bond length *R* (abscissa) and time *t* (ordinate). The values of ρ(*R*, *t*) and *j*(*R*, *t*) are indicated by colour codes on the right-hand side. The values of the control parameters of the laser sub-pulses (the duration τ and the phase θ of the second sub-pulse) are specified above the top panels. All other parameters of the laser pulses are fixed. The bottom panels show snapshots of ρ(*R*, *t*) (green lines) and *j*(*R*, *t*) (red lines) embedded in the PES of the electronic *B*-state (blue line) at specific times, which are indicated by horizontal lines in the top panels, and specified below the bottom panels. The new phenomena are discussed in detail in the text. This figure has been adopted from reference 2.

References

1) H. Katsuki, Y. Kayanuma and K. Ohmori, *Phys. Rev. B* **88**, 014507 (2013).

2) T. Bredtmann, H. Katsuki, J. Manz, K. Ohmori and C. Stemmle, *Mol. Phys.* **111**, 1691–1696 (2013). (invited paper).

Molecular Inner-Shell Spectroscopy: Local Electronic Structure and Intermolecular Interaction

Department of Photo-Molecular Science
Division of Photo-Molecular Science III

KOSUGI, Nobuhiro
Professor

YAMANE, Hiroyuki
Assistant Professor

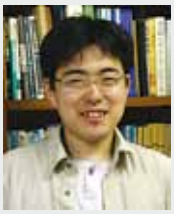

NAGASAKA, Masanari
Assistant Professor

YUZAWA, Hayato	IMS Fellow	NAKANE, Junko	Secretary
MOCHIZUKI, Kenji	Graduate Student		
WANG, Yu-Fu	Graduate Student*		

In order to reveal local electronic structures and weak intermolecular interactions in molecular systems such as organic solids, liquids, aqueous solutions, and molecular clusters, we are developing and improving several kinds of soft X-ray spectroscopic techniques, such as X-ray photoelectron spectroscopy (X-ray PES, XPS), X-ray absorption spectroscopy (XAS), resonant Auger electron spectroscopy (RAS), X-ray emission spectroscopy (XES), resonant XES (RXES), and resonant inelastic X-ray scattering (RIXS), at UVSOR in-vacuum undulator beamlines BL-3U and BL-6U with some international collaboration programs, and also an original *ab initio* quantum chemical program package GSCF, which is optimized to calculation of molecular inner-shell processes.

1. Electrochemical Reaction of Aqueous Iron Sulfate Solutions[1)]

The redox reactions of Fe ions are one of the most common electrochemical systems. Fe redox reactions have been mainly studied by voltammetric methods, but it is difficult to observe *in situ* change in valence of Fe ions in dilute electrolyte solutions. Recently, we have developed a liquid cell for soft X-ray absorption spectroscopy (XAS) in transmission mode. Furthermore, we have succeeded in development of an *in situ* XAS measurement system to study electrochemical reactions of electrolytes under realistic conditions by using a liquid cell with built-in electrodes. Change in valence of Fe ions in an aqueous iron sulfate solution at different potentials is investigated by Fe L-edge XAS.[1)]

Figure 1 shows the Fe L-edge XAS spectra of 0.5 M aqueous iron sulfate solutions at pH = 2.2 by variation of the potential at a gold electrode. Each XAS spectrum is measured at a constant potential. The XAS spectra reveal signals from Fe(II) and Fe(III) ions and show an isosbestic point, indicating only two species are involved. As seen in Figure 1(a), a nonlinear oxidation of Fe(II) to Fe(III) ions is observed when the potential is increased from 0.0 to 0.9 V. On the other hand, in Figure 1(b), the reduction of Fe(III) to Fe(II) ions shows linear dependence on the potential as decreased from 0.9 to –0.4 V.

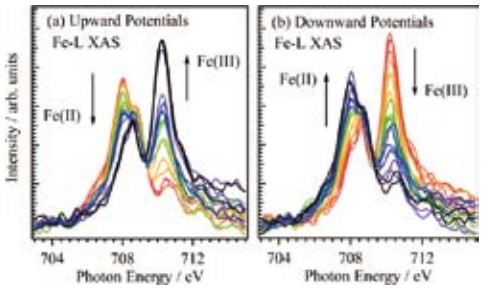

Figure 1. Fe L-edge XAS spectra of Fe ions in a 0.5 M aqueous iron sulfate at different potentials: (a) increasing from 0.00 to 0.90 V and (b) decreasing from 0.90 to –0.40 V.

Figure 2 shows the fraction of Fe(II) ions from total Fe ions as a function of potential and scanning direction, which is obtained from the XAS spectra. The fraction of Fe(II) ions decreases with increasing potential. Two processes are found in this oxidation process. The process at a high potential (0.72 V) is simple oxidation of Fe(II). The process at a low potential (0.34 V) involves the sulfate ions. The peak positions are dependent on the scanning rate because the rate of this process is dominantly influenced by the sulfate ions, which affect

electrode kinetic parameters and diffusion coefficients. On the other hand, the formation of Fe(II) with decreasing potential is a simple reduction of Fe(III) ions. We have discussed the mechanism of these Fe redox processes by correlating the XAS results with cyclic voltammetry results at different scanning rates.

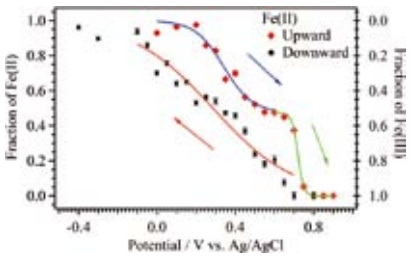

Figure 2. Fraction of Fe(II) ions as a function of potential and scanning direction versus Ag/AgCl with saturated KCl solutions.

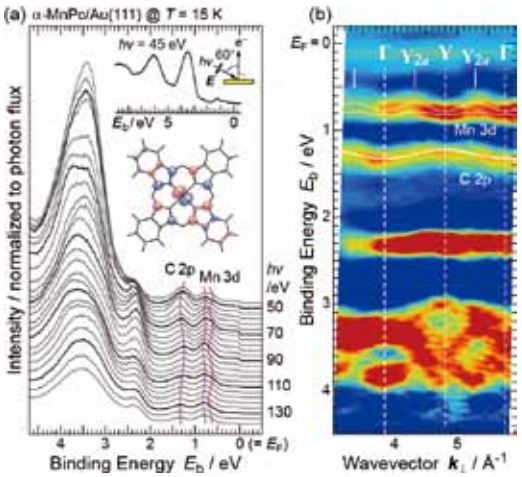

Figure 3. (a) $h\nu$-dependent normal-emission ARPES spectra ($h\nu$ step = 4 eV) of the MnPc crystalline film on Au(111) at 15 K. Inset shows the experimental geometry, wide valence-band spectrum at $h\nu$ = 45 eV, and the spatial distribution of the HOMO of MnPc. (b) Valence band map obtained from the second derivative of the ARPES spectra, with the tight-binding fitting (white curve).

2. Substituent-Induced Intermolecular Interaction in Organic Crystals Revealed by Precise Band-Dispersion Measurements[2)]

The intermolecular band dispersion, originating from the periodicity of the molecular stacking structure, is essential to investigate the charge transport mechanism related to organic electronics. Recently, we have succeeded in observation of quite small intermolecular band dispersions for crystalline films of metal phthalocyanine (MPc, M = metal) by the precise angle-resolved photoemission spectroscopy (ARPES) experiments.[2)] These observations enable us to perform systematic study of the intermolecular interaction in terms of the intermolecular distance along the π-π stacking direction ($a_\perp$) by changing terminal groups or central metals in MPc.

Figure 3(a) shows the photon energy ($h\nu$) dependence of normal-emission ARPES for the crystalline MnPc film on Au(111) at 15 K. The highest occupied molecular orbital (HOMO, Mn 3d) and HOMO-1 (C 2p) derived peaks of MnPc show a clear periodic shift. Moreover, we have found that the Mn 3d derived peak consists of two components with the different dispersion, indicating the relatively strong interaction at the Mn site. Figure 3(b) shows the valence band map for the crystalline MnPc film on Au(111), wherein the symmetric Γ and Y points are estimated from the lattice constant of 3.27 Å from the X-ray diffraction. The agreement between the periodicity of C 2p peak and the symmetric points indicates that the observed dispersion is ascribed to the intermolecular interaction. For the Mn 3d peak, the peak split and its dispersion are clearly seen in the band map. Furthermore, the periodicity of the Mn 3d dispersion is 1/2 times of that of the C 2p dispersion as labeled Y_{2a}. A possible origin of the Mn 3d dispersion is dimerization of the Mn d_π state.

From the observed band dispersions of the C-2p-derived band for crystalline films of various MPc molecules, the intermolecular transfer integral ($t_\perp$) can be evaluated with respect to the intermolecular distance ($a_\perp$) as shown in Figure 4. From the $t_\perp$-vs.-$a_\perp$ relation, we have found that (i) the $t_\perp$ value is getting large with decreasing the $a_\perp$ value due to the stronger intermolecular electronic coupling and that (ii) the $t_\perp$-vs.-$a_\perp$ relation seems to be fitted by a linear function in the present narrow $a_\perp$ range. From the least-squares fitting, the slope parameter of $t_\perp/a_\perp$ is determined to be 75±5 meV/Å for the C-2p-derived band of α-crystalline MPc films.

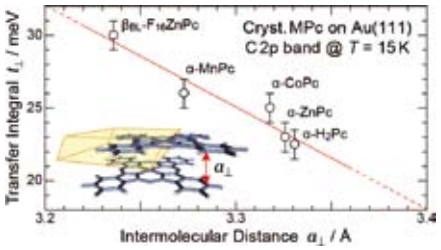

Figure 4. The $t_\perp$-versus-$a_\perp$ relation for the C 2p band in MPc crystals at 15 K obtained from the band dispersion measurement. The least-square fitting gives a slope parameter of $t_\perp/a_\perp$ = 75±5 meV/Å.

References

1) M. Nagasaka, H. Yuzawa, T. Horigome, A. P. Hitchcock and N. Kosugi, *J. Phys. Chem. C* **117**, 16343–16348 (2013).
2) H. Yamane and N. Kosugi, *Phys. Rev. Lett.* **111**, 086602 (2013).

Award

YAMANE, Hiroyuki; Young Researcher Award from National Institutes of Natural Sciences.

* carrying out graduate research on Cooperative Education Program of IMS with Tamkang University, Taiwan

Light Source Developments by Using Relativistic Electron Beams

UVSOR Facility
Division of Advanced Accelerator Research

KATOH, Masahiro
Professor

ADACHI, Masahiro
Assistant Professor

KONOMI, Taro
Assistant Professor

OHIGASHI, Takuji
Assistant Professor

TANAKA, Seiichi	Post-Doctoral Fellow	SEKITA, Sou	Graduate Student*
ARAI, Hidemi	Post-Doctoral Fellow	KAWAKAMI, Ryou	Graduate Student*
KAJIURA, Yohei	Graduate Student*		

This project involves researches and developments on synchrotron light source, free electron laser, beam physics and their related technologies, such as applications of the light sources. The most of the researches were carried out at the UVSOR facility.

1. Developments on UVSOR Accelerators

The magnetic lattice of UVSOR was modified in 2012. The new lattice gives small emittance of 15 nm-rad, which results in higher brightness of the synchrotron radiation. An in-vacuum undulator was successfully commissioned, which provides intense soft X-rays to a scanning transmission X-ray microscope (STXM). Although the storage ring was successfully commissioned in July, 2012,[1)] the machine tuning has been continued to achieve more stable operation. The beam injection efficiency has been gradually improved by the fine tuning of the injection system. Sudden beam losses frequently observed just after the commissioning have been gradually decreasing, as the vacuum conditioning via irradiation of synchrotron radiation was proceeding.

A new novel technique to inject the beam with a pulse sextupole magnet (Figure 1) was successfully demonstrated. By using this technique, the beam movement during the injection, which is inevitable with the traditional injection scheme with pulsed dipole magnets, can be avoided. As the result of the machine study just for two days, we could achieve the injection efficiency of about 20%. To introduce this scheme to the daily users operation, the efficiency should be higher than 50%. The study is going on.

Figure 1. Pulse sextupole magnet developed for UVSOR-III.

2. Improvements of STXM Beam-Line

After the successful commissioning of the STXM, the beamline BL4U (Figure 2), has been improved as an integrated system for upcoming user operation. For example, to bring out satisfactory performance of the STXM, 1) control

software of the beamline with sophisticated GUI, which makes linkage between the undulator, the monochromator and the STXM, was updated. 2) Wider energy range of incident X-rays, from 150 to 880 eV, became available by tuning the monochromator and the gap width of the undulator. 3) An experimental hutch was built at the end station of the beamline to stabilize temperature, to avoid from acoustic noise and to keep the air clean around the STXM.

On the other hand, two sample cells were designed for new applications of in-situ and polarization dependent observations. These sample cells will open new region of molecular science of the STXM.

Figure 2. BL4U Beam-line for STXM.

3. Light Source Technology Developments

We have demonstrated that coherent synchrotron radiation of various properties could be generated in an electron storage ring by using an external laser source. This research is supported by the Quantum Beam Technology Program of JST/MEXT. Under this support, a new experimental station has been constructed. The generation of coherent synchrotron radiation at the new site was successfully demonstrated. Some basic researches on coherent synchrotron radiation have been conducted as shown in Figure 3.[2] An ultrafast terahertz detector was tested.[3] Applications using coherent synchrotron radiation are under preparation and will be demonstrated in near future.

Laser Compton scattering is a method to produce monochromatic and energy-tunable gannma-ray pulses. Laser pulses are injected to the storage ring and are scattered by the relativistic electrons circulating in the ring. We developed a method to produce ultra-short gamma-ray pulses and have demonstrated a photon-induced positron annihilation lifetime spectroscopy experiment.[4]

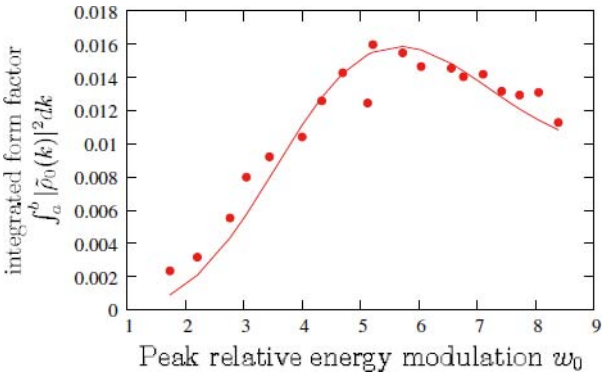

Figure 3. Observed saturation of coherent synchrotron radiation produced by the laser modulation method at UVSOR-II.

References

1) M. Adachi, H. Zen, T. Konomi, J. Yamazaki, K. Hayashi and M. Katoh, *J. Phys.: Conf. Ser.* **425**, 042013 (2013).
2) M. Hosaka, N. Yamamoto, Y. Takashima, C. Szwaj, M. Le Parquire, C. Evain, S. Bielawski, M. Adachi, T. Tanikawa, S. Kimura, M. Katoh, M. Shimada and T. Takahashi, *Phys. Rev. S. T. Accel. Beams* **16**, 020701 (2013).
3) P. Thoma, A. Scheuring, S. Wuensch, K. Il'In, A. Semenov, H-W Huebers, V. Judin, A-S. Mueller, N. Smale, M. Adachi, S. Tanaka, S. Kimura, M. Katoh, N. Yamamoto, M. Hosaka, E. Roussel, C. Szwaj, S. Bielawski and M. Siegel, *IEEE Trans. Terahertz Sci. Tech.* **3(1)**, 81–86 (2013).
4) Y. Taira, H. Toyokawa, R. Kuroda, N. Yamamoto, M. Adachi, S. Tanaka and M. Katoh, *Rev. Sci. Instrum.* **84**, 053305 (2013).

Awards

TAIRA, Yoshitaka; Young Scientist Award of the Physical Society of Japan.
TAIRA, Yoshitaka; 2012 Annual Meeting Award of the Particle Accelerator Society of Japan.
HIDA, Yohei; 2012 Annual Meeting Award of the Particle Accelerator Society of Japan.
NIWA, Takahiro; 2012 Annual Meeting Award of the Particle Accelerator Society of Japan.

* carrying out graduate research on Cooperative Education Program of IMS with Nagoya University

Synchrotron Radiation Spectroscopy on Strongly Correlated Electron Systems

UVSOR Facility
Division of Advanced Solid State Physics

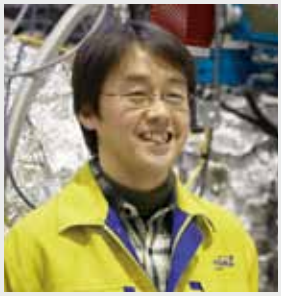

KIMURA, Shin-ichi
Associate Professor (–June, 2013)*

MATSUNAMI, Masaharu
Assistant Professor

HAJIRI, Tetsuya	Graduate Student†	KATO, Masaki	Graduate Student†
SHIMURA, Yusuke	Graduate Student†	KANEKO, Masaki	Graduate Student†
HIRATE, Satoshi	Graduate Student†	MOMIYAMA, Hakuya	Graduate Student†

Solids with strong electron–electron interaction, namely strongly correlated electron systems (SCES), have various physical properties, such as non-BCS superconducting, colossal magneto-resistance, heavy fermion and so on, which cannot be predicted by first-principle band structure calculation. Due to the physical properties, the materials are the candidates of the next generation functional materials. We investigate the mechanism of the physical properties as well as the electronic structure of SCES, especially rare-earth compounds, organic superconductors and transition-metal compounds, by infrared/THz spectroscopy and angle-resolved photoemission spectroscopy based on synchrotron radiation. Since experimental techniques using synchrotron radiation are evolved rapidly, the development of the synchrotron radiation instruments is also one of our research subjects.

1. Strongly Hybridized Electronic Structure of $YbAl_2$: An Angle-Resolved Photoemission Study[1)]

Heavy-fermion or valence fluctuation systems are characterized by the strong correlations of *f* electrons, resulting in an enhanced effective mass of quasiparticles due to the band renormalization effect. Consequently, the band structure and Fermi surface (FS) topology are modified from those predicted in band structure calculations based on local density approximation (LDA). To estimate the band renormalization effect, a direct comparison of the experimental band structure as well as the FS with the calculations is necessary. Angle-resolved photoemission spectroscopy (ARPES), which can probe both band structure and FS, is the most suitable tool for this purpose. Here we reported the electronic structure of a prototypical valence fluctuation system, $YbAl_2$, which is known as one of the prototypical valence fluctuation systems, using ARPES. In a recent hard X-ray photoemission spectroscopy study, the mean valence of Yb ions was estimated as +2.2 below 300 K. Correspondingly, an extremely high Kondo temperature (T_K) exceeding 2000 K has been suggested by the magnetic susceptibility or the inelastic neutron scattering. The mass enhancement factor is particularly small among heavy-fermion systems known so far, implying the small renormalization effect. Thus, $YbAl_2$ can be a suitable system to investigate the applicable limit of LDA calculation in relation with the fluctuating valence for the heavy-fermion systems. The observed band dispersions shown in Figure 1 are well described in terms of band structure calculations based on LDA calculation. Strong hybridization between the conduction and 4*f*

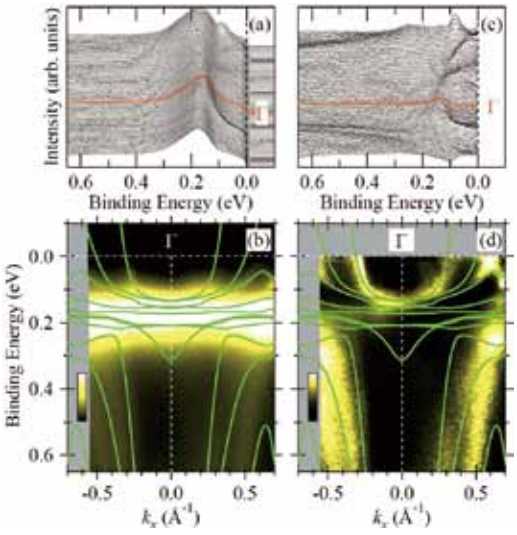

Figure 1. ARPES spectra (a) and intensity plot (b) near E_F along the Γ-K direction. (c), (d) The same data as in (a) and (b), normalized to the angleintegrated spectrum. The band dispersions obtained by the LDA calculation are overlapped in (b) and (d).

bands is identified on the basis of the periodic Anderson model. The evaluated small mass enhancement factor and the high Kondo temperature qualitatively agree with those obtained from thermodynamic measurements. Such findings suggest that the strong hybridization suppresses band renormalization and is responsible for the valence fluctuations in $YbAl_2$.

2. Optical Study of Archetypical Valence-Fluctuating Eu-Systems[2)]

Intermetallic compounds based on rare earth elements with an unstable valence, especially Ce, Eu and Yb, present many unusual properties and are therefore the subject of intense research since many years. Historically, the understanding of these compounds has been dominated by a dichotomy between the Kondo lattice/intermediate valence (KL/IV) scenario for Ce-/Yb-based systems and the valence fluctuating (VF) scenario for Eu-based systems. For Ce- or Yb-based KL/IV systems the nature of the electronic states and the low-energy excitations have been intensively investigated and are relatively well understood (with the exception of the immediate vicinity of the quantum critical point) while for Eu-based VF systems this knowledge is very limited. Then, we have investigated the optical conductivity of the prominent valence fluctuating compounds $EuIr_2Si_2$ and $EuNi_2P_2$ in the infrared energy range to get new insights into the electronic properties of valence fluctuating systems. For both compounds we observe upon cooling the formation of a renormalized Drude response, a partial suppression of the optical conductivity below 100 meV and the appearance of a mid-infrared peak at 0.15 eV for $EuIr_2Si_2$ and at 0.13 eV for $EuNi_2P_2$. Most remarkably, our results show a strong similarity with the optical spectra reported for many Ce- or Yb-based heavy fermion metals and intermediate valence systems, although the phase diagrams and the temperature dependence of the valence differ strongly between Eu- and Ce-/Yb-systems. This suggests that the hybridization between 4*f*- and conduction electrons, which is responsible for the properties of Ce- and Yb-systems, plays an important role in valence fluctuating Eu-systems.

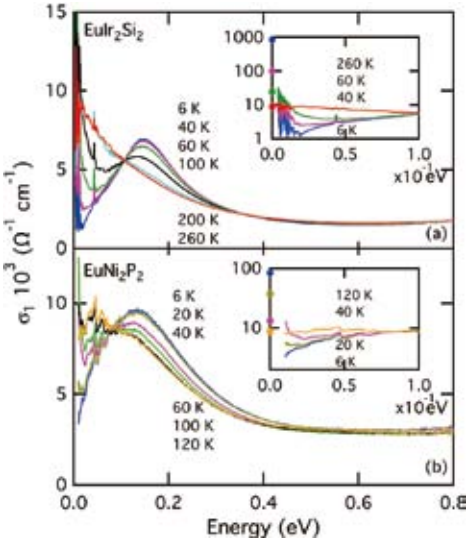

Figure 2. The real part of the optical conductivity spectra of $EuIr_2Si_2$ and $EuNi_2P_2$ at various temperatures. Insets: The low-energy optical conductivity spectra (solid lines) and the corresponding values for the dc conductivity, $\sigma_{dc} = \rho^{-1}$, (symbols) at 6, 40, 60 and 260 K for $EuIr_2Si_2$ and at 6, 20, 40 and 120 K for $EuNi_2P_2$.

3. Design of a Spin-, Symmetry-, and Momentum-Resolved Electronic Structure Analysis Instruments at UVSOR-III

UVSOR Facility equips two public undulator-beamlines for angle-resolved photoemission spectroscopy, one is BL5U in the photon energy $h\nu$ region of 20–200 eV and the other BL7U of $h\nu$ = 6–40eV. Since the monochromator of the former beamline is an old-style spherical grating type SGM-TRAIN constructed in 1990s and the throughput intensity and energy resolution are poor, the beamline was planned to be replaced to state-of-the-art monochromator and end station. Then we designed a new spin and angle-resolved photoemission spectroscopy instrument with variable photon energy and polarization. We employed a Monk-Gillieson-type variable-line-spacing plane-grating monochromator covering the photon energy of 20–200 eV. The end station shown in Figure 3 equips a VLEED spin detector. The beamline is constructed in FY2013-FY2014 and will be opened to users from FY2015.

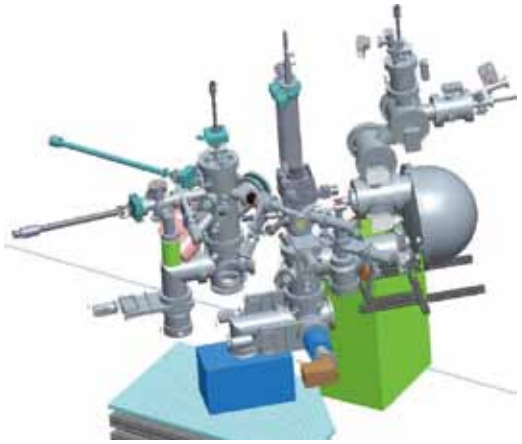

Figure 3. Schematic figure of the spin-, symmetry-, and momentum-resolved photoemission end station of BL5U, UVSOR-III.

References

1) M. Matsunami, T. Hajiri, H. Miyazaki, M. Kosaka and S. Kimura, *Phys. Rev. B* **87**, 165141 (2013).
2) V. Guritanu, S. Seiro, J. Sichelschmidt, N. Caroca-Canales, T. Iizuka, S. Kimura, C. Geibel and F. Steglich, *Phys. Rev. Lett.* **109**, 247207 (2012).

* Present Position; Professor, Graduate School of Frontier Bioscience, Osaka University
† carrying out graduate research on Cooperative Education Program of IMS with Nagoya University

Electronic Structure and Decay Dynamics in Atoms and Molecules Following Core Hole Creation

UVSOR Facility
Division of Advanced Photochemistry

SHIGEMASA, Eiji
Associate Professor

IWAYAMA, Hiroshi
Assistant Professor

The dynamics of the inner-shell photoexcitation, photoionization, and subsequent decay processes is much more complex, in comparison to outer-shell photo-processes. For instance, the inner-shell photoionization is concomitant with the excitation and ionization of valence electrons, which reveal themselves as shake-up and shake-off satellite structures in the corresponding photoelectron spectrum. The one-photon multi-electron processes, which are entirely due to the electron correlation in the system, are known to happen not only in the primary inner-shell hole creation processes, but also in their relaxation processes. Our research project is focused on elucidating the electronic structures and decay dynamics in core-excited atoms and molecules, by utilizing various spectroscopic techniques together with monochromatized synchrotron radiation in the soft x-ray region.

1. Ultrafast Dynamics in C 1s Core-Excited CF_4 Studied by Two-Dimensional Resonant Auger Spectroscopy

Excitation of a core electron to the lowest unoccupied antibonding orbital weakens the molecular bonding and populates generally a dissociative state. Morin and Nenner demonstrated that the 3d $\rightarrow \sigma^*$ excitation in HBr leads to a fast neutral dissociation which can precede the Auger relaxation; in other words, one can observe 'atomic' 3d hole decays in the Br fragment.[1)] The CF_4 molecule, tetrafluoro methane, has been a benchmark for several spectroscopic studies, due to its high symmetry, same as methane, CH_4. One of the most interesting observations deriving from the comparison between CH_4 and CF_4 is the relative intensity of below-threshold photoabsorption structures around the C 1s ionization threshold associated with transitions to empty molecular orbitals versus Rydberg states. CF_4 is a good candidate to investigate the dynamical properties of core-excited states with an electron in the antibonding lowest-unoccupied molecular orbital (LUMO) in a highly symmetric system.

Here an investigation of ultrafast dissociation following C1s-to-LUMO core excitation in CF_4, with high-resolution resonant Auger spectroscopy, is presented. The main novelty of this work is the use of two-dimensional (2D) maps to record resonant Auger spectra across the resonance as a function of photon energy with a small energy step and then to characterize ultrafast dynamics. This method allows one to follow in great detail the evolution of the resonant enhancement of spectral features corresponding to final ionic states while scanning the energy across the resonance, and to fully exploit the so-called detuning effects.

The experiment was performed on the soft X-ray beamline BL6U at UVSOR. The photon energy resolutions were set to 10000 and 4000 for total-ion yield and 2D map measurements, respectively. Kinetic energies of the emitted electrons were measured by a hemispherical electron energy analyzer (MBS-A1). The direction of the electric vector was set to be parallel to the axis of the electrostatic lens of the analyzer. The kinetic energy resolution of the analyzer was set to 60 meV. The 2D maps were obtained by taking decay spectra at regular photon energy intervals of 100 meV across the resonance.

Figure 1 shows the 2D map after subtraction of the non-resonant contributions, and with on-top two pseudo-absorption curves obtained by the CIS (Constant Ionic State) method, and namely plotting the integrated intensity of the two resonant features, the non-dispersive one related to the fragment and the dispersive one related to the $3t_2$ state, as a function of photon energy. The double feature with maxima at 297.7 and 298.4

eV is assigned to the Jahn-Teller-split transition to the LUMO (σ^* of t_2 symmetry), followed by the Rydberg series. It is seen that while the intensity of the molecular state closely mimics one of the absorption curve, the non-dispersive feature related to the fragment decreases in relative intensity across the resonance, and disappears in the photon energy region of the Rydberg states. Detailed calculations on the potential curves of the intermediate and final state would be needed to fully clarify this finding.

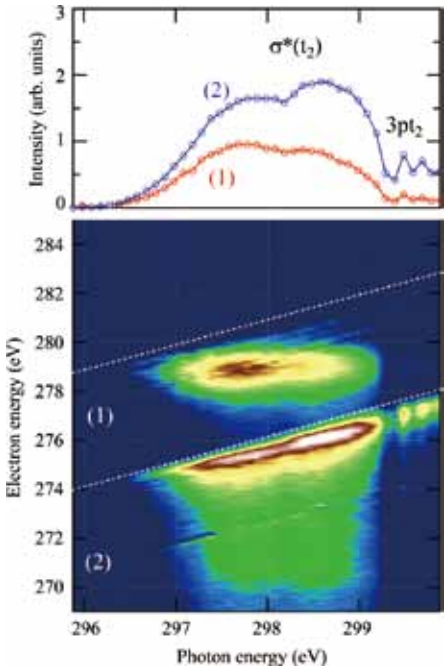

Figure 1. Top: CIS spectra of the fragment (1) and of the $3t_2$ (2) final states. Bottom: resonant Auger 2-D map showing only the resonant contributions: (1) the non-dispersive state and (2) the $3t_2$ spectral line.

2. High-Resolution Electron Spectroscopy for Ethyl Trifluoroacetate

Inner-shell photoionization of light elements is mostly relaxed via an Auger decay process, causing the emission of another electron from an outer-shell. Auger electron spectroscopy (AES) is thus an element-sensitive method with various analytical applications. Since a core hole can be regarded as being strongly localized at a particular atom, it can be expected that the Auger final dicationic state has two valence holes which are also localized near the inner-shell ionized atom. According to this simple atomic picture, the binding energies of the molecular Auger final states would also show chemical shifts. Owing to a hole–hole repulsion, the chemical shift in Auger electron spectra reflects any localization character of the two valence holes.

The interpretation of molecular Auger spectra is complex and the difficulties increase with increasing the number of atoms in a molecule. The Auger spectra become much more complicated in the case where a molecule is composed of several atoms of the same element. While well-defined photoelectron peaks reflecting the chemical shifts can be observed in photoelectron spectra, direct observations of the corresponding chemical shifts in molecular Auger spectra are practically impossible without using a coincidence technique. In order to stabilize the interpretation on the site-specific Auger spectra obtained by such coincidence experiments, however, high-resolution Auger electron spectra as well as theoretical calculations are indispensable. We have carried out high-resolution electron spectroscopic measurements on ethyl trifluoroacetate ($C_4H_5F_3O_2$).

The experiment was performed on the soft X-ray beamline BL6U at UVSOR. The radiation from an undulator was monochromatized by a variable included angle varied line-spacing plane grazing monochromator. The monochromatized radiation was introduced into a cell with sample gases. Kinetic energies of the emitted electrons were measured by a hemispherical electron energy analyzer (MBS-A1) placed at a right angle with respect to the photon beam direction. The direction of the electric vector was set to be parallel to the axis of the electrostatic lens of the analyzer. The energy resolution of the analyzer was set to 20 meV.

The oxygen and fluorine Auger electron spectra are displayed in Figure 2 (a) and (b), respectively. It is seen that the populations of the Auger final states strongly depend on which core electron is ionized. No fine structure is found in every Auger electron spectrum, in spite of the high-resolution. The Auger spectra have been simulated using a statistical approach. It is found that all Auger decays populate mainly localized dicationic states, with the two holes located either on the same fluorine atom or on adjacent fluorine atoms. While the decay of the F 1s hole populates exclusively the former states, the latter class of states is also populated by the decay of the C and O 1s holes.

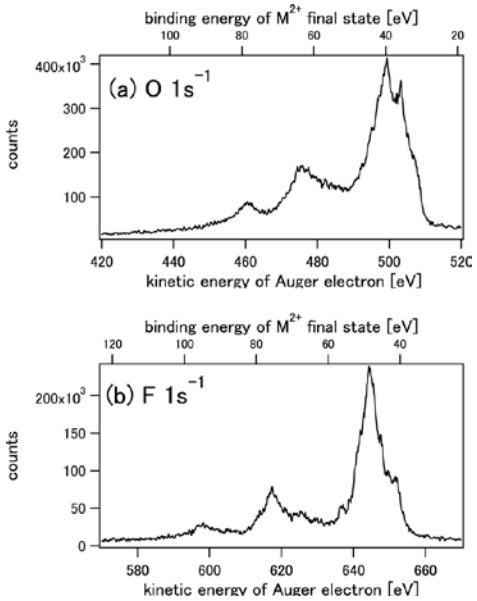

Figure 2. (a) Oxygen and (b) fluorine Auger electron spectra of $C_4H_5F_3O_2$.

References

1) P. Morin and I. Nenner, *Phys. Rev. Lett.* **56**, 1913–1916 (1986).
2) M. N. Piancastelli *et al.*, *J. Chem. Phys.* **138**, 234305 (2013).
3) H. Iwayama *et al.*, *J. Chem. Phys.* **138**, 024306 (2013).

Micro Solid-State Photonics

Laser Research Center for Molecular Science
Division of Advanced Laser Development

TAIRA, Takunori
Associate Professor

ISHIZUKI, Hideki
Assistant Professor

TSUNEKANE, Masaki	Post-Doctoral Fellow	BHANDARI, Rakesh	Post-Doctoral Fellow
SATO, Yoichi	Post-Doctoral Fellow	ARZAKANTSYAN, Mikayel	Post-Doctoral Fellow
KAUSAS, Arvydas	Post-Doctoral Fellow	KONG, Weipeng	Graduate Student
		ONO, Yoko	Secretary
		INAGAKI, Yayoi	Secretary

The artistic optical devices should be compact, reliable, efficient and high power light sources. With the approaches of domain structures and boundaries engineering, it is possible to bring the new interaction in their coherent radiation. The high-brightness nature of Yb or Nd doped single crystal or ceramic microchip lasers can realize efficient nonlinear wavelength conversion. In addition, designed nonlinear polarization under coherent length level allows us new function, such as the quasi phase matching (QPM). The development of "***Micro Solid-State Photonics***," which is based on the micro domain structure and boundary controlled materials, opens new horizon in the laser science.

1. High Peak Power, Passively Q-Switched Yb:YAG/Cr:YAG Micro-Lasers

High peak power (>MW), passively Q-switched Yb:YAG/Cr:YAG micro-laser end-pumped by fiber-coupled 120 W QCW LDs (Repetition rate < 100 Hz) was developed. The convex output coupler with a curvature of 2 m successfully enlarged the fundamental mode size in the micro-laser cavity, and the output pulse energy increased to 3.6 mJ at a Cr:YAG initial transmission of 89% without optical damage. The TEM_{00} transverse mode and the single-frequency oscillation were confirmed. The pulse duration was 1.3 ns, and then the peak power was estimated as 2.8 MW. To our knowledge, these are the highest pulse energy and peak power ever reported in Yb:YAG/Cr:YAG micro-lasers.

2. Palm-Top Size Megawatt Peak Power UV (266 nm) Microlaser

We have developed of a very compact, highly efficient, megawatt peak power, sub-nanosecond pulse width, 266 nm ultraviolet (UV) microlaser.

It contains a specially designed passively Q-switched Nd:YAG/Cr^{4+}:YAG microchip laser whose high output peak power of 13 MW enables efficient wavelength conversion without using any optics before the nonlinear crystals. The sub-nanosecond pulse width region, which delivers high peak power of several MW even for a moderate pulse energy of a few mJ, is very useful for efficient wavelength conversion.

We achieved 73% second harmonic generation efficiency using a LiB_3O_5 (Lithium Triborate, LBO) crystal and 45% fourth harmonic generation efficiency using a β-BaB_2O_4 (β-barium borate, BBO) crystal. As a result, we obtained 650 μJ, 4.3 MW peak power, 150 ps, 100 Hz pulse output at 266 nm. We used an original design for the nonlinear crystal holders to reduce the size of the microlaser.

This palm-top size 266 nm UV microlaser will be useful for many applications, such as, photoionization, UV laser induced breakdown spectroscopy (LIBS), pulsed laser deposition and materials microprocessing.

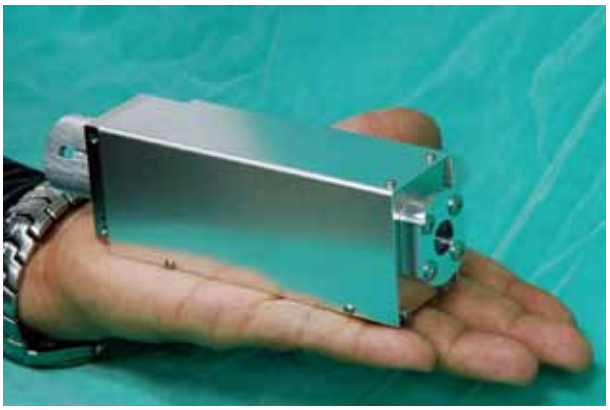

Figure 1. Palm-top size 266 nm UV microlaser.

3. Fundamental Investigations in Orientation Control Process for Anisotropic Laser Ceramics

We developed theoretical studies on the orientation control of micro-domains in anisotropic laser ceramics. The direction of the crystal axis that is parallel to easy magnetization in each micro-domain can be aligned via two steps of fabrication processes.

In the first step the alignment is performed during the slip-casting under the magnetic field, where directions of easy magnetization in primary particles are forced to align along applied magnetic field. The further orientation control can be processed by the preferential grain growth, where an adequate orientation distribution of primary articles in the casted green body is required for the nearly perfect alignment in sintered ceramics.

However, even though rare-earth trivalent ions doped into primary particles as luminous ions enhance their magnetic moment, the perfect alignment control is not always possible due to Brownian fluctuations by slurry solvent at this stage. By means of the distribution function for the crystal orientation in micro-domains under magnetic field, we confirmed the improvement in the orientation distribution contributed by preferential grain growth from detailed XRD analyses.

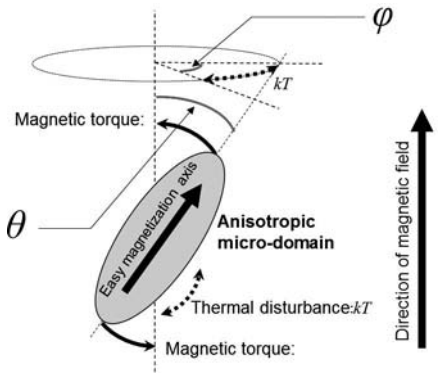

Figure 2. Conceptual diagram for the orientation control of anisotropic laser ceramics. Angle θ and φ are the angle between the control axis and the direction of easy magnetization axis and the precession angle of the micro-domain, respectively.

4. Half-Joule Output Optical-Parametric Oscillation by Using 10-mm-Thick PPMgLN Device

We presented a next generation of large-aperture periodically poled Mg-doped $LiNbO_3$ (PPMgLN) device with 10-mm thickness. Efficient optical parametric oscillation with 540 mJ output energy at 709 mJ pumping by 1.064 μm laser in 10 ns operation could be demonstrated using the 10-mm-thick PPMgLN with an inversion period of 32.2 μm at total conversion efficiency > 76%. We also confirmed that degradation effect of conversion-efficiency distribution by wedged inversion structures, which is inevitable in current poling condition of the large-aperture PPMgLN, can be ignored in high-intensity operation.

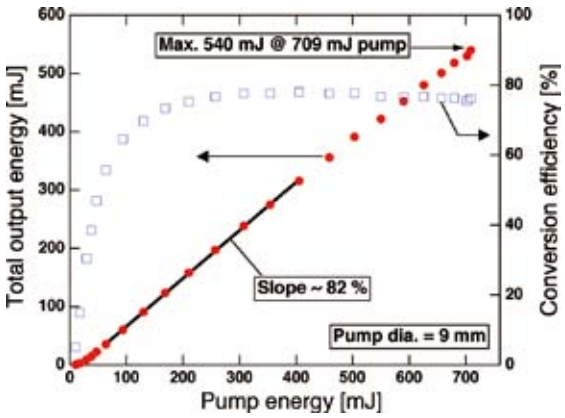

Figure 3. Characteristics of 10 nanoseconds OPO by using 10-mm-thick PPMgLN device.

References

1) M. Tsunekane and T. Taira, *IEEE J. Quantum Electron.* **49**, 454–461 (2013).
2) R. Bhandari and T. Taira, *Opt. Eng.* **52**, 076102 (6 pages) (2013).
3) Y. Sato, J. Akiyama and T. Taira, *Phys. Status Solidi C* **10**, 896 (2013), Y. Sato, J. Akiyama and T. Taira, *Opt. Mater. Express* **3**, 829 (2013).
4) H. Ishizuki and T. Taira, *Opt. Express* **20**, 20002–20010 (2012).

Ultrafast Laser Science

Laser Research Center for Molecular Science
Division of Advanced Laser Development

FUJI, Takao
Associate Professor

NOMURA, Yutaka
Assistant Professor

SHIRAI, Hideto IMS Fellow
KAWAI, Shigeko Secretary

Speed of ultrafast energy transfer from light to molecules (*i.e.* primary processes of photosynthesis, photoisomerization in visual pigments, *etc.*) is on the order of femtosecond (10^{-15} s). In our laboratory, we develop cutting edge lasers for such ultrafast molecular science, namely, femtosecond or attosecond (10^{-18} s) ultrashort pulse lasers.

For example, arbitrary waveform synthesis can be performed with simultaneous generation of femtosecond light pulses in various wavelength regions and superimposition of them with precisely controlled phases.

We would like to develop such advanced light control technology, which can push forward the research on ultrafast photochemical reactions.

1. Generation of Phase-Stable Sub-Cycle Mid-Infrared Pulses from Filamentation in Gases[1,2)]

Coherent light sources in the mid-infrared spectral region (MIR, 2.5–20 μm, 4000–500 cm^{-1}) are highly important for studies in molecular science since a number of molecular vibrations have resonance in this wavelength region. The light source can be applied to various advanced molecular spectroscopies, such as frequency comb spectroscopy for the molecular fingerprint region, pump–probe spectroscopy to trace ultrafast structural dynamics, and control of photodissociation by selective excitation of vibrational states.

Here we report the generation of sub-single-cycle pulses in the mid-infrared (MIR) region through a laser-induced filament in gases. Although the nonlinearity of gas media is much smaller than that of bulk media, the filamentation effect can be used to overcome the low efficiency. The balance between self-focusing and plasma self-defocusing in the filament makes the pulse propagate much longer than the Rayleigh range with a very high intensity. It results in a dramatic enhancement of nonlinear processes occurring in the filamentation zone.

The fundamental (ω_1) and second harmonic (ω_2) output of a 30-fs Ti:sapphire amplifier were focused into nitrogen gas and produce phase-stable broadband MIR pulses (ω_0) by using a four-wave mixing process ($\omega_1 + \omega_1 - \omega_2 \rightarrow \omega_0$) through filamentation. The spectrum spread from 400 cm^{-1} to 5500 cm^{-1}, which completely covered the MIR region. The low frequency components were detected by using an electro–optic sampling technique with a gaseous medium. The efficiency of the MIR pulse generation was very sensitive to the delay between the fundamental and second harmonic pulses. It was revealed that the delay dependence of the efficiency came from the interference between two opposite parametric processes, $\omega_1 + \omega_1 - \omega_2 \rightarrow \omega_0$ and $\omega_2 - \omega_1 - \omega_1 \rightarrow \omega_0$. The pulse duration was measured as 6.9 fs with cross-correlation frequency-resolved optical gating by using four-wave mixing in nitrogen. The carrier-envelope phase of the MIR pulse was passively stabilized. The instability was estimated as 154 mrad rms in

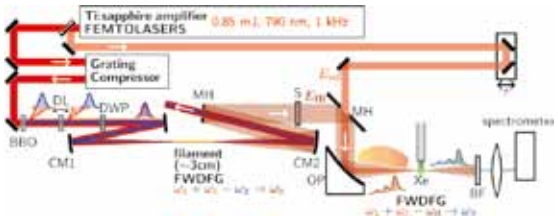

Figure 1. Schematic of the MIR pulse generation through filamentation and the chirped-pulse upconversion with FWDFG in xenon gas. BBO:β-BaB_2O_4 crystal (Type 1, θ = 29 deg, t = 100 μm), DP: delay plate (calcite crystal, t = 1.7 mm), DWP: dual wave plate (λ at 400 nm, λ/2 at 800 nm), CM1: r = 1 m concave mirror, CM2: r = 0.5 m concave mirror, MH: aluminium-coated mirror with a hole (ϕ = 7 mm), S: sample, OP: off-axis parabola (f = 50 mm), BF: blue filter.

2.5 hours. The beam profile and spectrum of the MIR field are accurately reproduced with a simple calculation based on a four-wave mixing process. Although the MIR pulse had ring-shaped beam profile, it was well-focusable. The ring-shaped pattern was originated from a dramatic confocal-parameter mismatch between the MIR field and the laser beams.

2. Single-Shot Detection of Mid-Infrared Spectra by Chirped-Pulse Upconversion with Four-Wave Difference Frequency Generation in Gases[3)]

Single-shot detection of the entire MIR supercontinuum (500–4000 cm^{-1}) with reasonable resolution has been required for the above mentioned advanced molecular spectroscopies. It is straightforward to measure the MIR spectrum with a dispersive MIR spectrometer consisting of a grating and a multichannel MIR detector. However, the bandwidth of this method has been limited to about 500 cm^{-1} due to the low sensitivity and the high cost of the multichannnel MIR detectors.

An alternative approach to detect the MIR supercontinuum with single-shot is optically converting the spectra into visible region and recording them with a visible spectrometer, which has much higher performance than the MIR spectrometers. However, the bandwidths of these upconversion methods have still been limited to about 600 cm^{-1} because of the limited phase matching bandwidth of the nonlinear solid crystals for the upconversion.

Here we report the demonstration of ultrabroadband detection of MIR spectra on a single-shot basis using chirped-pulse upconversion with gas media. By using a gas as a nonlinear medium, the detection bandwidth dramatically broadens to more than 5000 cm^{-1} due to the wide transmission range and the broadband phase matching condition of the gas medium. Although the low frequency conversion efficiency due to the low nonlinearity of the gas media is the large drawback of the method, it was possible to measure spectra over the range of MIR region, specifically 200–5500 cm^{-1}, with about 2 cm^{-1} resolution on a single-shot basis.

Experimental demonstration of the method was realized with the system shown in Figure 1. The ultrabroadband MIR continuum was generated by using FWDFG of the fundamental and the second harmonic of Ti:sapphire amplifier (790 nm, 30 fs, 0.85 mJ at 1 kHz) output through filamentation in gases, which is basically the same generation scheme as that reported in the previous section. A small portion of the fundamental pulse ($E_{ref}(t)$, 0.1 mJ, ω_1) before the compressor of the Ti:sapphire amplifier system was used as a chirped pulse. The pulse duration of the chirped pulse was estimated as 10.3 ps. The chirped pulse and the MIR pulse ($E_{IR}(t)$, ω_0) were combined with a delay time τ through a mirror with a hole. The combined beam was focused into a xenon gas at about atmospheric pressure with a parabolic mirror (f = 50 mm) and generated visible light $E_{ref}^2(t-\tau)E_{IR}^*(t)$ through an FWDFG process, $\omega_1 + \omega_1 - \omega_0 \rightarrow \omega_2$. Since gas media are centrosymmetric, it is not possible to use second-order nonlinear processes but possible to use third-order nonlinear processes for frequency conversion, such as FWDFG or four-wave sum frequency generation (FWSFG). The spot size of the chirped pulse at the focus was about 12 μm. The pulse energy of the upconverted signal was several pJ. The spectrum of the FWDFG signal at a fixed delay was measured with a conventional spectrometer with an EMCCD camera. The camera was synchronized with the repetition rate of the laser and the spectrum was measured with a single shot, namely within 1 ms.

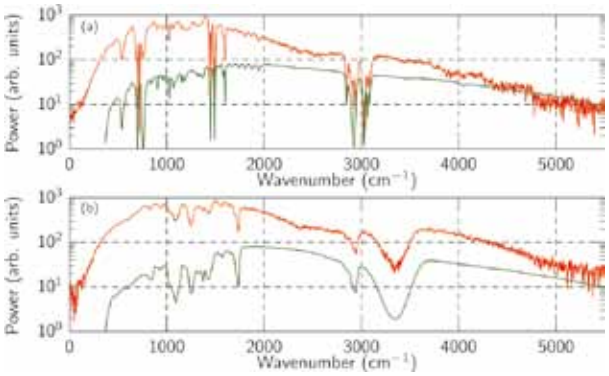

Figure 2. The spectra of the MIR pulse passed through (a) polystyrene and (b) polyvinyl alcohol films measured with the chirped pulse upconversion (red curves). The MIR absorption spectrum for each sample measured with a conventional Fourier-transform spectrometer is also shown (green curves).

We have applied the method to measure the absorption spectra of polystyrene and polyvinyl alcohol films, whose thicknesses were 38 μm and 12 μm, respectively. The MIR pulse transmitted through each film was upconverted and measured with a visible spectrometer. The path of the MIR pulse was purged with argon. The MIR spectra retrieved from the visible spectra are shown in the Figure 2. Several absorption lines of the polystyrene and polyvinyl alcohol films are clearly observed. For comparison, the MIR absorption spectrum of each sample was measured with a conventional Fourier-transform spectrometer with the resolution of 1.3 cm^{-1}. As can be seen in Figure 2, the fine structures of the MIR absorption lines are very well reproduced.

One of the most interesting applications of the chirped-pulse upconversion method is MIR spectroscopy with attenuated total reflectance (ATR) because there should be no change of temporal and spatial overlap of the MIR pulse and the chirped pulse by exchanging the sample at the chirped pulse upconversion system with the ATR.

References

1) Y. Nomura, H. Shirai, K. Ishii, N. Tsurumachi, A. A. Voronin, A. M. Zheltikov and T. Fuji, *Opt. Express* **20**, 24741–24747 (2012).
2) T. Fuji and Y. Nomura, *Appl. Sci.* **3**, 122–138 (2013).
3) Y. Nomura, Y.-T. Wang, T. Kozai, H. Shirai, A. Yabushita, C.-W. Luo, S. Nakanishi and T. Fuji, *Opt. Express* **21**, 18249–18254 (2013).

Dissociative Photoionization Studies of Fullerenes and Carbon Nanotubes and Their Application to Dye-Sensitized Solar Cells

Department of Photo-Molecular Science
Division of Photo-Molecular Science III

KATAYANAGI, Hideki
Assistant Professor

We have observed the dissociative photoionization of the fullerenes. We studied the mechanisms and kinetics of C_2 release reactions from the fullerenes on the basis of the yield curves and the scattering velocity distributions of the fragments $C_{60(70)-2n}^{z+}$ ($n \geq 1$; z = 1–3). We now intend to apply the above gas phase spectroscopy to functional materials such as carbon nanotubes (CNTs). Additionally we utilize the CNT as catalytic counter electrodes in dye-sensitized solar cells (DSSCs). This research aims at understanding the electron transfer reactions from CNTs both in gas phase and in condensed phase.

1. Mass Resolved Velocity Map Imaging of Doubly Charged Photofragments from C_{60}

We observed mass resolved velocity map images of fragments produced by the photodissociation of the fullerenes.[1,2] However we have not obtained a two-dimensional (2D) projection of three-dimensional (3D) velocity distribution of each fragment. We installed a four-element imaging lens which enables us to completely resolve the fragment signals. We thus observed the 2D velocity image of each fragment. The 2D velocity image of C_{58}^{2+} was found to be a convolution of isotropic barycentric velocity distribution of C_{58}^{2+} and anisotropic velocity of C_{60} in the parent molecular beam.

2. Gas Phase Spectroscopy of CNTs

The gas phase spectroscopy used to elucidate the dissociation dynamics of the fullerenes is now applied to the CNT. We have started to design a vacuum chamber for the gas phase spectroscopy of CNTs. Meanwhile we have examined properties and suitable vaporization conditions of CNT samples using AFM and MALDI equipment. We are also seeking for methods for controlling the length of CNT. The gas phase spectroscopy of length selected CNT will allow us to understand properties of the CNTs as functions of their length.

3. Development and Evaluation of CNT Catalytic Counter Electrodes for DSSCs

To improve photovoltaic energy conversion efficiency of the DSSC, the rate of charge transfer reaction on the counter electrode is important. We prepared the counter electrodes using commercial CNT aqueous dispersions. We found a simple method to produce the CNT counter electrodes with comparable efficiency to Pt electrodes.

References

1) H. Katayanagi and K. Mitsuke, *J. Chem. Phys. (Communication)* **133**, 081101 (4 pages) (2010).
2) H. Katayanagi and K. Mitsuke, *J. Chem. Phys.* **135**, 144307 (8 pages) (2011).

Visiting Professors

Visiting Professor
NODA, Susumu *(from Kyoto University)*

Strong Coupling of Single Atoms to Photonic Crystal Cavity Field

We have investigated photonic crystal structures which enable modification of propagation properties of an electromagnetic field and also tight confinement of the field to a tiny resonator. Accordingly the field strength inside the resonator is much enhanced and therefore the field can be strongly coupled to a quantum emitter such as a quantum dot even at a single photon level. Such a nanostructure device would be suitable for applications in optical communication and future quantum information processing in terms of its scalability. We have studied the strong coupling of the cavity field with a quantum dot and also the Purcell effect. Recently we have been interested in adopting a single cold atom as a quantum emitter, which shows much longer coherence time and therefore would be desirable for future application. Cold atoms are first loaded into a magneto-optical trap and then one of them is captured in tightly-focused optical tweezers. A movable lens-positioner can translate the position of the focal point, thereby transferring the trapped atom to the vicinity of the photonic crystal cavity. With this technique, the strong coupling of the single atom with the cavity field will be studied.

Visiting Professor
ITO, Atsushi *(from Tokai University)*

X-Ray Spectromicroscopy of Biomedical Specimens

Soft X-ray microscopy has a great advantage over other microscopies in the mapping of light elements or molecules containing such elements at high resolution. The mapping is realized by X-ray spectro-microscopy which utilizes distinctive spectral features of elements and molecules, that is, absorption edges and XANES profiles observed in the vicinity of the absorption edge. For applying this method to biomedical specimens, XANES profiles have been surveyed for a variety of biomolecules such as DNA, proteins (histone and albumin), sulfur-containing amino acids, calcium-containing biomolecules and iron-containing proteins at the C-K, N-K, O-K, S-L, Ca-L and Fe-L absorption edges. One of the most interesting and useful results obtained in this survey is that DNA and histone, a nuclear protein, exhibited significantly different spectra at the N-K edge, suggesting the possibility to image DNA and proteins in cellular nuclei separately. Spectromicroscopy at the N-K edge for a whole cell or an isolated nucleus would provide a unique method to image DNA distribution in a nucleus.

Visiting Associate Professor
TSUBOUCHI, Masaaki *(from Japan Atomic Energy Agency)*

THz Pulse Shaping by Interaction between THz Light and Photo-Induced Carrier

We are developing pulse shaping techniques in the THz frequency region to realize precise control of molecular rotation. First, we have developed the THz tomography of photo-induced carriers in a semi-conductor. Since the photo-induced carrier strongly interacts with THz light, the measurement and control of the carrier distribution and dynamics are significantly important to design THz optics. For the aim of pulse shaping, we have demonstrated an etalon with an optical shutter that can generate a THz pulse train with high efficiency. Our THz etalon consists of a Si plate as an input coupler and an ITO coated glass plate as an output coupler. After the THz pulse is transmitted from the Si plate, the Si is irradiated by a UV light to generate the plasma layer which strongly reflects the THz light. The UV light operates as an optical shutter which traps the THz pulse in the etalon cavity.

Visiting Associate Professor
HATSUI, Takaki *(from RIKEN SPring-8 Center)*

Theoretical Study on the Interaction between Matter and X-Ray Free Electron Laser

This year, we have investigated on the valence excitations of multiply ionized states for envelope measurement of X-ray free electron laser. Multiply ionized ground/excited anilines created by X-ray free electron lasers (XFELs) were analyzed by first-principles calculations. The analyses revealed that red shift of the optical absorption appear dominantly during XFEL illumination owing to the ultra-short lifetime of the core-hole states. The XFEL pulse envelope information is thus transferred from X-ray to optical frequency domain, where precise measurement is feasible. The predictions give foundation of novel pulse envelope monitor indispensable for future envelope-controlled XFEL experiments, such as seeded XFEL.

RESEARCH ACTIVITIES

Materials Molecular Science

Extensive developments of new functional molecules and their assemblies are being conducted in three Divisions of Electronic Structures, Electronic Properties, and Molecular Functions, and one division for visiting professors, in an attempt to discover new phenomena and useful functions. The physical (electric, optical, thermal and magnetic) properties on new functional materials, the chemical properties like enzymes, catalysis and photochemistry, the exploitation of new spectroscopic methods for materials molecular science, and technological applications like solar cells and transistors are investigated in this department.

Exploitations of Novel Spectroscopic Methods Using Synchrotron Radiations and Lasers for Materials Science

Department of Materials Molecular Science
Division of Electronic Structure

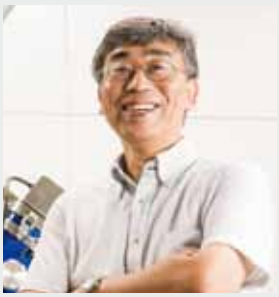

YOKOYAMA, Toshihiko
Professor

TAKAGI, Yasumasa
Assistant Professor

UEMURA, Yohei
Assistant Professor

NAKAGAWA, Takeshi	Assistant Professor*
WANG, Heng	Post-Doctoral Fellow
EGUCHI, Keitaro	Graduate Student
NAKANO, Hirohito	Graduate Student
UOZUMI, Madoka	Technical Fellow
USUI, Chika	Technical Fellow
FUNAKI, Yumiko	Secretary
TOYAMA, Yu	Secretary
FUKUTOMI, Yukiyo	Secretary
YASUI, Yuco	Secretary
WATANABE, Yoko	Secretary
KANEKO, Yasushi	Nano. Platform Manager
INOUE, Mika	Nano. Platform Manager

To develop novel functional materials, it is also essentially important to exploit new characterization methods that improve spatial and time resolving powers substantially and allow one to investigate the materials in operand conditions. In our group, we are interested in the developments of new spectroscopic methods for materials science using synchrotron radiation and lasers. Especially, we have been investigated surface and thin-film magnetism and related magnetic materials for the last decade. Recently, to investigate surface reaction process in working condition, we began to exploit hard x-ray photoelectron spectroscopy at ambient pressure.

1. Novel Magnetic Nanoscope: Ultraviolet Magnetic Circular Dichrosim Photoelectron Emission Microscope (UVMCD PEEM)[1)]

Since we discovered dramatic enhancement of visible and ultraviolet photoemission magnetic circular dichroism of 3d transition metal ultrathin films in the vicinity of the work function threshold,[1)] we have been exploiting UVMCD PEEM to visualize magnetic domains with a spatial resolution of ~30 nm and a time resolution of ~100 fs. Compared to X-ray MCD PEEM that has now become a widely established technique, this technique is advantageous in that the measurements can be performed in laboratory and the time resolution of ~100 fs can easily be achieved by using ultrashort pulsed lasers that are commercially available.

The light source is a wavelength-tunable high-power mode-locked Ti:Sapphire laser, and by using the second-, third- and fourth-order harmonics available photon energies are 3.0–6.0 eV with sufficient intensity. Two-photon processes are also available for the requirement of higher photon energies. The pulse width is ~200 fs and the ultrafast pump-and-probe experiment can be performed. Figure 1 is the demonstrative magnetic domain images of ~15 monolayer Ni films grown epitaxially on Cu(001) during hydrogen adsorption with almost real-time observation interval. Bright and dark contrasts stand for upward and downward magnetic domains. As H_2 adsorbs on the Ni surface, it is clearly found that the shape of the magnetic domains becomes simpler so that the length of domain wall may be reduced. This originates from stabilization of the perpendicular magnetic anisotropy of the Ni films upon hydrogen adsorption. To reduce unstability at the domain walls with a large perpendicular magnetic anisotropy, the domain wall length is shorter with H_2 adsorption.

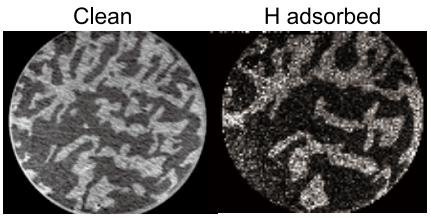

Figure 1. Magnetic domain images of ~15 ML Ni on Cu(001) at 300 K before and after hydrogen adsorption. The field of view is 100 μm.

2. Ambient Pressure Hard X-Ray Photo-Electron Spectroscopy

In order to investigate Pt-based catalysts in polymer electrolyte fuel cells under working conditions, we are exploiting hard x-ray photoelectron spectroscopy in an ambient pressure. Ambient pressure soft x-ray photoelectron spectroscopy is now available in several third-generation synchrotron facilities

in the world and allows one to characterize the surface of the specimen at ~100 Pa. However, the maximum pressure is still too small to study wet materials. Because of substantially longer mean free paths of electrons with much higher electron kinetic energies, the usage of hard x-rays can extend the pressure range up to ~3000 Pa that corresponds to the vapor pressure of water at room temperature. Up to now, no reports concerning this technique are seen in the literatures.

We have joined NEDO (New Energy and Industrial Technology Development Organization) fuel cell project and installed an ambient pressure hard x-ray photoelectron spectrometer in Beamline 36XU of SPring-8, as shown in Figures 2(a) and 2(b). The hard x-rays from the undulator source with photon energies of 6–8 keV, are monochromatized by four Si crystals, and the total energy resolution including the electron energy analyzer is ~0.35 eV for practical use. Figure 2(c) shows the Au 4f spectra of Au foil by varying the environmental pressure. Up to 3000 Pa N_2, we have successfully obtained good Au 4f spectra of Au foil without any discharging problem concerning high voltages applied to the electron lenses. We have tried to measure Pt 3d spectra [Figure 2(d)] of the Pt-C electrode in sulfuric acid solution with Nafion membrane by applying the voltage to conduct water electrolysis. With increasing the applied voltage, Pt is gradually oxidized to provide larger Pt–OH and Pt–O signals. At 1.8 V, the electrolysis of water takes place and again the Pt–O signal is reduced. Since the performance of the spectrometer is found to be excellent, an application to real fuel cell systems is desired as soon as possible.

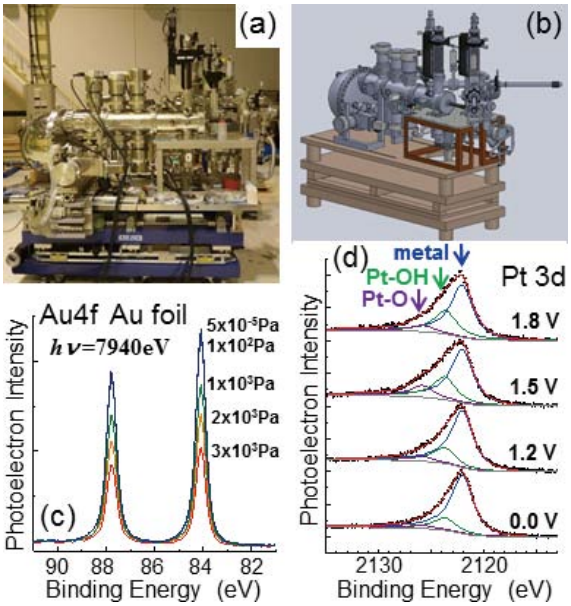

Figure 2. Photo (a) and schematic drawing (b) of the ambient pressure hard x-ray electron spectrometer. (c) Au 4f photoelectron spectra of Au foil under N_2. (d) Pt 3d photoelectron spectra of the Pt-C/Nafion/H_2SO_4(aq)/Pt system under 2000 Pa O_2 atmosphere by varying the voltage applied to the Pt-C electrode.

3. Anisotropic Thermal Expansion and Invar/Anti-Invar Effects in MnNi[3)]

An Invar alloy $Fe_{66}Ni_{34}$ that shows anomalously small thermal expansion over a wide temperature range was discovered in 1897. Basically, the coexistence of the different electronic states in Fe compensates for thermal expansion. The detailed origin of the Invar effect is however a famous long-standing problem. Previously we have studied local thermal expansion and its quantum effect.[2)] In this work, anisotropic thermal expansion in fct $Mn_{88}Ni_{12}$ alloy, which has a martensitic shape memory effect, was investigated by EXAFS and the path-integral simulations.[3)]

In the lattice constants, the *a* axis shows somewhat larger thermal expansion than usual, while the *c* axis exhibits almost no thermal expansion. The environment around Mn is found to be really tetragonally distorted, while the Ni environment is regarded as cubic. It should be noted here that in spite of the fact that the average x-ray structure is fct, the local structures of Mn and Ni are essentially different. It is also clearly found that the theoretical simulations based on the low-spin/high-spin two-state model successfully reproduce all the experimental lattice constants and bond distances. This confirms that the two inequivalent bonds around Mn are regarded as the bonds within the *bc*/*ca* and *ab* planes. Consequently, the present anisotropic thermal expansion is explained by the cooperative Invar/anti-Invar effects in the Mn atom, where the tetragonally distorted more stable low-spin Mn state gives a smaller atomic radius within the *ab* plane and a larger radius along the *c* axis than the spherical one of the HS state, as depicted in Figure 3(c).

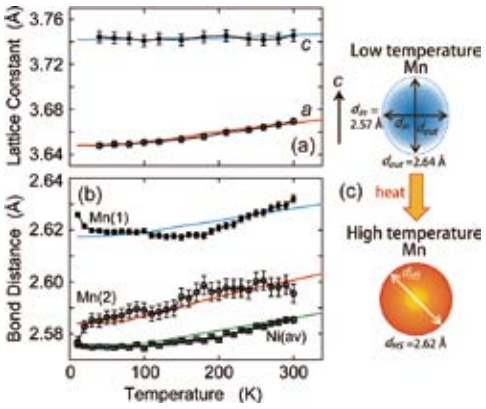

Figure 3. Experimental and simulated (a) lattice constants and (b) bond distances. (c) Schematic model of electronic structure change in Mn at low and high temperatures.

References

1) T. Nakagawa and T. Yokoyama, *J. Electron Spectrsc. Relat. Phenom.* **185**, 356 (2012).
2) T. Yokoyama and K. Eguchi, *Phys. Rev. Lett.* **107**, 065901 (2011).
3) T. Yokoyama and K. Eguchi, *Phys. Rev. Lett.* **110**, 075901 (2013).

* Present Address; Department of Molecular and Material Sciences, Interdisciplinary Graduate School of Engineering Sciences, Kyushu University, Kasuga Koen 6-1, Kasuga, Fukuoka 816-8580, Japan

Design and In-Situ Characterization of Catalyst Surfaces

Department of Materials Molecular Science
Division of Electronic Structure

MURATSUGU, Satoshi
Assistant Professor†

TADA, Mizuki
Associate Professor (–March, 2013)*

MAITY, Niladri	Post-Doctoral Fellow	SODE, Aya	Post-Doctoral Fellow
ZHANG, Shenghong	Post-Doctoral Fellow	KITYAKARN, Sutasinee	Post-Doctoral Fellow
SAIDA, Takahiro	Post-Doctoral Fellow	TRAN, Quang Thuong	JENESYS Program Visiting Scientist
WAKI, Minoru	Post-Doctoral Fellow	WANG, Fei	Graduate Student
		ISHIGURO, Nozomu	Graduate Student‡
		USUI, Chika	Technical Fellow
		GONDO, Makiko	Technical Fellow
		FUKUTOMI, Yukiyo	Secretary

We have focused on the preparation of new catalyst surfaces by using metal complexes, metal nanoparticles, and metal oxides and in situ characterization of solid catalysts under catalyst working conditions.

1. Preparation and Discontinuous Property of Methane Steam Reforming of Ni/Ordered $Ce_2Zr_2O_x$ Catalysts[1)]

Methane steam reforming is one of the key reactions to produce hydrogen. We prepared Ni catalysts on an ordered $Ce_2Zr_2O_x$ solid-solution support (x = 7–8) with a regular arrangement of Ce and Zr ions for CH_4 steam reforming to produce H_2 and CO. The catalytic performance of the Ni/$Ce_2Zr_2O_x$ catalysts strongly depended on the oxygen content of $Ce_2Zr_2O_x$, and we found a unique discontinuity in the CH_4 steam-reforming activity at x = 7.5 (Figure 1).

Ni/$Ce_2Zr_2O_7$ catalyst was stable, resulting in a remarkably catalytic performance. The discontinuity in the catalytic performance at x = 7.5 may be related to the oxygen storage capacity of $Ce_2Zr_2O_x$. The reduction of NiO_y strongly depended on the nature of the $Ce_2Zr_2O_x$ support. In the range of $7 \leq x < 7.5$, Ni and $Ce_2Zr_2O_x$ were reduced to the metallic state and the $Ce_2Zr_2O_7$ phase, respectively, under the reaction conditions; the reduction was due to CH_4. In the range of $7.5 \leq x \leq 8$, however, NiO_y was converted to NiO and $Ce_2Zr_2O_x$ remained unchanged under the reaction conditions. The oxidation of Ni nanoparticles on $Ce_2Zr_2O_x$ ($7.5 \leq x \leq 8$) was due to H_2O.

The oxygen storage and release processes rapidly occur at $x < 7.5$ compared with $x \geq 7.5$. In the range of $7 \leq x < 7.5$, lattice oxygen atoms in $Ce_2Zr_2O_x$ readily migrate from the bulk to the surface, at which they react with CH_4 to form the resultant $Ce_2Zr_2O_7$ phase. The transport of oxygen atoms at the interface between NiO_y nanoparticles and a $Ce_2Zr_2O_x$ support and/or the spillover of oxygen atoms at the boundary may be key issues in the chemical event.

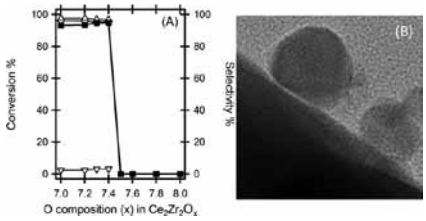

Figure 1. (A) CH_4 steam-reforming performance of Ni/$Ce_2Zr_2O_x$ at 973 K. The oxygen content x was changed by the reaction with O_2 and Ni/$Ce_2Zr_2O_7$ at 773 K ■ (with bold line): CH_4 conv.%, △: CO selectivity %, ▽: CO_2 selectivity %, and ◇: H_2 selectivity %. (B) A TEM image of the Ni catalyst.

2. Imaging of Pt/C Cathode Catalyst Layers in MEA for PEFC by X-Ray Laminography XAFS[2)]

Polymer electrolyte fuel cells (PEFCs) are among the most efficient clean energy technologies, but practical application in automobiles remains challenging because of the high cost and insufficient durability of cathode catalysts. The deactivation and unfavorable dissolution of Pt catalysts at cathode under PEFC operating conditions are serious to be tackled. However, direct observation of the chemical states of Pt catalysts in a membrane electrode assembly (MEA) for PEFC is not achieved in a non-destructive manner.

X-ray Computed Laminography (XCL) is applicable to partial three-dimensional imaging of such a shaped sample. In XCL, the rotation axis of a sample is not fixed at 90° with respect to incident X-ray beam, and the sample is inclined. We succeeded in measuring XCL-XAFS combining XCL imaging

technique and XAFS spectroscopy by changing the energies of incident X-rays for XCL. The reconstruction images of XCL-XAFS revealed not only the morphology of cathode catalyst layer but also the distribution of Pt catalysts inside the catalyst layer.

The spatio-distribution of the Pt catalysts was visualized by mapping Pt L_{III}-edge intensity, which corresponds to a difference in the intensity of X-ray absorption at 11.572 keV (isosbestic point of Pt and PtO_2) from that at 11.496 keV (before Pt L_{III}-edge). We reconstructed 3D images of the distributions of Pt nanoparticles in the cathode catalyst layer in the fresh and degraded MEAs. The distribution of the Pt catalyst remarkably changed after the degradation process of MEA, and several aggregation spots of the Pt catalyst and large cavities in the cathode catalyst layer were observed (Figure 2 (A)). The Pt distribution was heterogeneous throughout the entire cathode catalyst layer, which suggests that Pt migration, aggregation, and cracking spread throughout the cathode catalyst layer in the degraded MEA.

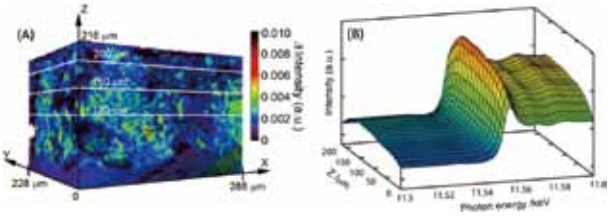

Figure 2. (A) The distribution of the Pt catalyst inside the cathode catalyst layer of the degraded MEA by XCL-XAFS. (B) Depth-resolved XCL-XANES spectra for the degraded MEA.

Depth-resolved XANES spectra were successfully obtained by integrating 3D-Laminography-XANES spectra over the X–Y plane at each depth in the X-ray energy range of 11.439–11.608 keV (Figure 2 (B)). Difference in the edge intensity of the Pt L_{III}-edge XANES spectra indicates difference in the Pt quantity in the MEAs along the *Z* depth. A series of depth-resolved Laminography-XANES spectra of the degraded MEA were wavy to the *Z* depth, probably reflecting the degradation of the MEA.

The newly developed XCL-XAFS technique provided the three-dimensional images of Pt quantity in the fresh and degraded MEAs enabled the visualization of aggregation behavior induced under PEFC operating processes. The 3D-Laminography-XAFS method would be promising for visualizing heterogeneous structural information in MEAs in order to address critical issues on the performance and property of practical PEFCs.

3. Ethynylpyridine-Functionalized Pt/Al_2O_3 Catalyst with Induced Chirality for Hexose Sugar Oxidation[3)]

Uronic acids are monosaccharide derivatives in which primary hydroxyl group at the terminal carbon is oxidized to a carboxylic acid. To prepare glucuronic acid, the hydroxyl group at the 6-position of glucose must be selectively oxidized without over-oxidizing the secondary alcohols at other positions. We prepared a heterogeneous Pt nanoparticle catalyst with a sugar-binding ethynylpyridine (EPy) site ($EPy/Pt/Al_2O_3$) for the selective oxidation of hexose sugars to their corresponding uronic acids. Compared with a non-EPy-functionalized Pt/Al_2O_3 catalyst, $EPy/Pt/Al_2O_3$ enhanced reaction rates for the selective oxidation of the 6-OH groups of hexose sugars.

Titration with octyl β-D-glucopyranoside monitored by UV/vis and CD spectroscopy revealed that EPy acted as a binding site for hexose sugar, resulting in a complex of the EPy moiety and the hexose sugar with induced chirality. When Oct-β-D-Glc was added, an induced CD (ICD) signal with negative Cotton effect was observed in the region of the EPy ligand absorption (Figure 3 (A)). An ICD signal with positive Cotton effect was also observed after the addition of the enantiomer, octyl β-L-glucopyranoside. The ICD signals of the EPy ligand on the $EPy/Pt/Al_2O_3$ catalyst surface depended on the chirality of the hexose sugars, which demonstrated that binding interaction between the EPy ligand and the hexose sugars existed on the catalyst surface (Figure 3 (B)). The positive binding of the hexose sugars to EPy through intermolecular host–guest interaction would be enhanced the reaction rates of the selective oxidation on the Pt nanoparticle catalyst.

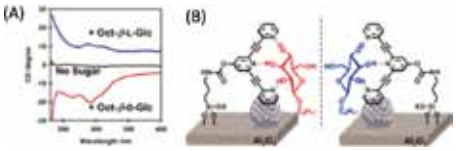

Figure 3. (A) CD spectra of the mixture of Pt/Al_2O_3 and octyl β-glucopyranoside in CH_2Cl_2. (B) The suggested host–guest interaction of EPy and the hexose sugar.

References

1) M. Tada, S. Zhang, S. Malwadkar, N. Ishiguro, J. Soga, Y. Nagai, K. Tezuka, H. Imoto, S. O. –Y. –Matsuo, S. Ohkoshi and Y. Iwasawa, *Angew. Chem., Int. Ed.* **51**. 9361–9365 (2012) (Hot Paper).
2) T. Saida, O. Sekizawa, N. Ishiguro, K. Uesugi, M. Hoshina, T. Uruga, S. Ohkoshi, T. Yokoyama and M. Tada, *Angew. Chem., Int. Ed.* **51**. 10311–10314 (2012).
3) M. Waki, S. Muratsugu and M. Tada, *Chem. Commun.* **49**. 7283–7285 (2013) (Inside Back Cover).

Award

KITYAKARN, Sutasinee; Poster Prize Award (ISHHC-16).

* Present Position; Professor, Research Center for Materials Science, Nagoya University
† Present Address; Graduate School of Science, Nagoya University
‡ carrying out graduate research on Cooperative Education Program of IMS with The University of Tokyo

Magnetic Resonance Studies for Functional Molecular-Based Solids

Department of Materials Molecular Science
Division of Electronic Properties

NAKAMURA, Toshikazu
Associate Professor

FURUKAWA, Ko
Assistant Professor*

TAKAHASHI, Seiya — Graduate Student†
ABE, Hitomi — Secretary

Magnetic resonance measurements are advantageous for studying fundamental electronic properties and for understanding the detailed electronic structures of molecular based compounds. Developing an understanding of the electronic phases and functionality of these materials enables us to perform systematic investigations of low-dimensional, highly-correlated electron systems and functional materials. Competition between the electronic phases in molecular-based conductors has attracted much attention. The investigations of such electronic phases by magnetic resonance measurements are important to understanding unsolved fundamental problems in the field of solid state physics, and to explore novel functionalities in the field of material science.

In this study, we performed broad-line NMR and ESR measurements on molecular-based conductors to understand electron spin dynamics and functionality in low-temperature electronic phases.

1. Time-Resolved ESR Spectroscopy Investigation of Photoconduction Mechanism in Covalent Organic Framework (COF) Materials

Covalent organic framework (COF) materials are porus crystalline materials. They attracted much attention because of their functionalities. Recently, a variety of COF materials based on the Donor-Acceptor (D-A) system have been developed. Jiang and coworkers synthesized a variety of D-A type COFs such as NDI-ZnPc, PyDI-ZnPC and ZnPc-NDI-HHTP. While molecules are connected by tight covalent bonds within the two-dimensional layers, the molecules stack to form one-dimensional columns perpendicular to the planes. They show pronounced photo-conducting behavior. The possible photo-conduction origin is the electron transfer between donor and acceptor. However, the detail mechanism is an open question. We performed time-resolved photo-excited ESR spectroscopy for a series of D-A type COF materials to investigate the photo-conduction mechanism. After photo-excitation to D-A type COFs, an ESR signal originated from the charge-separated state was observed, which could not be observed in isolated molecules. As for ZnPc-NDI-COF, we can observe the charge-separated ESR signal even at R.T., indicating long lifetime of the photo-excited carriers. Actually, the lifetime of the photo-excited charge-separated states in ZnPc-NDI-COF are estimated as 865 μs at 80 K and 1.8 μs at 280 K.

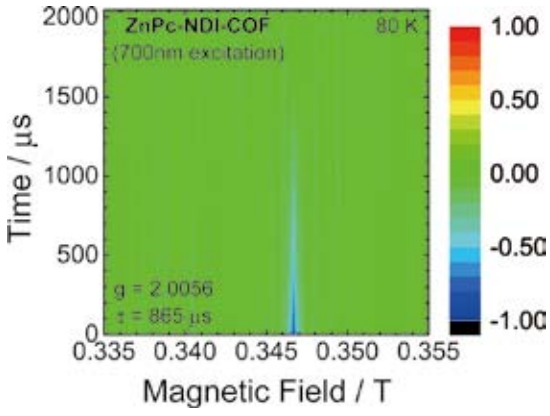

Figure 1. 2D pulsed TR-ESR spectra for ZnPc-NDI-COF. The normal axis represents the ESR signal intensity. The color scale denotes the signal intensity. Positive and negative values indicate the absorption and emission of microwaves, respectively.

2. Simultaneous Control of Carriers and Localized Spins with Light in Organic Materials

Photoconduction and its related phenomena have been known for quite some time, and have attracted a significant amount of scientific attention. Photoconduction is applied in devices, sensors, detectors, and energy converters, such as charge-coupled devices, complementary metal oxide-semiconductor image sensors, and photovoltaic cells, in addition to other advanced applications under investigation. In all known photoconductors, photoexcitation (PE) controls only the carriers. Herein, a new photoconductor is reported, in which the carriers and localized spins can be simultaneously controlled with UV irradiation. This material transforms from a semiconductor to a metal under irradiation, distinguishing it from all existing photoconductors. Furthermore, an interaction between the carriers and localized spins has been discovered, which enables the localized spins to be controlled and detected by the carriers and vice versa. In addition, the photoconduction is unique because it exhibits wavelength selectivity. The selectivity means that the photoconduction mechanism is different from currently known mechanism. No material has been found in which the carriers and localized spins can be simultaneously generated with light. If the carriers and localized spins are controlled using light (i.e., via PE), it may be possible to enhance this control over a wider range, beyond the restrictions of thermodynamic equilibrium. In order to find such a material, a promising starting point is to investigate charge-transfer salts consisting of a photochemical redox pair, because, under irradiation, the redox reaction transfers a larger number of electrons between pairs, and thus produces, by far, a larger number of carriers and localized spins than using PE alone. Following a series of examinations of a variety of charge-transfer salts, focus was placed on salts of $[Ni(dmit)_2]_n^-$ (dmit = 1,3-dithiol-2-thione-4,5-dithiolate; $0 \leq n \leq 2$) and methyl viologen (MV_n^+). $Ni(dmit)_2$ molecules are known to form conducting solids with multiredox properties, while the MV is expected to be a spin source under irradiation because of its characteristic photochemical redox reactivity. Herein, a strategy for realizing photomagneticconductors is proposed and demonstrated based on the electrical and magnetic properties of $MV[Ni(dmit)_2]_2$.

3. Organometallic Ionic Liquids from Alkyloctamethylferrocenium Cations: Thermal Properties, Crystal Structures, and Magnetic Properties

Alkyloctamethylferrocenium salts with the Tf_2N anion ($[Fe(C_5Me_4C_nH_{2n+1})(C_5Me_4H)][Tf_2N]$; Tf_2N = bis-(trifluoromethanesulfonyl)amide) were prepared, and their ionic liquid properties, thermal properties, crystal structures, and magnetic properties were investigated. The melting points of the Tf_2N salts were near room temperature, and decreased with increasing alkyl chain length up to $n = 8$ and then increased.

The salts with PF_6 and NO_3 anions were also prepared. The melting points of the PF_6 salts were higher than 100 °C. Most of these salts exhibited phase transitions in the solid state. The sum of the entropies of the melting and solid phase transitions was nearly independent of the alkyl chain length for salts with short alkyl chains, whereas those for salts with longer alkyl chains ($n \geq 10$ for Tf_2N salts, $n \geq 6$ for PF_6 salts) increased with increasing alkyl chain length. Crystal structure determinations revealed that the short chain salts form simple alternately packed structures of cations and anions in the solid state, and that the long chain salts form lamellar structures, in which the alkyl chains are aligned parallel between the layers. The effects of magnetic fields on the crystallization of the paramagnetic ionic liquids were investigated, and revealed that the Tf_2N salts with $n = 4$ exhibited magnetic orientation when solidified under magnetic fields. The magnetic orientation was shown to be a bulk phenomenon, and the importance of the magnetic anisotropy of the crystal structure was suggested in comparison with the response of other Tf_2N salts.

4. Magnetic Resonance Investigation of Self-Doped Type TTFCOO and TTPCOO Family Salts

^{1}H-NMR and High-Field ESR measurements were carried out for self-doped type organic conductor, TTFCOO and TTPCOO derivatives. We found the conducting electrons both for TTFCOO and TTPCOO derivatives. But the spin susceptibility shows significant activation-type contribution and the ^{1}H-NMR spin-lattice relaxation rate, $^1H\text{-}T_1^{-1}$, shows a 1D electron spin-diffusion type relaxation for TTFCOO derivative. On the other hand, TTPCOO derivative shows metallic behavior down to the lowest temperatures. Detailed comparison between TTFCOO and TTPCOO salts is investigated.

References

1) S. Jin, X. Ding, X. Feng, M. Supur, K. Furukawa, S. Takahashi, M. Addicoat, M. E. El-Khouly, T. Nakamura, S. Irle, S. Fukuzumi, A. Nagai and D. Jiang, *Angew. Chem., Int. Ed.* **52**, 2017–2021 (2013).

2) T. Naito, T. Karasudani, K. Ohara, T. Takano, Y. Takahashi, T. Inabe, K. Furukawa and T. Nakamura, *Adv. Mater.* **24**, 6153–6157 (2012).

3) Y. Funasako, T. Inagaki, T. Mochida, T. Sakurai, H. Ohta, K. Furukawa and T. Nakamura, *Dalton Trans.* **42**, 8317–8327 (2013).

Award

FURUKAWA, Ko; SEST Young Investigator Award (2012).

* Present Address; Institute for Research Promotion Center for Instrumental Analysis, Niigata University

† carrying out graduate research on Cooperative Education Program of IMS with Yokohama National University

Organic Solar Cells

Department of Materials Molecular Science
Division of Molecular Functions

KAJI, Toshihiko
Assistant Professor

HIRAMOTO, Masahiro
Professor

NAKAO, Satoru	Post-Doctoral Fellow	YOKOYAMA, Kazuya	Research Fellow
SHINMURA, Yusuke	Research Fellow	YOSHIOKA, Tadashi	Research Fellow
KUBO, Masayuki	Research Fellow	KIKUCHI, Mitsuru	Research Fellow
		YAMASHINA, Yohei	Research Fellow
		ISHIYAMA, Norihiro	Graduate Student
		SUGIHARA, Hidemi	Secretary

Organic solar cell (OSC) is recognized as a next generation solar cell. *pn*-control and nanostructure control of co-deposited films consisting two kinds of organic semiconductors are key issues for the development of OSC. Recently, we have established *pn*-control technique for single and co-deposited films of organic semiconductors.[1–3] Moreover, we have developed a new method for producing phase-separated co-deposited films by introducing a co-evaporant molecules, which improves the carrier transport in the co-deposited film.[4]

Here, we show the recent results on co-evaporant effect (Topic-1) and combination of doping and co-evaporant (Topic-2).

1. Nano-Structure Control of Organic Thin Films by Co-Evaporant Induced Crystallization

Nano-structure control of organic thin films is important for fabricating high performance organic electronic devices, such as organic transistors and OSCs. Especially, needle growths of organic semiconductors sometimes roughen their film surface and the electronic devices composed of such films lose their robustness. Recently, we have proposed a new method of organic film growth, "co-evaporant induced crystallization," and succeeded in crystallizing donor–acceptor blends, the key part of OSCs, based on small molecules by using a liquid as a non-sticking co-evaporant source during vacuum deposition of the blend film and showed striking enhancements of photocurrent. In this study, this new method is utilized for controlling the needle growth of metal-free phthalocyanine (H_2Pc) thin films. Nominally 200 nm of H_2Pc films were grown on indium tin oxide (ITO) coated glass substrates with substrate heating of 70 and 40 °C. The morphologies were observed by using scanning electron microscopy (SEM), and the crystallinities were confirmed by X-ray diffraction (XRD). Figure 1 shows SEM images of H_2Pc thin films grown at the substrate temperature of 40 °C with and without a co-evaporant, PDMS (polydimethylsiloxane). Similar lengths of H_2Pc needles are observed in the both films with/without co-evaporant. From grain size comparison, in contrast, the effect of the co-evaporant is clearly noticed as the grain size enlargement typically from 20 to 50 nm. This difference implies that the co-evaporant itself does not induce the needle growth, and that the needle growth is caused by the substrate heating, which is conventionally known effective for the crystallization of organic thin films. These results suggest that the co-evaporant enhances rather 2-dimensional-growth than 3-dimensional-growth of organic films.

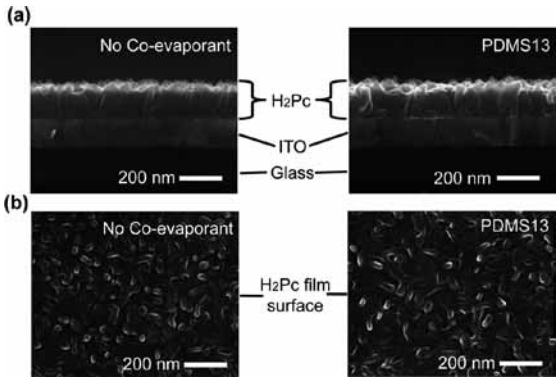

Figure 1. SEM images of 200-nm-thick H_2Pc film grown at 40 °C without co-evaporant/with PDMS. (a) Cross-sections. (b) Film surfaces.

2. *pn*-Homojunction Organic Solar Cells Formed in Phase-Separated Co-Deposited Films

Since the conductivity (σ) is the product of the mobility (μ) and the carrier concentration (n), *i.e.*, $\sigma = en\mu$, the resist-

ance (σ^{-1}) can be reduced by increasing both n, by means of doping, and μ, by means of co-evaporant introduction. Simultaneous control of the doping and phase-separation in co-deposited films was performed by using 4-sources co-evaporation consisting of H_2Pc, C_{60}, dopants, and co-evaporant (PDMS).

Figure 2 shows the energy diagram for the phase-separated H_2Pc:C_{60} co-deposited films. For donor (Cs_2CO_3) doping, Fermi level (E_F) has shifted from the undoped value of 4.48 eV to 4.22 eV (green broken line, left) and is close to the C_{60} conduction band (CB_{C60}). In contrast, for acceptor (V_2O_5) doping, E_F has shifted to 4.95 eV (green broken line, right) and is close to the H_2Pc valence band (VB_{H2Pc}). Clearly, the *pn*-control in the phase-separated co-deposited films were accomplished. Moreover, the shift in E_F is revealed to occur within the "bandgap of the co-deposited film."

The doping was used to form *pn*-homojunctions in the phase-separated co-deposited films (Figure 3). In order to determine the precise extent of the photoactive layer beyond the depletion layer (Figure 4, blue shaded area), the J_{SC} for various *p*-type layer thickness (X) was calculated with the carrier generation efficiency following Gaussian profiles (Figure 3). Clearly, the curve with σ = 250 nm (green curve) agrees well with the observed short-circuit photocurrent (J_{SC}) (black dots), indicating that the photoactive layer extends 250 nm from the edge of the depletion layer.

This result means that the diffusion length of the minority carrier (electrons) reached extremely large value of 0.25 μm. Thus, photogenerated electrons far from the *pn*-homojunction can reach the edge of the depletion region and be collected by the Ag electrode. Large minority carrier diffusion length is due to the large electron mobility (μ = 0.1 $cm^2V^{-1}s^{-1}$). On the other hand, a high hole concentration ($n = 1 \times 10^{17}$ cm^{-3}) in the *p*-type C_{60}:H_2Pc film ensures hole extraction by the ITO electrode. This allows the fabrication of very thick cells up to 0.5 μm thick with large values of fill factor (FF) of around 0.56.

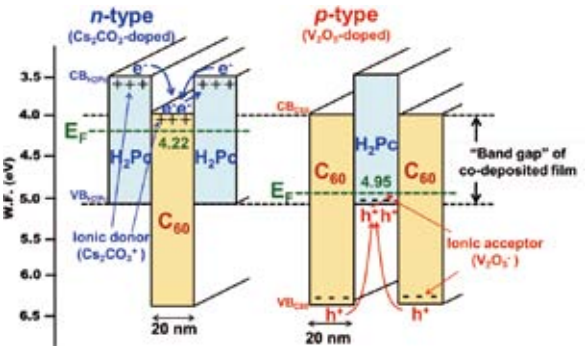

Figure 2. Phase-separated energy structure of C_{60}:H_2Pc co-deposited film doped with Cs_2CO_3-doped (*n*-type) and V_2O_5-doped (*p*-type) films.

The present cell is the first example of organic solar cell utilizing long minority carrier diffusion length like inorganic Si solar cells.

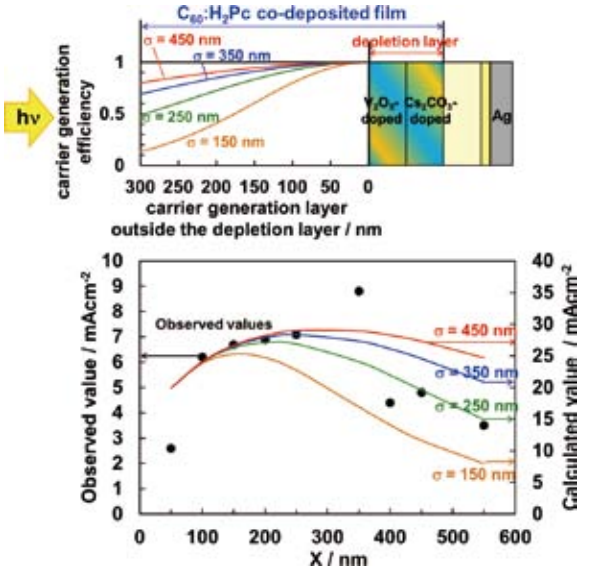

Figure 3. Dependence of calculated J_{SC} (solid lines) and observed J_{SC} (black dots) on *p*-layer thickness (X). Gaussian profiles of minority carriers outside the depletion layer are also shown.

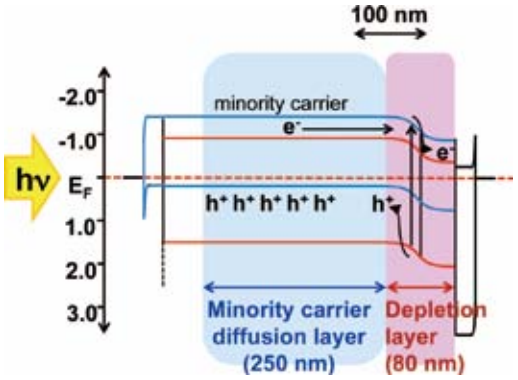

Figure 4. Energy structure of the cell. The depletion and minority carrier diffusion regions are indicated by the red and blue shaded areas, respectively.

References

1) M. Kubo, K. Iketaki, T. Kaji and M. Hiramoto, *Appl. Phys. Lett.* **98**, 073311 (2011).
2) Y. Shinmura, M. Kubo, N. Ishiyama, T. Kaji and M. Hiramoto, *AIP Adv.* **2**, 032145 (2012).
3) N. Ishiyama, M. Kubo, T. Kaji and M. Hiramoto, *Org. Electron.* **14**, 1793 (2013).
4) T. Kaji, M. Zhang, S. Nakao, K. Iketaki, K. Yokoyama, C. W. Tang and M. Hiramoto, *Adv. Mater.* **23**, 3320 (2011).

Award

KAJI, Toshihiko; Young Scientist Research Paper Award from Molecular Electronics and Bioelectronics division of Japan Society of Applied Physics (2013).

Two-Dimensional Polymers and Covalent Organic Frameworks

Department of Materials Molecular Science
Division of Molecular Functions

JIANG, Donglin
Associate Professor

NAGAI, Atsushi
Assistant Professor

GU, Cheng	IMS Fellow
DALAPATI, Sasanka	IMS Fellow
XU, Yan	Post-Doctoral Fellow
NI, Huagang	Visiting Scientist
JIN, Shangbin	Graduate Student
CHEN, Xiong	Graduate Student
CHEN, Long	Graduate Student
XU, Hong	Graduate Student
WU, Yang	Graduate Student
XU, Fei	Graduate Student
HUANG, Ning	Graduate Student
SUZUKI, Hiroko	Secretary
HAMADA, MASAKO	Secretary

Two-dimensional polymers and their layered frameworks (covalent organic frameworks: COFs) are a class of crystalline porous materials that allow an atomically precise integration of components into a 2D or 3D periodicity. The recent synthetic progress has shown that 2D COFs are useful platform for designing conducting, where 2D polymer sheets are organized in a superimposed way to generate a layered architecture that provides periodic π pathways for charge-carrier transport.[1–7]

We pioneered the design and synthesis of COFs by integrating π-electronic units into the 2D polygon skeletons. In this year, we focus on our challenge for the molecular design of donor–acceptor COFs with periodically ordered electron donor–acceptor π-columnar structure and maximized bicontinuously segregated p-n interface, which provide a new molecular configuration and mechanism for optoelectronics and photovoltaics.

1. Charge Dynamics in 2D Polymers and COFs

The donor–acceptor heterojunction is a key structure in current technologies, including transistors, light-emitting diodes, and photovoltaics, because it controls the charge dynamics in the devices. Covalent organic frameworks (COFs) are crystalline molecular skeletons that allow atomically precise integration of building blocks into periodic array structures. In this regard, we have demonstrated arene, porphyrin, and phthalocyanine COFs that provide periodically ordered columnar arrays of π-components and show outstanding semiconducting and photoconductive properties. We recently synthesized a donor–acceptor COF that gives rise to a periodically ordered bicontinuous heterojunction structure. This heterojunction structure provides ambipolar pathways for charge collection, and would be ideal for the current semiconducting devices that involve photoenergy transformations; however, the charge dynamics, which is a key mechanism that controls the energy transformation, remains unclear.

We determined the charge dynamics of a donor–acceptor COF using time-resolved spectroscopy. In the COF, the heterojunctions allow an ultrafast electron transfer from the donor to the acceptor columns. The light absorption is directly coupled with charge dissociation to generate free charges in the donor and acceptor π-columns within 2 ps. The stacked π-columns delocalize the charges, suppress charge recombination, and retain the charges for a prolonged period of time. The COFs enable rapid charge separation and exceptional long-term charge retention, thereby providing a key mechanistic basis to envisage the high potential of donor–acceptor COFs for photoelectric applications.

To clarify the charge dynamics in the solid-state COFs, we performed time-resolved electron-spin resonance (TR-ESR) spectroscopy. Before the 700-nm laser flash, the TR-ESR was silent over the entire magnetic field range. After the laser flash, the TR-ESR signal rapidly increased in intensity as a result of a very rapid charge separation. The TR-ESR signal exhibited an increase up to t = 1.5 μs and then decayed slowly. Therefore, we monitored the TR-ESR spectra at t = 1.5 μs as a function of the magnetic field and obtained a time-slice profile, which can be reproduced with a single emission-type Lorentzian with a g value of 2.0059 and a narrow spectral width of 0.75 mT. The g value of 2.0059 confirms the forma-

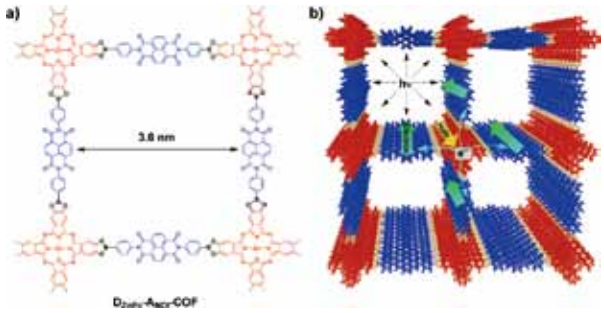

Figure 1. a) Structural representation of a donor–acceptor COF (D_{ZnPc}-A_{NDI}-COF). Donor and acceptor units are shown in red and blue, respectively. The dotted black lines suggest the extension of periodic structures. b) Illustration of a 2 × 2 cell of the 0.8-Å slipped AA-stacking COF and photochemical events.

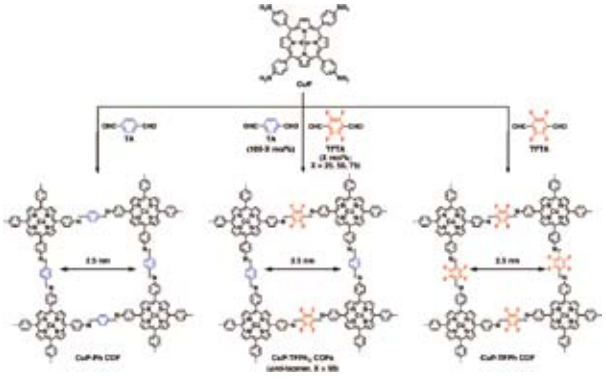

Figure 2. Schematic representation of the synthesis of COFs integrated with self-complementary π-electronic interactions (CuP-TFPhX COFs, X = 25, 50, and 75) and the CuP-Ph COF and CuP-TFPh COF controls.

tion of $ZnPc^{\bullet+}$ and $NDI^{\bullet-}$ species. The narrow spectral width of the COF is consistent with a weak magnetic dipolar interaction between two spins because they are spatially separated and delocalize in the donor and acceptor columns. The TR-ESR measurements at 80 K also confirmed the charge-separated state, as evidenced by a single emission-type Lorentzian profile with the same *g* value of 2.0059. Through curve-fitting of the time profiles to an exponential function given by $\Phi = \alpha\exp[-t/\tau_{CS}]$, where α, *t*, and τ_{CS} are the proportional factor, time, and lifetime, respectively, the τ_{CS} values of the solid-state COFs at 280 K was determined to be 1.8 μs.

These dynamics provide mechanistic insights into the key photochemical processes involved in optoelectronics and photoenergy conversion systems and suggest that the donor–acceptor COFs are promising high-performance semiconducting materials for use in applications.

2. Control Crystallinity and Porosity of Covalent Organic Frameworks through Managing Interlayer Interactions Based on Self-Complementary π-Electronic Force

COFs provide a useful skeleton for designing a new sort of organic semiconductors that feature columnar π-arrays periodically aligned at a nanometer-scale precision.[3,6] In this sense, the 2D COFs serve as a new platform for designing organic 2D materials with structural periodicity that is difficult to be achieved with other molecular architectures. However, controls over the crystallinity and porosity, which are key parameters in the applications, have been elusive.

We demonstrated the strategy using imine-linked porphyrin COFs, in which fluoro-substituted and non-substituted arenes at different molar ratios were integrated into the edge units (Figure 2). The porphyrins occupy the vertices and the arene units locate the edges of mesoporous two-dimensional COFs.

We demonstrated the control of COFs using self-complementary π-electronic interactions. Computational studies in conjunction with structural resolutions reveal that the self-complementary π-electronic force maximizes the total crystal stacking energy and minimizes the unit cell size. As a result, the COFs show an improved crystallinity and enhanced porosity, with the greatest effects observed when the interactions are strongest. Together with a prominent effect on changing the π-cloud distribution in the framework and lowering the HOMO-LUMO gap, the present work suggests a new means to designing COFs through managing the interlayer interactions.

References

1) Y. Xu, S. Jin, H. Xu, A. Nagai and D. Jiang, *Chem. Soc. Rev.* **42**, 8012–8031 (2013) (Cover Page).
2) X. Liu, Y. Xu, Z. Guo, A. Nagai and D. Jiang, *Chem. Commun.* **49**, 3233–3235 (2013).
3) A. Nagai, X. Chen, X. Feng, X. Ding, Z. Guo and D. Jiang, *Angew. Chem., Int. Ed.* **52**, 3770–3774 (2013) (Hot Paper).
4) S. Jin, X. Ding, X. Feng, M. Supur, K. Furukawa, S. Takahashi, M. Addicoat, M. E. El-Khouly, T. Nakamura, S. Irle, S. Fukuzumi, A. Nagai and D. Jiang, *Angew. Chem., Int. Ed.* **52**, 2017–2021 (2013) (Inside Cover).
5) X. Chen, M. Addicoat, S. Irle, A. Nagai and D. Jiang, *J. Am. Chem. Soc.* **135**, 546–549 (2013).
6) Y. Xu, A. Nagai and D. Jiang, *Chem. Commun.* **49**, 1591–1593 (2013) (Inside Cover).
7) X. Feng, Y. Dong and D. Jiang, *CrystEngComm.* **15**, 1508–1511 (2013).

Award

JIN, Shangbin; CSJ presentation Award.

Solid State NMR for Molecular Science

Department of Materials Molecular Science
Division of Molecular Functions

NISHIMURA, Katsuyuki
Associate Professor

IIJIMA, Takahiro
Assistant Professor

TANIO, Michikazu
IMS Research Assistant Professor

We are working on methodology and hardware developments of solid state NMR and structural biology and materials science. In the following, we show studies of peripheral membrane proteins and inorganic compounds based on NMR.

1. NMR Analysis of Intramolecular Allostery in the Phosopholipase C-δ1 Pleckstrin Homology Domain

Proteins are generally activated by interactions with ligands, such as proteins, lipids, peptides, nucleotides, ions, photons, odorants, or other chemical compounds. Ligand binding usually induces changes in the protein conformation and dynamics, which also occur at distal sites away from the ligand-binding site in the protein molecule through intramolecular signal transductions, causing allosteric regulation of protein functions. Although elucidation of allosteric mechanisms is expected to be useful for regulations of protein functions and for allosteric drug designs, the detailed molecular mechanisms remain unclear.

Our previous study suggested the existence of intramolecular allosteric interactions in the phospholipase C (PLC)-δ1 pleckstrin homology (PH) domain.[1)] The PLC-δ1 PH domain binds to phosphatidylinositol 4,5-bisphosphate (PIP_2) in the cell membrane, and inositol 1,4,5-triphosphate (IP_3), a product of PIP_2 hydrolysis by PLC-δ1. Mutational analyses of the PLC-δ1 PH domain demonstrated that conformational disruption of the characteristic short α-helix (α2) from residues 82 to 87 results in reduced affinity for IP_3 and in thermal instability, and that the phenyl ring of Phe-87 contributes to effective stabilization of the IP_3-binding state.[1)] However, the α2-helix does not make direct contact with IP_3 in the crystal structure of the PLC-δ1 PH domain complexed with IP_3, and our findings therefore indicate that the α2-helix indirectly interacts with the IP_3-binding site through intramolecular allosteric interactions. In this study, we investigated the detailed molecular mechanisms of intramolecular allosteric interactions among spatially separated sites in the PLC-δ1 PH domain by using NMR.[2)]

To detect the local environmental changes in the protein induced by ligand binding and site-specific mutations, we analyzed the ^{1}H-^{15}N HSQC NMR spectra of selectively [α-^{15}N]Lys-labeled PLC-δ1 PH domain and its mutants in the presence and absence of IP_3. In the wild-type protein, IP_3-dependent chemical shift changes were observed for all lysine signals, indicating that IP_3 binding affects the local environments at all lysine residues. Chemical shift perturbation (CSP) analyses for the wild-type protein demonstrated that more

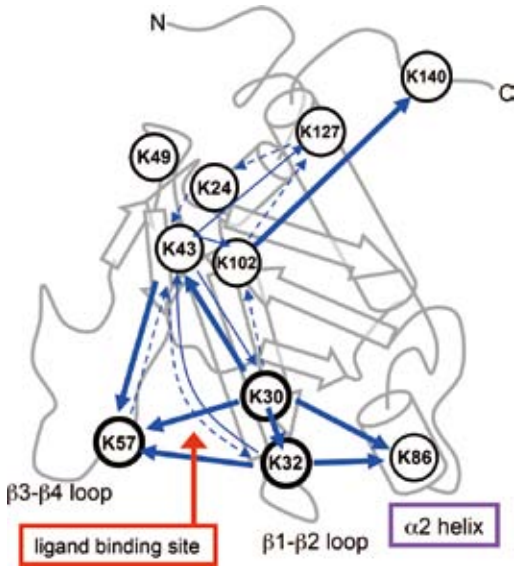

Figure 1. Graphical summary of the mutational effects on the PLC-δ1 PH domain. The bold, thin and dashed blue arrows indicate directions from mutated residues to affected residues with major, medium and minor CSP changes, respectively.

marked changes of chemical shifts were observed for Lys-43, Lys-102, and Lys-127, of which the α-nitrogen atoms are located far from the IP_3-binding site consisting of Lys-30, Lys-32, and Lys-57, suggesting that more drastic changes occurs at these distal sites on IP_3 binding.

If specific IP_3 binding induces local environmental changes at distal sites, mutations at the ligand-binding site would also affect local environments at spatially separated sites in the PLC-δ1 PH domain. The mutational analyses for signal assignments demonstrated that the single lysine mutants, K30A, K32A, K43A and K102A, showed significant chemical shift changes of at least two signals with drastic CSP changes as compared with the lysine chemical shifts of the wild-type protein under the ligand-free state. The effects of single lysine mutations on the other lysine residues are graphically summarized in Figure 1. These results indicate that an interaction network mainly consisting of the side chains of Lys-30, Lys-32, and Lys-43, but not Lys-57 or Lys-86, exists in the ligand-free protein.

The IP_3 titration experiment of the wild-type protein also demonstrated that in the ligand-free state, the α2-helix undergoes intermediate chemical exchange between at least two conformations with different population, and that IP_3 binding stabilizes one of the two conformations.[2] Interestingly, such stabilization of the α2-helix (Lys-86) induced by IP_3 binding was also observed in F87Y, but not in K57A or F87A (Figure 2) , indicating that the side chains of Lys-57 and Phe-87 contribute to stabilization of the IP_3-binding state, although Lys-57 does not contribute to the interaction network in the ligand-free state. Our results therefore strongly suggested that the pre-existing interaction network, mainly consisting of Lys-30, Lys-32 and Lys-43, in the ligand-free state is modified by IP_3 binding, resulting in formation of a new interaction network, in which Lys-57 and Phe-87 contribute to stabilization of IP_3-binding state.[2]

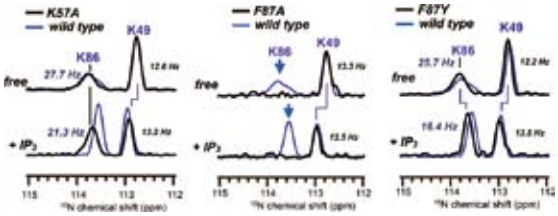

Figure 2. ^{15}N projections around the Lys-86 signal of the ^{1}H-^{15}N HSQC NMR spectra of [α-^{15}N]labeled K57A (left), F87A (middle) and F87Y (right) in the absence (top) and presence of IP_3 (bottom) as compared with those of the wild-type protein (blue).

2. A DFT Study of Electron Absorption of Polyoxomolybdates with d^1 Electrons

Among molybdenum with an integer valence from Mo^0 to Mo^{VI}, many Mo^V species are included in polyoxomolybdates of ε-Keggin anions and nano-sized oxides with characteristic shape. Localization of d^1 electrons of the Mo^V species has attracted much attention in terms of molecular design and solid state physics. Recently, we have found from solid-state ^{95}Mo NMR and DFT calculation that for $\{Mo_{12}(La)\}$ ($[PMo_{12}O_{36}(OH)_4\{La(H_2O)_{2.75}Cl_{1.25}\}_4]\cdot 27H_2O$) having eight d^1 electrons in a molecule, (i) there are two different molybdenum sites with population of 2:1 and (ii) they are basically corresponding to the species of Mo^V and Mo^{VI}, but some of the d^1 electrons are delocalized. This is a somewhat surprising result, because no intervalence charge-transfer bands for Mo^V to Mo^{VI} have been observed so far. In this work, we calculated electron absorption spectra of some polyoxomolybdates including $\{Mo_{12}(La)\}$ by DFT.

DFT calculation of the absorption spectra was implemented by the ADF2013.01 software. The local density approximation of VWM augmented with the Becke-Perdew GGA was employed for the exchange-correlation functional. The TZ2P or DZ all-electron basis set was used. Only allowed transitions were used for calculation of the absorption spectra.

Figure 3 shows the electron absorption spectra of polyoxomolybdates in the range of wavelength 400–1,400 nm obtained by DFT. Figure 3(i) is the spectrum of $\{Mo_{16}\}$ ($[Me_3NH]_6[H_2Mo^V_{12}O_{28}(OH)_{12}(Mo^{VI}O_3)_4]\cdot 2H_2O$), where twelve d^1 electrons are localized to form six Mo^V–Mo^V bonds of the ε-Keggin core. The relatively strong peak is only at around 430 nm that explains the brown color of this crystal. The weak peaks at ca. 590 and 655 nm are due to the d–d transition of the d^1 electrons of Mo^V. Figure 3(ii) shows the electron absorption spectrum of $\{Mo_{12}(La)\}$. It is found that the number of the peak increased both in the visible-light and near-infrared regions for $\{Mo_{12}(La)\}$. However, the absorption with short-wavelength visible light is consistent with the bark color of the crystal. Also, the intensity of the increased d–d transitions with wavelength of the near-infrared region would be not enough for the electron transition to be observed. Therefore, the slight delocalization of the d^1 electrons of $\{Mo_{12}(La)\}$ seems to be plausible.

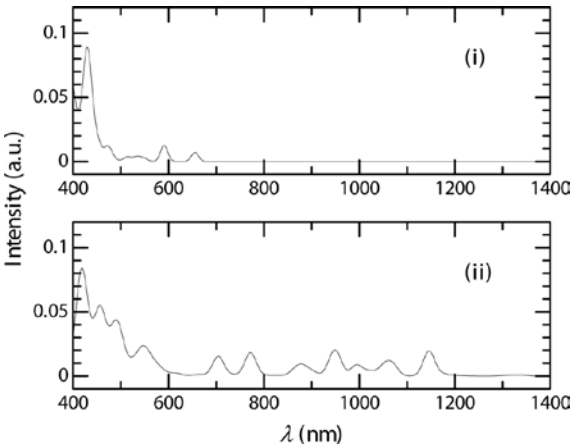

Figure 3. Electron absorption spectra for the polyoxomolybdates of (i) $\{Mo_{16}\}$ and (ii) $\{Mo_{12}(La)\}$ obtained by DFT calculation.

References

1) M. Tanio and K. Nishimura, *Anal. Biochem.* **431**, 106–114 (2012).
2) M. Tanio and K. Nishimura, *Biochim. Biophys. Acta* **1834**, 1034–1043 (2013).

Development of Novel Heterocyclic Compounds and Their Molecular Assemblies for Advanced Materials

Safety Office

TOMURA, Masaaki
Assistant Professor

Heterocycles containing sulfur and/or nitrogen atoms are useful as components of functional organic materials since heteroatoms in their rings are helpful to stabilize ions or ion-radical species. In addition, intermolecular interactions caused by heteroatom contacts can be expected to form unique molecular assemblies. In this project, novel functional organic materials based on various heterocycles were synthesized and their physical and structural properties were investigated.

1. Molecular and Crystal Structure of Cyananilic Acid Dihydrate

Cyananilic acid shows both electron accepting and proton donating properties. Supramolecular synthons formed with cyananilic acid have been used for constructing a variety of molecular networks. A molecular and crystal structure of cyananilic acid was reported as its hexahydrate derivative in 1975.[1)] We have found a novel hydrate isomer of cyananilic acid, dihydrate derivative. Cyananilic acid dihydrate crystallizes in the triclinic $P\bar{1}$ space group with one molecule in the unit cell. Cell parameters are a = 4.940(6) Å, b = 7.064(8) Å, c = 7.404(8) Å, α = 109.20(2)°, β = 94.73(1)°, γ = 102.27(1)° and V = 235.2(5) Å^3. The cyananilate dianion molecule is planar with an r.m.s. deviation of 0.011(2) Å and is located on an inversion center. The cyananilate molecules are linked via the oxonium ions with intermolecular O–H···O and O–H···N interactions.

Reference

1) E. K. Anderson and I. G. K. Anderson, *Acta Crystallogr., Sect. B* **31**, 379–383 (1975).

Multifunction Integrated Macromolecules for Molecular-Scale Electronics

Safety Office

TANAKA, Shoji
Assistant Professor

Recently a single electron tunnel device (**SET**) has attracted much attention. In this project, to establish an innovative fabrication process for **SET** systems, we have been developing stepwise synthetic protocols for mono-molecular single-electron tunnel devices (**MOSET**) and their integrated circuits.

1. Upgrade of Building Blocks toward Higher Integration of Single-Electron Tunnel Devices

We have developed a generally applicable stepwise synthetic protocol for basic mono-molecular single-electron tunnel devices starting with our versatile building blocks (**1-4**) (Figure 1(a-b)). In order to advance to the next stage of nanofabrication, we have prepared a new set of molecular building blocks (**5-16**) in view of recent progress in cross coupling reactions of C–Cl and C–H bonds of heterocycles. The end points of these molecular blocks have significantly different reactivity for metal-catalyzed coupling reactions. Thus, a selective and stepwise cross coupling will lead to more complicated macromolecular systems. Now we have been developing the synthetic protocols for mono-molecular integrated circuits such as single electron memory and counter, using these building blocks **1-16** (Figure 1(b)).

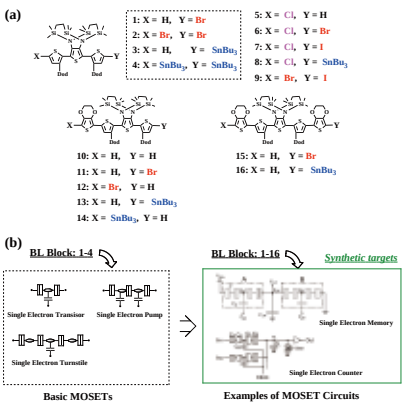

Figure 1. (a) Molecular structure of building blocks. (b) A strategy for mono-molecular MOSETs integration.

Visiting Professors

Visiting Professor
ASAKURA, Tetsuo *(from Tokyo University of Agriculture and Technology)*

Determination of Molecular Structure with Ultra Fast MAS under High-Field NMR

In single crystal X-ray diffraction analyses of peptides and proteins, it is well-known that the co-ordinates of carbon, nitrogen and oxygen atoms can be obtained in high accuracy, but enough accuracy cannot be obtained for those of hydrogen. Therefore we are trying to determine the accurate ^{1}H positions by the combination of NMR observation by ultra fast magic angle spinning under high field magnetic field and accurate ^{1}H NMR chemical shift calculation. We are applying this novel analytical technique to determine the structures of silk fibroins before and after spinning together with their model peptides. Since such a ^{1}H information is sensitive to both the intra- and inter -molecular structures, it is especially useful in molecular design of biomaterials with silks.

Visiting Professor
TAKENOBU, Taishi *(from Waseda University)*

Electronic Phase Control of Molecular Materials by Electric Double Layer Transistors

Charge carrier control is one of the key issues in the development of solid state physics and novel functional devices. Beyond the simple enhancement of conductivity, high charge carrier accumulation can realize various phenomena, such as phase transition, magnetic ordering, and superconductivity. Electric double layers, formed at solid/electrolyte interfaces, induce extremely large electric fields, huge specific capacitance and high charge carrier accumulation, and, as the results, this method opens new route for novel functionalities. Because molecular materials have large variety of electronic and magnetic properties, we are trying the combination of molecular solid and electric double layer transistors to discover novel phase transitions and functional devices.

Visiting Associate Professor
KANEMOTO, Katsuichi *(from Osaka City University)*

Optical and ESR Characterizations of Organic Semiconductor Devices

π-conjugated molecules and polymers have been the subject of much interest due to their potential device applications such as LEDs, solar cells, and field-effect transistors. Their remarkable electronic properties are owing to excitons and carriers created by photoexcitation or bias impression. The main purpose of our research is to characterize the determinant roles of the excitons and carriers on the device operation, through *in situ* optical and ESR measurements for operating organic devices. Recently, we found that a transient current is induced at the moment of ESR in polymer diodes under photoirradiation. The transient current was compatible with a steady-state photocurrent and found to arise from a change of polarization induced by ESR.

RESEARCH ACTIVITIES

Life and Coordination-Complex Molecular Science

Department of Life and Coordination-Complex Molecular Science is composed of two divisions of biomolecular science, two divisions of coordination-complex molecular science, and one adjunct division. Biomolecular science divisions cover the studies on functions, dynamic structures, and mechanisms for various biomolecules such as sensor proteins, membrane-anchored proteins, biological-clock proteins, metalloproteins, glycoconjugates, and molecular chaperone. Coordination complex divisions aim to develop molecular catalysts and functional metal complexes for transformation of organic molecules, water oxidation and reduction, and molecular materials such as molecular wires. Interdisciplinary alliances in this department aim to create new basic concepts for the molecular and energy conversion through the fundamental science conducted at each division. Professor Kunihiro Kuwajima was retired at the end of March, 2013. Professors Shuji Akiyama and Tetsuro Murahashi (Division of Biomolecular Sensing and the Division of Functional Coordination Chemistry, respectively) have moved to the Research Center of Integrative Molecular Systems in April 2013, who have been contributing this department under concurrent appointments.

Bioinorganic Chemistry of Metal-Containing Sensor Proteins

Department of Life and Coordination-Complex Molecular Science
Division of Biomolecular Functions

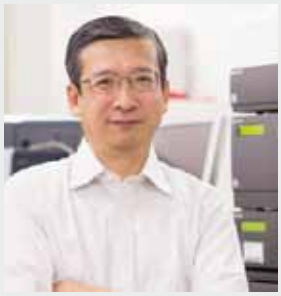

AONO, Shigetoshi
Professor

YOSHIOKA, Shiro
Assistant Professor

SAWAI, Hitomi
IMS Research Assistant Professor*

MURAKI, Norifumi
IMS Research Assistant Professor

KITATSUJI, Chihiro	Post-Doctoral Fellow
OKAMOTO, Yasunori	Graduate Student†
TANIZAWA, Misako	Secretary

The widely studied biological function of heme is to act as a prosthetic group in hemeproteins that show a variety of functions, including oxygen storage and transport, electron transfer, redox catalysis, and sensing of gas molecules. Besides acting as a prosthetic group in a protein matrix, it has become apparent that free heme molecules can act as physiological effectors of several proteins, including transcriptional regulators, heme-regulated eIF2α kinase, and sensor kinases in two-component signal transduction systems. Reversible heme binding regulates the physiological function of these proteins. Though research on these proteins has shown new physiological functions of heme as a signaling molecule, the detailed molecular mechanisms by which heme regulates the functions of these proteins remain to be elucidated, mainly because the three-dimensional structures of these regulatory proteins have not yet been solved. Our research interests are focused on the elucidation of the molecular mechanisms of how heme molecule acts as a signaling molecule. We are also studying about the structure–function relationships of the heme-based gas sensor proteins.

1. Structural Basis for the Transcriptional Regulation of Heme Homeostasis in *Lactococcus lactis*[1)]

Though heme is a crucial element for many biological processes including respiration, heme homeostasis should be regulated strictly due to the cytotoxicity of free heme molecules. Numerous lactic acid bacteria, including *Lactococcus lactis*, acquire heme molecules exogenously to establish an aerobic respiratory chain. A heme efflux system plays an important role for heme homeostasis to avoid cytotoxicity of acquired free heme, but its regulatory mechanism is not clear. Here, we report that the transcriptional regulator HrtR senses and binds a heme molecule as its physiological effector to regulate the expression of the heme-efflux system responsible for heme homeostasis in *L. lactis*. To elucidate the molecular mechanisms of how HrtR senses a heme molecule and regulates gene expression for the heme efflux system, we determined the crystal structures of the apo-HrtR/DNA complex, apo-HrtR, and holo-HrtR at a resolution of 2.0, 3.1, and 1.9 Å, respectively. These structures revealed that HrtR is a member of TetR family of transcriptional regulators. The residue pair Arg46 and Tyr50 plays a crucial role for specific DNA-binding through hydrogen-bonding and a CH–π interaction with the DNA bases (Figure 1).

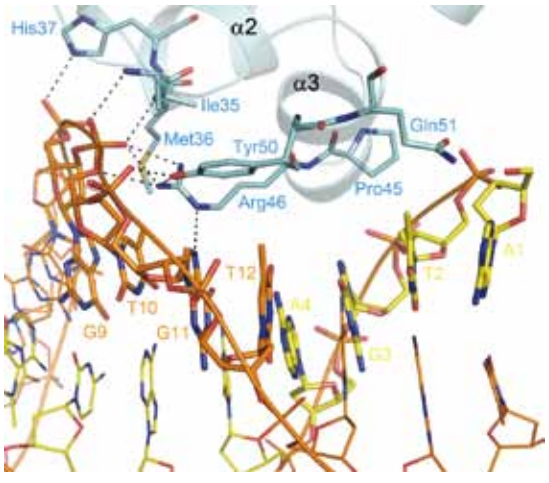

Figure 1. Interaction between apo-HrtR and DNA.

HrtR adopts a unique mechanism for its functional regulation upon heme-sensing. A comparison of the apo-HrtR/DNA complex and holo-HrtR structures revealed that heme-binding triggers a coil-to-helix transition at the α4a-α4b region (Figure 2 (A), (B)). In apo-HrtR, a loop (residues 68-71) intervenes between α4a and α4b helices. Glu70 in the middle of this intervening loop forms a hydrogen bond with Trp123 in apo-HrtR (Figure 2 (A)). Upon heme-binding, a coil-to-helix transition occurs in this intervening loop, which results in the formation of a long α4 helix in holo-HrtR. As the location of Glu70 is largely altered by this coil-to-helix transition, the hydrogen bond between Glu70 and Trp123 is lost in holo-HrtR as shown in Figure 2B. Heme-binding to HrtR causes a coil-to-helix transition of the α4 helix in the heme-sensing domain, which triggers a structural change of HrtR causing it to dissociate from the target DNA for de-repression of the genes encoding the heme efflux system. HrtR uses a unique heme-sensing motif with *bis*-His (His72 and His149) ligation to the heme, which is essential for the coil-to-helix transition of the α4 helix upon heme-sensing.

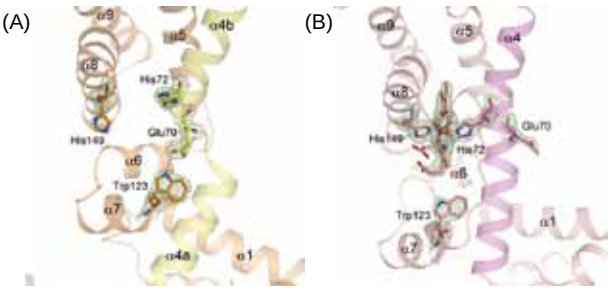

Figure 2. (A) Crystal structure of apo-HrtR. (B) Crystal structure of holo-HrtR.

2. A Model Theoretical Study on Ligand Exchange Reactions of CooA[2)]

Rr-CooA is a CO-sensor heme protein, where binding of CO with the heme group stimulates a transcriptional activator activity of CooA. In this process, the heme undergoes a series of ligand exchanges. In the ferric form, the heme has Cys75 and Pro2 as the axial ligands. In the reduced ferrous form, the heme has His77 instead of Cys75 as an axial ligand with Pro2. Only in the reduced form, CooA can bind CO that replaces Pro2. Model calculations are carried out to elucidate the ligand exchange reactions of CooA. The coordinated proline is found to be the neutral, protonated form. The ligand exchange of cysteine for histidine is reproduced by a relatively small model. This exchange would be mainly due to difference in stability of the non-bonding sulfur p-orbital in Cys75 between the ferric and ferrous states. The selectivity of gas molecules among CO, NO, and O_2 in the proteins is explained by the relative stability of products for Rr-CooA. This is also the case for Ch-CooA, where the amino group of the N-terminus and a histidine are coordinated to the iron ion both in the ferric and ferrous states. The ability to bind the gas molecules is a little stronger in Rr-CooA than in Ch-CooA. In the ferric form of Rr-CooA, heme is deformed to a ruffled form whereas heme is planar in the ferrous form, which leads to a red-shifted Q-band in the former.

3. Molecular Mechanisms of Heme Transport in Gram-Positive Bacteria

Iron, the second-most abundant metal in the Earth's crust, forms a water insoluble oxyhydroxide polymer in water under aerobic conditions, resulting in poor bio-availability. As it is an essential nutrient for prokaryotes and eukaryotes, they develop sophisticated iron acquisition systems to overcome this problem. A gram-positive bacterium *Listeria monocytogenes* has several iron (and iron complexes) transport systems, one of which is an ABC-type transporter (HupCGD) that transports heme as an iron source for this bacterium. HupC, HupG, and HupD proteins are an ATPase component, a membrane permease, and substrate (heme) biding protein, respectively. We have charezterized HupD protein to elucidate the molecular mechanisms of heme transport in *L. monocytogenes*.

HupD contains a typical N-terminal sequence of lipoprotein signal peptide. The amino acid sequence of LLASC is present at the C-terminus of the signal peptide, of which the cysteine residue is the target for lipid modification and becomes the first residue of the mature lipoprotein after cleavage by SPase II protease. When HupD with the signal peptide is expressed in *E. coli*, the recombinant HupD forms aggregates probably due to a hydrophobic signal peptide. Mature HupD lacking the signal peptide is expressed as a soluble protein, which is a mixture of apo- and holo-forms. Purified holo-HupD shows the Soret, α, and β peaks at 413, 565, and 530 nm, respectively, which are typical for 6-coordinated ferric heme proteins with two His as the axial ligands. Ferric HupD shows EPR signals with g = 3.27 and 2.08, which are consistent with a bis-His type ligation of the heme. Site-directed mutagenesis studies suggest that His105 and His259 act as the axial ligands of the heme in HupD. Crystallization experiments are now in progress to obtain structural information of HupD.

References

1) H. Sawai*, M. Yamanaka*, H. Sugimoto, Y. Shiro and S. Aono, *J. Biol. Chem.* **287**, 30755–30768 (2012). (*equal contribution)
2) T. Ishida and S. Aono, *Phys. Chem. Chem. Phys.* **15**, 6139–6148 (2013).

* Present Address; University of Hyogo
† carrying out graduate research on Cooperative Education Program of IMS with Osaka University

Elucidation of the Molecular Mechanisms of Protein Folding

Department of Life and Coordination-Complex Molecular Science
Division of Biomolecular Functions

KUWAJIMA, Kunihiro
Professor (–March, 2013)*

NAKAMURA, Takashi
IMS Research Assistant Professor

TAKENAKA, Toshio	Post-Doctoral Fellow
MIZUKI, Hiroko	Technical Fellow
TANAKA, Kei	Secretary

Kuwajima group is studying mechanisms of *in vitro* protein folding and mechanisms of molecular chaperone function. Our goals are to elucidate the physical principles by which a protein organizes its specific native structure from the amino acid sequence. In this year, they studied molecular mechanisms of the cytotoxicity of human α-lactalbumin made lethal to tumor cells (HAMLET) and other protein-oleic acid complexes, in which a protein folding intermediate forms a complex with oleic acid, and this complex has a unique apoptotic activity for the selective killing of tumor cells.

1. Molecular Mechanisms of the Cytotoxicity of Human α-Lactalbumin Made Lethal to Tumor Cells (HAMLET) and Other Protein-Oleic Acid Complexes

Although HAMLET (human α-lactalbumin made lethal to tumor cells), a complex formed by human α-lactalbumin and oleic acid, has a unique apoptotic activity for the selective killing of tumor cells, the molecular mechanisms of expression of the HAMLET activity are not well understood. Therefore, we studied the molecular properties of HAMLET and its goat counterpart, GAMLET (goat α-lactalbumin made lethal to tumor cells), by pulse field gradient NMR and 920-MHz two-dimensional NMR techniques. We also examined the expression of HAMLET-like activities of complexes between oleic acid and other proteins that form a stable molten globule state. We observed that both HAMLET and GAMLET at pH7.5 were heterogeneous, composed of the native protein, the monomeric molten globule-like state, and the oligomeric species. At pH 2.0 and 50 °C, HAMLET and GAMLET appeared in the monomeric state, and we identified the oleic acid-binding site in the complexes by two- dimensional NMR. Rather surprisingly, the binding site thus identified was markedly different between HAMLET and GAMLET. Furthermore, canine milk lysozyme, apo- myoglobin, and β_2-microglobulin all formed the HAMLET- like complex with the anti-tumor activity, when the protein was treated with oleic acid under conditions in which their molten globule states were stable. From these results, we conclude that the protein portion of HAMLET, GAMLET, and the other HAMLET-like protein-oleic acid complexes is not the origin of their cytotoxicity to tumor cells and that the protein portion of these complexes plays a role in the delivery of cytotoxic oleic acid molecules into tumor cells across the cell membrane.

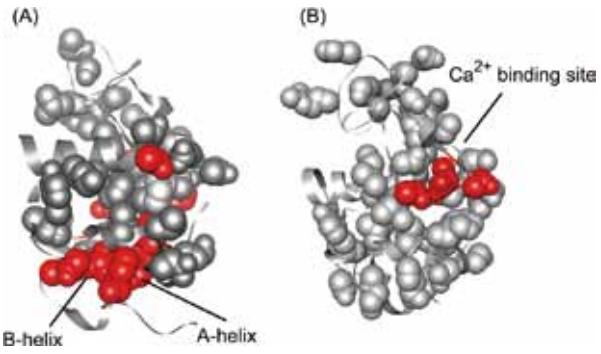

Figure 1. The oleic acid-binding sites of human α-lactalbumin in HAMLET (A) and of goat α-lactalbumin in GAMLET (B) as determined by differences in cross-peaks between the free molten globule state and the α-lactalbumin-olecic acid complex (HAMLET or GAMLET). The amino acid residues represented by the space-filling model are those whose cross-peaks in the ^{1}H-^{15}N HSQC spectra are assigned. The red residues indicate the oleic acid-binding site of each protein.

2. Native-State Heterogeneity of β_2-Microglobulin as Revealed by Kinetic Folding and Real-Time NMR Experiments

The kinetic folding of β_2-microglobulin from the acid-denatured state was investigated by interrupted-unfolding and interrupted-refolding experiments using stopped-flow double-jump techniques. In the interrupted unfolding, we first unfolded the protein by a pH jump from pH 7.5 to pH 2.0, and the kinetic refolding assay was carried out by the reverse pH jump by monitoring tryptophan fluorescence. Similarly, in the interrupted refolding, we first refolded the protein by a pH jump from pH 2.0 to pH 7.5 and used a guanidine hydrochloride (GdnHCl) concentration jump as well as the reverse pH jump as unfolding assays. Based on these experiments, the folding is represented by a parallel-pathway model, in which the molecule with the correct Pro32 *cis* isomer refolds rapidly with a rate constant of 5–6 s^{-1}, while the molecule with the Pro32 *trans* isomer refolds more slowly (pH 7.5 and 25 °C). At the last step of folding, the native-like *trans* conformer produced on the latter pathway isomerizes very slowly (0.001–0.002 s^{-1}) into the native *cis* conformer. In the GdnHCl-induced unfolding assays in the interrupted refolding, the native-like *trans* conformer unfolded remarkably faster than the native *cis* conformer, and the direct GdnHCl-induced unfolding was also biphasic, indicating that the native-like *trans* conformer is populated at a significant level under the native condition. The one-dimensional NMR and the real-time NMR experiments of refolding further indicated that the population of the *trans* conformer increases up to 7–9% under a more physiological condition (pH 7.5 and 37 °C).

3. Structural Insights into the Stability Perturbations Induced by N-Terminal Variation in Human and Goat α-Lactalbumin

Addition of an extra methionine at the N-terminus by recombinant expression of α-lactalbumin in *Escherichia coli* significantly destabilizes the protein, and this destabilization has hampered mutational analyses such as the mutational phi-value analysis of the protein. Deletion of residue 1 from the recombinant form recovers the stability in human and goat α-lactalbumin. Here, we thus determined the crystal structures of the residue 1-deletion variants of recombinant human and goat α-lactalbumin, and compared the structures with those of the authentic and recombinant forms. The results demonstrate the importance of the N-terminal backbone structure and hydrogen- bonding pattern for the stability of α-lactalbumin.

4. The H/D-Exchange Kinetics of the *Escherichia coli* Co-Chaperonin GroES Studied by 2D NMR and DMSO-Quenched Exchange Methods

We studied hydrogen/deuterium-exchange reactions of peptide amide protons of GroES using two different techniques: (1) two-dimensional ^1H–^{15}N transverse-optimized NMR spectroscopy and (2) the dimethylsulfoxide-quenched hydrogen-exchange method combined with conventional ^1H–^{15}N heteronuclear single quantum coherence spectroscopy. By using these techniques together with direct heteronuclear single quantum coherence experiments, we quantitatively evaluated the exchange rates for 33 out of the 94 peptide amide protons of GroES and their protection factors, and for the remaining 61 residues, we obtained the lower limits of the exchange rates. The protection factors of the most highly protected amide protons were on the order of 10^6–10^7, and the values were comparable in magnitude to those observed in typical small globular proteins, but the number of the highly protected amide protons with a protection factor larger than 10^6 was only 10, significantly smaller than the numbers reported for the small globular proteins, indicating that significant portions of free heptameric GroES are flexible and natively unfolded. The highly protected amino acid residues with a protection factor larger than 10^5 were mainly located in three β-strands that form the hydrophobic core of GroES, while the residues in a mobile loop (residues 17–34) were not highly protected. The protection factors of the most highly protected amide protons were orders of magnitude larger than the value expected from the equilibrium unfolding parameters previously reported, strongly suggesting that the equilibrium unfolding of GroES is more complicated than a simple two-state or three-state mechanism and may involve more than a single intermediate.

References

1) T. Nakamura, T. Aizawa, R. Kariya, S. Okada, M. Demura, K. Kawano, K. Makabe and K. Kuwajima, *J. Biol. Chem.* **288**, 14408–14416 (2013).
2) A. Mukaiyama, T. Nakamura, K. Makabe, K. Maki, Y. Goto and K. Kuwajima, *J. Mol. Biol.* **425**, 257–272 (2013).
3) K. Makabe, T. Nakamura and K. Kuwajima, *Protein Eng., Des. Sel.* **26**, 165–170 (2013).
4) M. S. Chandak, T. Nakamura, K. Makabe, T. Takenaka, A. Mukaiyama, T. K. Chaudhuri, K. Kato and K. Kuwajima, *J. Mol. Biol.* **425**, 2541–2560 (2013).

* Present Address; The Center for the Promotion of Integrated Sciences, The Graduate University for Advanced Studies

Elucidation of Dynamical Structures of Biomolecules toward Understanding the Mechanisms Underlying Their Functions

Department of Life and Coordination-Complex Molecular Science
Division of Biomolecular Functions

KATO, Koichi
Professor

YAMAGUCHI, Takumi
Assistant Professor

YAGI-UTSUMI, Maho
OIIB Research Assistant Professor

YANAGI, Kotaro	IMS Fellow
TANADA, Norio	IMS Fellow
UEKUSA, Yoshinori	Post-Doctoral Fellow
WANG, Ying-Hui	Post-Doctoral Fellow
CHANDAK, Mahesh	Graduate Student
ZHANG, Ying	Graduate Student
ZHU, Tong	Graduate Student
WANG, Jinzheng	Graduate Student
KUNIHARA, Tomoko	Graduate Student
KUMOI, Kentaro	Graduate Student*
OKAWA, Keisuke	Graduate Student*
INAGAKI, Kouya	Graduate Student*
SUZUKI, Kousuke	Graduate Student*
THAMMAPORN, Ratsupa	Graduate Student†
SUZUKI, Mariko	Technical Fellow
ISONO, Yukiko	Technical Fellow
IKEDA, Yukako	Technical Fellow
MIZUKI, Hiroko	Technical Fellow
OKADA, Tomo	Technical Fellow
TANAKA, Kei	Secretary

Our biomolecular studies are based on detailed analyses of dynamical structures of various biological macromolecules and their complexes at atomic level, using NMR spectroscopy in conjunction with other biophysical, biochemical and molecular biology techniques. Here we report our recent structural studies of biomolecular complexes for exploring their functional relevance.

1. NMR Characterization of Specific Glycolipid-Protein/Peptide Interactions

Lipid membranes provide active platforms for dynamic interactions of a variety of biomolecules on cell surfaces, where oligosaccharides covalently modifying lipids are involved in divergent molecular recognition events. Sarcotoxin IA, a ecropin-type peptide from *Sarcophaga peregrine*, exhibits antibacterial activity against Gram-negative bacteria through its interaction with lipid A, a core component of lipopolysaccharides. To acquire detailed structural information on this specific interaction, we performed NMR analysis using bacterially expressed sarcotoxin IA analogs with isotope labeling along with lipid A-embedding micelles composed of dodecylphosphocholine. By inspecting the NMR data, we revealed that the N-terminal segment of sarcotoxin IA formed an amphiphilic α-helix upon its interaction with the aqueous micelles, thereby identifying key lysine residues in the interaction with lipid A and the consequent antibacterial activity.[1)] These results offer unique information for designing chemotherapeutics based on antibacterial peptide structures.

Gangliosides, glycosphingolipids possessing a sialyl oligosaccharide moiety, can be targets for various amyloidogenic proteins that are associated with neurodegenerative disorders. We successfully displayed a series of gangliosides on small bicelles with a uniform confined size, offering nanoscale standardized membrane mimics for spectroscopic characterization of weak encounter complexes formed between ganglioside clusters and amyloidogenic proteins.[2)] This enabled probing of initial membrane-landing processes of α-synuclein as therapeutic target by NMR spectroscopy.

2. NMR Characterization of Interactions of Molecular Chaperones with Model Ligands

Molecular chaperones are involved in various cellular processes in which proteins undergo folding, unfolding, and/or refolding under physiological and stress conditions. It has been proposed that molecular chaperones actively contribute to the suppression of toxic aggregate formation of various amyloidogenic proteins associated with neurodegenerative disorders. Furthermore, molecular chaperones have attracted attention due to their potential applicabilities as intelligent nanodevices in bioenginnering fields.

The chaperonin of *Escherichia coli* GroEL forms a large cylindrical complex that assists in the folding of nascent polypeptides. We characterized GroEL–protein interactions by stable isotope-assisted NMR spectroscopy using chemically

denatured bovine rhodanese and an intrinsically disordered protein, α-synuclein, as model ligands. NMR data indicated that proteins tethered to GroEL remain largely unfolded and highly mobile, enabling identification of the interaction hot spots displayed on intrinsically disordered proteins.[3] Furthermore, we found that GroEL could suppress Aβ amyloid formation by interacting with its two hydrophobic segments involving key residues in fibril formation. The binding site of Aβ was mapped on a pair of α-helices located in the GroEL apical domain.[4] These results provide insights into chaperonin recognition of amyloidogenic proteins of pathological interest.

Moreover, we successfully identified ligand-binding site of Hsp47, a client-specific chaperone for collagen, by NMR spectroscopy in conjunction with mutational analysis.[5] Our findings provide a molecular basis for the design of drugs that target the interaction between Hsp47 and procollagen in therapeutics for fibrotic diseases.

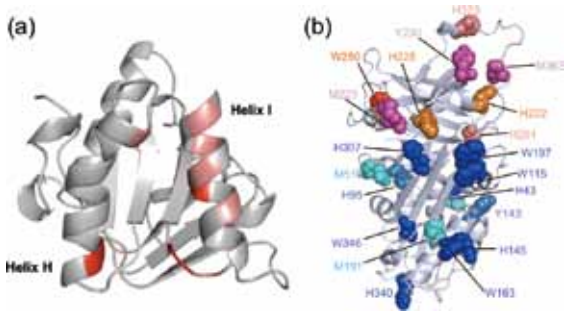

Figure 1. Mapping of (a) the Aβ-binding site on the GroEL apical domain and (b) the collagen-binding site of Hsp47.

3. Elucidation of the Functional Relevance of Quaternary Structures of Proteasome-Associated Proteins

Assembly of the eukaryotic 20S proteasome is an ordered process involving several proteins operating as proteasome assembly factors including PAC1-PAC2 but that of the archaeal 20S proteasome involves spontaneous self-assembly. Recent bioinformatic analysis identified archaeal PAC1-PAC2 homologs PbaA and PbaB. However, it remains unclear whether such assembly factor-like proteins play an indispensable role in orchestration of proteasome subunits in archaea. We revealed that PbaB forms a homotetramer and exerts a dual function as an ATP-independent proteasome activator and a molecular chaperone through its tentacle-like C-terminal segments.[6] Our findings provide insights into molecular evolution relationships between proteasome activators and assembly factors.

In mammals, a major form of proteasome activator PA28 is a heteroheptamer composed of interferon-γ-inducible α and β subunits, which share approximately 50% amino acid identity and possess distinct insert loops. Using deuteration-assisted small-angle neutron scattering, we demonstrated three α and four β subunits are alternately arranged in the heteroheptameric ring.[7] In this arrangement, PA28 loops surround the central pore of the heptameric ring, suggesting that the flexible PA28 loops act as gatekeepers, which function to select the length of peptide substrates to be transported between the proteolytic chamber and the extra-proteasomal medium.

We have also succeeded in encapsulation of ubiquitin, a protein modifier recognized by the proteasome, within synthetic hosts in collaboration with Dr. Makoto Fujita (The University of Tokyo) and his colleagues.[8]

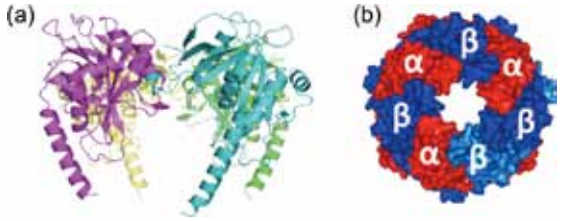

Figure 2. Quaternary structures of (a) the PbaB homotetramer and (b) the PA28 heteroheptamer.

References

1) M. Yagi-Utsumi, Y. Yamaguchi, P. Boonsri, T. Iguchi, K. Okemoto, S. Natori and K. Kato, *Biochem. Biophys. Res. Commun.* **431**, 136–140 (2013).
2) T. Yamaguchi, T. Uno, Y. Uekusa, M. Yagi-Utsumi and K. Kato, *Chem. Commun.* **49**, 1235–1237 (2013).
3) N. Nishida, M. Yagi-Utsumi, F. Motojima, M. Yoshida, I. Shimada and K. Kato, *J. Biosci. Bioeng.* **116**, 160–164 (2013).
4) M. Yagi-Utsumi, T. Kunihara, T. Nakamura, Y. Uekusa, K. Makabe, K. Kuwajima and K. Kato, *FEBS Lett.* **587**, 1605–1609 (2013).
5) M. Yagi-Utsumi, S. Yoshikawa, Y. Yamaguchi, Y. Nishi, E. Kurimoto, Y. Ishida, T. Homma, J. Hoseki, Y. Nishikawa, T. Koide, K. Nagata and K. Kato, *PLoS One* **7**, e45930 (2012).
6) K. Kumoi, T. Satoh, K. Murata, T. Hiromoto, T. Mizushima, Y. Kamiya, M. Noda, S. Uchiyama, H. Yagi and K. Kato, *PLoS One* **8**, e60294 (2013).
7) M. Sugiyama, H. Sahashi, E. Kurimoto, S. Takata, H. Yagi, K. Kanai, E. Sakata, Y. Minami, K. Tanaka and K. Kato, *Biochem. Biophys. Res. Commun.* **432**, 141–145 (2013).
8) D. Fujita, K. Suzuki, S. Sato, M. Yagi-Utsumi, Y. Yamaguchi, N. Mizuno, T. Kumasaka, M. Takata, M. Noda, S. Uchiyama, K. Kato and M. Fujita, *Nat. Commun.* **3**, 1093 (2012).

Award

YAMAGUCHI, Takumi; Poster Award, The 31st Annual Meeting of The Japanese Society of Carbohydrate Research (2012).

* carrying out graduate research on Cooperative Education Program of IMS with Nagoya City University
† carrying out graduate research on Cooperative Education Program of IMS with Kasetsart University

Structure-Function Relationship of Metalloenzymes

Department of Life and Coordination-Complex Molecular Science
Division of Biomolecular Functions

FUJII, Hiroshi
Associate Professor

KURAHASHI, Takuya
Assistant Professor

CONG, Zhiqi	Post-Doctoral Fellow
WANG, Chunlan	Graduate Student
TANIZAWA, Misako	Secretary

Metalloproteins are a class of biologically important macromolecules, which have various functions such as oxygen transport, electron transfer, oxidation, and oxygenation. These diverse functions of metalloproteins have been thought to depend on the ligands from amino acid, coordination structures, and protein structures in immediate vicinity of metal ions. In this project, we are studying the relationship between the electronic structures of the metal active sites and reactivity of metalloproteins.

1. Comparative Spectroscopic Studies of Iron(III) and Manganese(III) Salen Complexes Having a Weakly-Coordinating Triflate Axial Ligand[1)]

Salen and porphyrin are among the most versatile synthetic ligands that are widely utilized as catalysts and materials. Both ligands are four-coordinate dianionic ligands that bind a metal ion in a tetradentate fashion, forming a similar square-planar metal complex. Prominently, iron and manganese, which are abundant transition metals in nature, become functional in combination with these ligands. In the case of porphyrin complexes, spectroscopic properties and electronic structures of iron(III) and manganese(III) complexes have been extensively studied, and some unique properties have been found, such as an intermediate spin state of an iron(III) ion in the presence of weak-field anionic axial ligands such as perchlorate (ClO_4^-) and triflate ($CF_3SO_3^-$).

However, relatively less has been investigated for salen complexes bearing these weak-field anionic axial ligands, while spectroscopic and magnetic properties of iron and manganese salen complexes with strongly-coordinating axial ligands such as imidazole are well documented. This is mostly because a monomeric iron(III) salen complex is quite prone to dimerization in the absence of a strongly-coordinating axial ligand. We previously designed a sterically-hindered salen ligand, and successfully synthesized a monomeric iron(III) and manganese(III) complex bearing a weakly-coordinating ClO_4^- ligand. But the sterically-hindered salen ligand is not necessarily suited for electronic tuning by modification of the phenolate rings, which prevented us to obtain in-depth insight into their spectroscopic properties.

We herein prepare mononuclear manganese(III) and iron(III) salen complexes bearing a weakly-coordinating triflate axial ligand, using salen ligands with differing electron-donating properties (Chart 1). We also synthesize nonsymmetrical salen ligands (Chart 1), in order to precisely understand spectroscopic properties. Magnetic susceptibility and dual-mode electron paramagnetic resonance (EPR) data show that iron(III) and manganese(III) salen complexes adopt high-spin d^5 (S = 5/2) and d^4 (S = 2) electronic configurations, respectively, in all the cases in Chart 1. Further insights into electronic structures of central metal are obtained from ^{2}H NMR spectra of selectively-deuterated complexes, in which Fe^{III}(salen)(OTf) and Mn^{III}(salen)(OTf) exhibit well-resolved paramagnetic NMR signals of quite different shift patterns, due to the presence or absence of the unpaired electron in the dx^2–y^2 orbital.

2. Synthesis, Characterization, and Reactivity of Hypochlorito-Iron(III) Porphyrin Complexes[2)]

Myeloperoxidase (MPO) and chloroperoxidase (CPO) are unique heme peroxidases that catalyze oxidation of chloride ion to hypochlorite ion (OCl^-). MPO is loctaed in azurophil

granules of neutrophils and produces OCl^- or hypochlorous acid (HOCl), which works as an antimicrobial agent, from hydrogen peroxide and chloride ion. On the other hand, CPO is an enzyme of *Caldariomyces fumago* and catalyzes chlorination reactions in the biosynthesis of the chlorinated metabolite caldariomycin. It has been proposed that ferric MPO and CPO initially react with hydrogen peroxide to form an oxoiron(IV) porphyrin π-cation radical species known as compound I. Compound I then reacts with chloride ion to form a transient hypochlorito-iron(III) porphyrin intermediate, which finally releases HOCl with the protonation of the heme-bound hypochlorite. In addition, hypochlorito-metal complexes have been proposed as key intermediates in catalytic oxygenation reactions catalyzed by transition-metal complexes. Because of its significant importance, a hypochlorito-iron(III) porphyrin intermediate has been examined to detect in MPO and CPO reactions and to synthesize its model complex. Although previous reports have indicated the possibility of formation of hypochlorito-iron(III) porphyrin intermediates, spectroscopic evidence for the formation of such species has not been reported until now. The reactivity of a hypochlorito-iron(III) porphyrin complex has been also received much attention in relation to those of other terminal oxidant-metal complexes such as hypochlorite, hydroperoxide, and iodosylarene. Herein, we report the preparation, spectroscopic characterization, and reactivity of hypochlorito-iron(III) porphyrin complexes, including a bis-hypochlorite complex, $[(TPFP)Fe^{III}(OCl)_2]^-$ (**1**), and imidazole-hypochlorite complexes, $(TPFP)Fe^{III}(OCl)$(1-R-Im), where TPFP is 5,10,15,20-tetrakis(pentafluorophenyl) porphyrinate and R is $–CH_3$ (**2**), –H (**3**), or $–CH_2CO_2H$ (**4**). (see Figure 1).

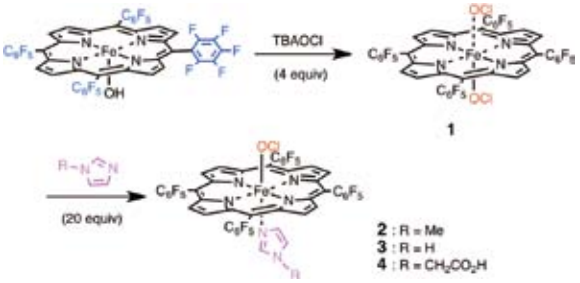

Figure 1. Preparation of hypochlorito-iron(III) porphyrin complexes.

3. Unique Ligand Radical Character of an Activated Cobalt Salen Catalyst that Is Generated by Aerobic Oxidation of a Cobalt(II) Salen Complex[3)]

The Co(salen)(X) complex, where salen is chiral *N*,*N*'-bis(3,5-di-*tert*-butylsalicylidene)-1,2-cyclohexanediamine, and X is an external axial ligand, has been widely utilized as a versatile catalyst. The Co(salen)(X) complex is a stable solid that has been conventionally described as a Co^{III}(salen)(X) complex. Recent theoretical calculations raised a new proposal that the Co(salen)$(H_2O)(SbF_6)$ complex contains appreciable contribution from a $Co^{II}(salen^{+\bullet})$ electronic structure (Kochem, A.; Kanso, H.; Baptiste, B.; Arora, H.; Philouze, C.; Jarjayes, O.; Vezin, H.; Luneau, D.; Orio, M.; Thomas, F. *Inorg. Chem.* **51**, 10557–10571 (2012)), while other theoretical calculations for Co(salen)(Cl) indicated a triplet Co^{III}(salen) electronic structure (Kemper, S.; Hrobárik, P.; Kaupp, M.; Schlörer, N. E. *J. Am. Chem. Soc.* **131**, 4172–4173 (2009)). However, there has been no experimental data to evaluate these theoretical proposals. We herein report key experimental data on the electronic structure of the Co(salen)(X) complex (X = $CF_3SO_3^-$, SbF_6^-, and *p*-$MeC_6H_4SO_3^-$). The X-ray crystallography shows that Co(salen)(OTf) has a square-planar N_2O_2 equatorial coordination sphere with OTf as an elongated external axial ligand. Magnetic susceptibility data indicate that Co(salen)(OTf) complexes belong to the S = 1 spin system. ^{1}H NMR measurements provide convincing evidence for the $Co^{II}(salen^{+\bullet})$(X) character, which is estimated to be about 40% in addition to 60% Co^{III}(salen)(X) character. The CH_2Cl_2 solution of Co(salen)(X) shows an intense near-infrared absorption, which is assigned as overlapped transitions from a ligand-to-metal charge transfer in Co^{III}(salen)(X) and a ligand-to-ligand charge transfer in $Co^{II}(salen^{+\bullet})$(X). The present experimental study establishes that the electronic structure of Co(salen)(X) contains both $Co^{II}(salen^{+\bullet})$(X) and Co^{III}(salen)(X) character.

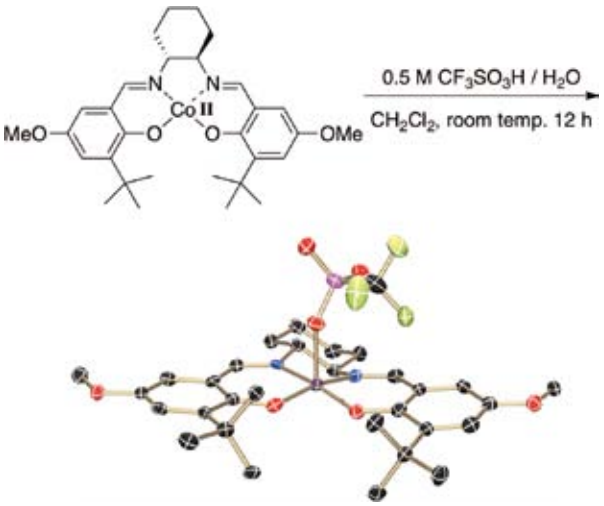

Figure 2. Preparation and Structure of Co(salen)(OTf) complex.

References

1) T. Kurahashi and H. Fujii, *Bull. Chem. Soc. Jpn.* **85**, 940–947 (2012). (BCSJ Award Article)
2) Z. Cong, S. Yanagisawa, T. Kurahashi, T. Ogura, S. Nakashima and H. Fujii, *J. Am. Chem. Soc.* **134**, 20617–20620 (2012).
3) T. Kurahashi and H. Fujii, *Inorg. Chem.* **52**, 3908–3919 (2013).

Award

KURAHASHI, Takuya and FUJII, Hiroshi; BCSJ Award Article, September, 2012.

Investigation of Molecular Mechanisms of Channels, Transporters and Receptors in Cell Membrane

Department of Life and Coordination-Complex Molecular Science
Division of Biomolecular Sensing

FURUTANI, Yuji
Associate Professor

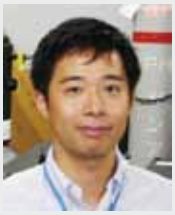

KIMURA, Tetsunari
Assistant Professor

TSUKAMOTO, Hisao
IMS Research Assistant Professor

INAGUMA, Asumi	Research Fellow	SHIMIZU, Atsuko	Secretary
MEENA SINGH, Yatindra	Visiting Scientist		
FUJIWARA, Kuniyo	Graduate Student		

Membrane proteins are important for homeostasis of living cells, which work as ion channels, transporters, various types of chemical and biophysical sensors, and so on. These proteins are considered as important targets for biophysical studies.

Our main goal is to clarify molecular mechanisms of channels, transporters and receptors in cell membrane mainly by using stimulus-induced difference infrared (IR) spectroscopy, which is sensitive to the structural and environmental changes of bio-molecules.

1. O–H Stretching Vibrations of Dangling Bonds of Water Molecules in *pharaonis* Halorhodopsin Studied by Time-Resolved FTIR Spectroscopy

Ion transportation via the chloride ion pump protein *pharaonis* halorhodopsin (*p*HR) occurs through the sequential formation of several intermediates during the photocyclic reaction. Although the structural details of each intermediate state have been studied, the role of water molecules in the translocation of chloride ions inside the protein at physiological temperatures remains unclear. To analyze the structural dynamics of water inside the protein, we performed time-resolved Fourier transform infrared (FTIR) spectroscopy under H_2O or $H_2{}^{18}O$ hydration and successfully assigned water O–H stretching bands.[1)] We found that a dangling water band at 3626 cm^{-1} in *p*HR disappears in the L_1 and L_2 states. On the other hand, relatively intense positive bands at 3605 and 3608 cm^{-1} emerged upon the formation of the N and O states, respectively, suggesting that the chloride transportation is accompanied by dynamic rearrangement of the hydrogen-bonding network of the internal water molecules in *p*HR (Figure 1) .

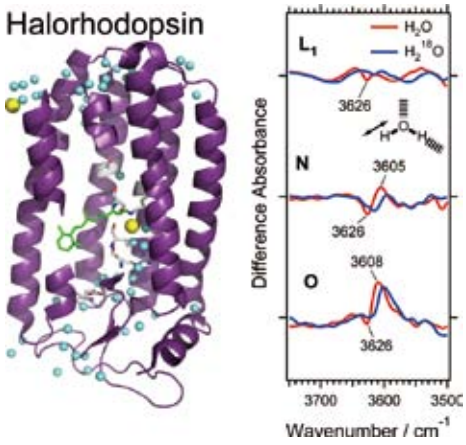

Figure 1. X-ray crystal structure of halorhodopsin (left). The O–H stretching bands of dangling bonds of water molecules inside the protein(right). The figure is adapted with permission from ref. 1. Copyright 2012 American Chemical Society.

2. Perfusion-Induced ATR-FTIR Spectroscopy for Studying Ion-Protein Interactions of a Potassium Ion Channel, KcsA

The potassium channel is highly selective for K^+ over Na^+,

and the selectivity filter binds multiple dehydrated K^+ ions upon permeation. Here, we applied attenuated total reflection Fourier-transform infrared (ATR-FTIR) spectroscopy to extract ion-binding-induced signals of the KcsA potassium channel at neutral pH.[2] Shifts in the peak of the amide-I signal towards lower vibrational frequencies were observed as K^+ was replaced with Na^+ (Figure 2). These ion species-specific shifts deduced the selectivity filter as the source of the signal, which was supported by the spectra of a mutant for the selectivity filter (Y78F). The difference FTIR spectra between the solution containing various concentrations of K^+ and that containing pure Na^+ demonstrated two types of peak shifts of the amide-I vibration in response to the K^+ concentration. These signals represent the binding of K^+ ions to the different sites in the selectivity filter with different dissociation constants (K_D = 9 or 18 mM).

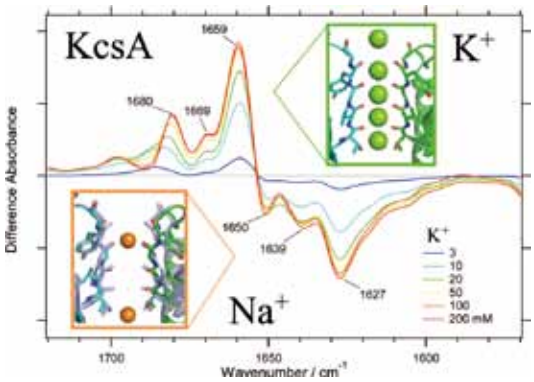

Figure 2. The K^+-minus-Na^+ difference spectra measured with different K^+ concentration. The insets show the X-ray crystal structures of KcsA. The figure is reprinted with permission from ref. 2. Copyright 2012 American Chemical Society.

3. Development of the Measurement Condition of Surface-Enhanced Infrared Absorption Spectroscopy on Membrane Proteins

Surface-enhanced infrared absorption with attenuated total reflection (ATR-SEIRA) is a powerful tool for exploring molecular mechanisms of membrane proteins at the monolayer level. However, the band intensity, position, and direction can be largely influenced by the presence of a thin gold film, as observed for small molecules existing in close proximity to the surface. Here we investigated influence on the band shapes of an α-helical membrane protein, *p*HR, attached on the gold surface through a complex formation between a six-histidines tag and a Ni-nitrilotriacetic acid (Ni-NTA) linker.[3] Normal, bipolar, and inverted shapes of amide-I and -II bands were observed with an increase in film thickness, although *p*HR molecules would locate relatively far from the surface. The physical origin of this interesting phenomenon has been identified by changing incident angle, polarization, and film deposition rate. We find the observed absorption anomalies are due to the influence of perpendicularly polarized light. Furthermore, it is shown that the band shapes are normal below the percolation threshold, and bipolar ones occur when an anomalous absorption by the films is strong, while the inverted ones develop with films in which surface scattering is predominant.

4. Development of a Rapid Buffer-Exchange System for Time-Resolved ATR-FTIR Spectroscopy with the Step-Scan Mode

Attenuated total reflectance (ATR)-FTIR spectroscopy has been widely used to probe protein structural changes under various stimuli, such as light absorption, voltage change, and ligand binding, in aqueous conditions. Time-resolved measurements require a trigger, which can be controlled electronically; therefore, light and voltage changes are suitable. Here we developed a novel, rapid buffer-exchange system for time-resolved ATR-FTIR spectroscopy to monitor the ligand- or ion-binding reaction of a protein.[4] By using the step-scan mode (time resolution; 2.5 ms), we confirmed the completion of the buffer-exchange reaction within ~25 ms; the process was monitored by the infrared absorption change of a nitrate band at 1350 cm^{-1} (Figure 3). We also demonstrated the anion-binding reaction of a membrane protein, *p*HR, which binds a chloride ion in the initial anion-binding site near the retinal chromophore. The formation of chloride- or nitrate-bound *p*HR was confirmed by an increase of the retinal absorption band at 1528 cm^{-1}. It also should be noted that low sample consumption (~1 μg of protein) makes this new method a powerful technique to understand ligand–protein and ion–protein interactions, particularly for membrane proteins.

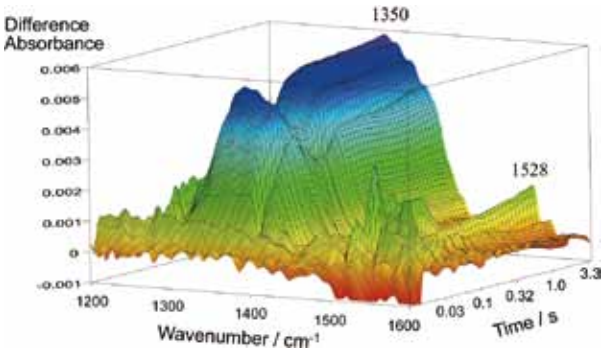

Figure 3. The time-resolved FTIR spectra of the rapid-buffer exchange reaction of pHR. The figure is reprinted with permission from ref 4. Copyright 2013 The Biophysical Society of Japan.

References

1) Y. Furutani *et al.*, *J.Phys. Chem. Lett.* **3**, 2964–2969 (2012).
2) Y. Furutani *et al.*, *J. Phys. Chem. Lett.* **3**, 3806–3810 (2012).
3) H. Guo *et al.*, *Chem. Phys.* **419**, 8–16 (2013).
4) Y. Furutani *et al.*, *Biophysics* **9**, 123–129 (2013).

Heterogeneous Catalytic Systems for Organic Chemical Transformations in Water

Department of Life and Coordination-Complex Molecular Science
Division of Complex Catalysis

UOZUMI, Yasuhiro
Professor

OSAKO, Takao
Assistant Professor

HAMASAKA, Go
Assistant Professor

NAGAOSA, Makoto	Post-Doctoral Fellow	TSUJI, Hiroaki	Graduate Student
KOBAYASHI, Noboru	Graduate Student	TORII, Kaoru	Technical Fellow
SAKURAI, Fumie	Graduate Student	TAZAWA, Aya	Technical Fellow
		SASAKI, Tokiyo	Secretary
		FUKUSHIMA, Tomoko	Secretary

Various transition metal-catalyzed organic molecular transformations in water were achieved under heterogeneous conditions by use of a self-assembled polymeric imidazole-copper catalyst, a boron-iridium heterobimetallic polymeric catalyst, or resin-supported iron nanoparticles which were designed and prepared by this research group. In particular, development of a highly active reusable poly(imidazole-copper) and an iron-catalyzed hydrogenation of under flow conditions are highlights among the achievements of the 2012–2013 period to approach what may be considered ideal chemical process of next generation. Representative results are summarized here under.

1. Amphiphilic Self-Assembled Polymeric Copper Catalyst to Parts per Million Levels: Click Chemistry[1)]

Self-assembly of copper sulfate and a poly(imidazole–acrylamide) amphiphile provided a highly active, reusable, globular, solid-phase catalyst for click chemistry. The self-assembled polymeric Cu catalyst was readily prepared from poly(*N*-isopropylacrylamide-co-*N*-vinylimidazole) and $CuSO_4$ via coordinative convolution. The surface of the catalyst was covered with globular particles tens of nanometers in diameter, and those sheetlike composites were layered to build an aggregated structure. Moreover, the imidazole units in the polymeric ligand coordinate to $CuSO_4$ to give a self-assembled, layered, polymeric copper complex. The insoluble amphiphilic polymeric imidazole Cu catalyst with even 4.5–45 mol ppm drove the Huisgen 1,3-dipolar cycloaddition of a variety of alkynes and organic azides, including the three-component cyclization of a variety of alkynes, organic halides, and sodium azide. The catalytic turnover number and frequency were up to 209000 and 6740 h^{-1}, respectively. The catalyst was readily reused without loss of catalytic activity to give the corresponding triazoles quantitatively.

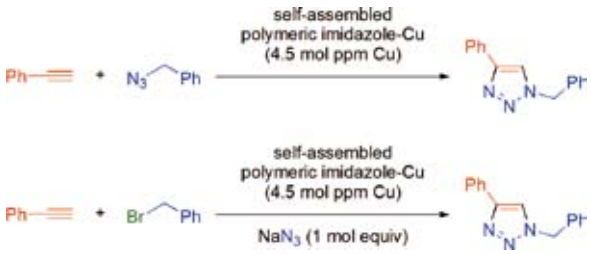

Figure 1. Click reaction catalyzed by self-assembled polymeric imidazole-Cu.

2. Polymeric Bimetallic Catalyst-Promoted In-Water Dehydrative Alkylation of Ammonia and Amines with Alcohols[2)]

A dehydrative alkylation with three kinds of Ir/B heterobimetallic polymeric catalysts in water is reported. The poly-

meric heterobimetallic catalysts were readily prepared by ionic convolution of a poly(catechol borate) and iridium complexes. The N-alkylation of ammonia and amines with alcohols, as alkylating agents, was carried out with a heterogeneous catalyst (1 mol% Ir) at 100 °C without the use of organic solvents under aerobic and aqueous conditions to afford the corresponding alkylated amines in high yield.

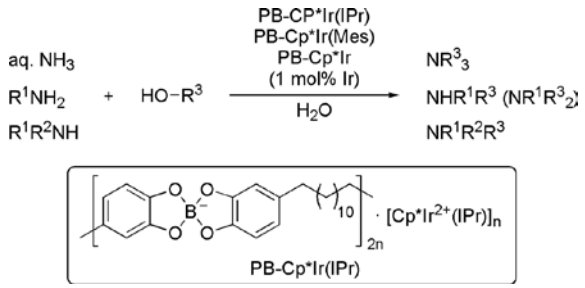

Figure 2. In-water dehydrative alkylation of ammonia and amines with alcohols using polymeric bimetallic catalysts.

3. Highly Efficient Iron(0) Nanoparticle-Catalyzed Hydrogenation in Water in Flow[3)]

Highly efficient catalytic hydrogenations are achieved by using amphiphilic polymer-stabilized Fe(0) nanoparticle (Fe NP) catalysts in ethanol or water in a flow reactor. Alkenes, alkynes, aromatic imines and aldehydes were hydrogenated nearly quantitatively in most cases. Aliphatic amines and aldehydes, ketone, ester, arene, nitro, and aryl halide functionalities are not affected, which provides an interesting chemoselectivity. The Fe NPs used in this system are stabilized and protected by an amphiphilic polymer resin, providing a unique system that combines long-term stability and high activity. The NPs were characterized by TEM of microtomed resin, which established that iron remains in the zero-valent form despite exposure to water and oxygen. The amphiphilic resin-supported Fe(0) nanoparticles in water and in flow provide a novel, robust, cheap and environmentally benign catalyst system for chemoselective hydrogenations.

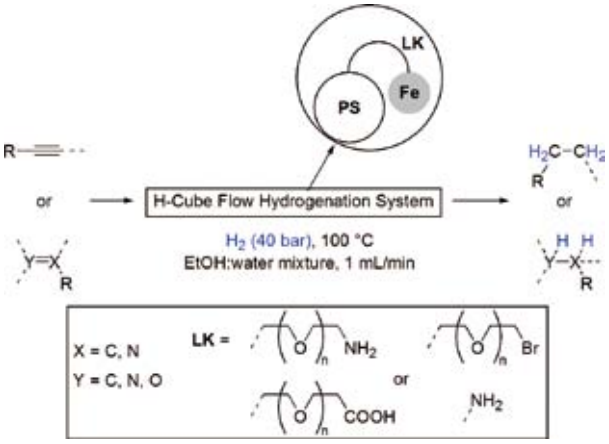

Figure 3. Schematic of hydrogenation reactions undertaken with polymer supported iron nanoparticles, under flow conditions (PS = polystyrene).

References

1) Y. M. A. Yamada, S. M. Sarkar and Y. Uozumi, *J. Am. Soc. Chem.* **134**, 9285–9290 (2012).
2) Y. M. A. Yamada, H. Ohta, Y. Yuyama and Y. Uozumi, *Synthesis* **45**, 2093–2100 (2013).
3) R. Hudson, G. Hamasaka, T. Osako, Y. M. A. Yamada, C.-J. Li, Y. Uozumi and A. Moores, *Green Chem.* **15**, 2141–2148 (2013).

Awards

OSAKO, Takao; Shionogi & Co. Ltd., Award in Synthetic Organic Chemistry, Japan.
HAMASAKA, Go; Nagoya University Ishida Prize.

Development of Functional Metal Complexes for Artificial Photosynthesis

Department of Life and Coordination-Complex Molecular Science
Division of Functional Coordination Chemistry

MASAOKA, Shigeyuki
Associate Professor

KONDO, Mio
Assistant Professor

YOSHIDA, Masaki	Post-Doctoral Fellow
NAKAMURA, Go	Graduate Student
OKAMURA, Masaya	Graduate Student
MURASE, Masakazu	Graduate Student*
ITOH, Takahiro	Graduate Student
FUKAHORI, Yukino	Graduate Student
FUKATSU, Arisa	Graduate Student
LIU, Ke	Graduate Student
KUGA, Reiko	Technical Fellow
KANAIKE, Mari	Technical Fellow
WAKABAYASHI, Kaori	Technical Fellow
SHIBATA, Akane	Technical Fellow
TANIWAKE, Mayuko	Secretary

1. Controlled Self-Assembly of Paddle-Wheel Dimers via Multipoint Arene-Perfluoroarene Interactions[1)]

Control over the self-assembling process of metal complexes is of key importance to construct supramolecular materials in which desirable bulk properties emerge as a consequence of specific intermolecular orientations. Paddle-wheel complexes which are described as M_2L_4 (M = metal ion, L = monoanionic bidentate ligand) attract much attention because of their highly symmetric (D_{4h}) structures suitable for the construction of continuous structures. Moreover, the existence of free coordination sites at the axial positions (open axial sites) and their Lewis acidity play a crucial role in catalysis or selective guest recognition. Therefore, the construction of continuous structures of paddle-wheel units with open axial sites is of significance to develop functional materials.

In this study we firstly report the self-assembly of Rh(II) and Cu(II) paddle-wheel complexes with open axial sites controlled via *unidirectional* interaction realized by multipoint arene-perfluoroarene interactions (Scheme 1). Two kinds of paddle-wheel dimers, the I-shaped complex (**1**), which has only two *unidirectional* interaction sites and is expected to one-dimensional chain assembly, and the cross-shaped complex (**2**), which has four *unidirectional* interaction sites in one molecule and is expected to have two-dimensional sheet-structure, are chosen to examine the molecular arrangements in the crystalline state (Scheme 1).

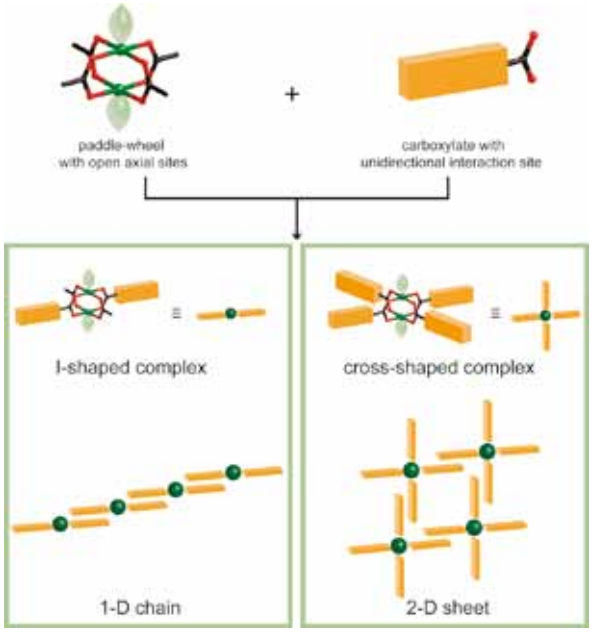

Scheme 1. Schematic illustration of I- and cross-shaped paddle-wheel complexes with open axial sites and their self-assembled structures.

In the crystal packing structures of **1** and **2**, intermolecular multipoint arene-perfluoroarene interactions are observed. **1** is arranged in one-dimensional chain due to face-to-face overlap of phenylene and perfluorophenyl rings. Interchain stacking are stabilized by π–π interactions between perfluorophenyl

rings to form the two-dimensional sheet structure. In the crystal packing structures of **2**, an infinite two-dimensional square-grid sheet structure is formed via multipoint arene-perfluoroarene interaction between ligands.

Moreover, porous structure was formed by the stacking of the two dimensional sheets via π–π interaction between ligands along the *a* axis and open axial sites are oriented to the channel.

The results presented in this contribution offer a new strategy to assemble paddle-wheel units of various metal ions with open axial sites at room temperature. This can be a powerful tool to construct supramolecular structures applied for heterogeneous catalytic system or sensor.

2. Photoinduced Hydrogen Evolution from Water by a Simple Platinum(II) Terpyridine Derivative[2)]

Hydrogen energy has been one of the most important targets as a renewable clean energy. Particularly, hydrogen generation based on water splitting by solar energy has attracted considerable attention for many years. Up to now, photochemical hydrogen production catalyzed by metal complexes has been extensively studied using a so-called three-component system consisting of tris(2,2'-bipyridine)ruthenium(II) ($Ru(bpy)_3^{2+}$) as a photosensitizer, methylviologen (N,N'-dimethyl-4,4'- bipyridinium, MV^{2+}) as an electron relay, and ethylenediaminetetraacetic acid disodium salt (EDTA) as a sacrificial electron donor, for which colloidal platinum was often employed as a H_2-evolving catalyst. Previously, we reported on the photochemical hydrogen production from water catalyzed by $[PtCl(terpy)]^+$ (terpy = 2,2':6',2"-terpyridine) in the presence of EDTA, where the platinum(II) complex is known to serve as a photosensitizer as well as a H_2-evolving catalyst. Thus this work was considered as the first example of 'bifunctional single-component photocatalysts' driving visible light-induced H_2 production from water (Figure 1).

In this work, we reported the novel platinum(II) complex (PV^{2+}) as the first example of 'trifunctional single-component photocatalysts' for visible light-induced H_2 production from water (Figure 1).

The H_2-evolving activity of PV^{2+} evaluated in the presence of EDTA showed that the stability of the PV^{2+} catalyst during the photolysis is much higher than that of the parent compound $[PtCl(tpy)]^+$. This is due to the improved electron-accepting ability of PV^{2+} compared with $[PtCl(tpy)]^+$. It is also found that the photolysis of PV^{2+} first generates a one-electron-reduced species (PV^+) as an initial photoproduct and this further undergoes a photoinduced process leading to H_2 generation from water. Therefore, this is the first demonstration of Z-scheme photosynthesis within the family of artificial molecular systems, although these two-step reductive quenching processes do not perfectly match with the oxidative ones in natural photosynthesis. The present study also demonstrates that the PHE activity can be dramatically enhanced by the presence of a Pt^{II}-based molecular co-catalyst, such as *cis*-$[PtCl_2(NH_3)_2]$.

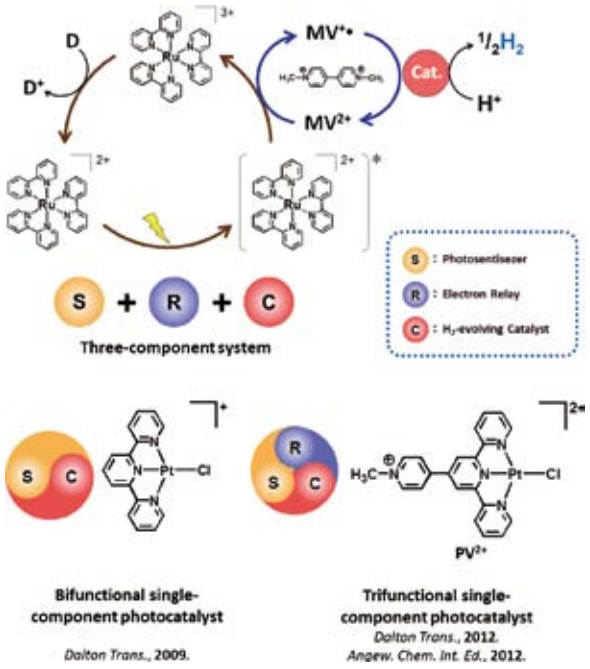

Figure 1. Three-component, bifunctional single-component and trifunctional single-component photocatalysts for hydrogen production from water.

References

1) T. Itoh, M. Kondo, M. Kanaike and S. Masaoka, *CrystEngComm* **15**, 6122–6126 (2013).
2) M. Kobayasi, S. Masaoka and K. Sakai, *Angew. Chem., Int. Ed.* **51**, 7431–7434 (2012).

Awards

NAKAMURA, Go; FY2013 (the 4th) Sokendai President's Award (2013).
NAKAMURA, Go; Student Poster Award, 2nd CSJ Chemistry Festa (2012).
YOSHIDA, Masaki; Student Poster Award, 2nd CSJ Chemistry Festa (2012).
MURASE, Masakazu; Student Poster Award, 2nd CSJ Chemistry Festa (2012).
OKAMURA, Masaya; Student Poster Award, 2nd CSJ Chemistry Festa (2012).

* carrying out graduate research on Cooperative Education Program of IMS with Nagoya Institute of Technology

Visiting Professors

Visiting Professor
SASAI, Hiroaki *(from Osaka University)*

Design and Synthesis of Novel Enantioselective Catalysts

Synthesis of optically active complex molecules using catalytic amount of chiral compounds plays an important role in pharmaceutical industrial processes. Our group engages in the development of novel enantioselective catalyses which involve asymmetric domino reaction promoted by an acid-base type organocatalyst, oxidative coupling of 2-naphthol derivatives using dinuclear vanadium(V) catalysts, spiro bis(isoxazoline) ligand (SPRIX) accelerated transition metal catalyses, *etc.* Recently we have realized a highly enantioselective Pd(II)/Pd(IV) catalysis, formal [n+2] type cycloadditions of a ketimine with an alkyl 2,3-butadienoate, and an enantioselective Friedel-Crafts type reaction using chiral dinuclear vanadium catalyst.

Visiting Associate Professor
UEMURA, Takashi *(from Kyoto University)*

Highly Ordered Polymers by Host-Guest Cross-Polymerization

Chain alignment can deeply influence the ultimate macroscopic properties of a polymeric material; however, a general and versatile methodology for attaining highly ordered crystalline packing of polymer chains with high stability has not been reported so far. We have disclosed a strategy to produce polymeric materials that exhibit a crystalline arrangement promoted by “ordered cross-links.” Divinyl cross-linkers were embedded into a porous coordination polymer (PCP). During the polymerization of vinyl monomers in the channels, the divinyl species crosslink vinyl polymer chains that have formed within adjacent channels of the PCP. This bridging ensures that, on selective removal of the PCP, the polymer chains remained aligned even in the absence of stereoregularity.

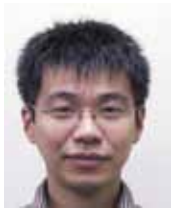

Visiting Associate Professor
SUDO, Yuki *(from Nagoya University)*

Understanding and Controlling the Photoactive Proteins

Light absorbing photoactive proteins show characteristic colors originating from a species specific energy gap between their ground state and excited state, which leads to different characteristic absorption maxima (λ_{max}). Among these proteins and their cognate chromophores, the rhodopsins are known to show a large variation in their absorption spectra depending on the interaction between the apoprotein (opsin) and the retinal chromophore. Another striking characteristic of the rhodopsins is their wide range of seemingly dissimilar functions. Our research are roughly divided into three topics as follows; i) Discovery of novel microbial rhodopsins from the nature, ii) Identification of the biological function and investigation of the structure and the structural change during the photoreaction, and iii) Development of the rhodopsin-based optical tools for the life scientists.

RESEARCH ACTIVITIES

Research Center of Integrative Molecular Systems

The mission of CIMoS is to analyze molecular systems in nature to find the logic behind the sharing and control of information between the different spatiotemporal hierarchies, with the ultimate goal of creating novel molecular systems on the basis of these findings.

Molecular Origin of 24 Hour Period in Cyanobacterial Protein Clock

Research Center of Integrative Molecular Systems
Division of Trans-Hierarchical Molecular Systems

AKIYAMA, Shuji
Professor

MUKAIYAMA, Atsushi
Assistant Professor

ABE, Jun	Post-Doctoral Fellow	SHINTANI, Atsuko	Technical Fellow
HIYAMA, Takuya	Post-Doctoral Fellow	SUZUKI, Hiroko	Secretary
FUNAKI, Yukino	Technical Fellow		

Circadian (approximately 24 h) clocks are endogenous time-keeping systems encapsulated in living cells, enabling organisms to adapt to daily fluctuation of exogenous environments on the Earth. These time-keeping systems, found ubiquitously from prokaryotes to eukaryotes, share the three characteristics. First, the circadian rhythmicity of the clocks persists even without any external cues (self-sustainability). Second, the period is little dependent on ambient temperature (temperature compensation). Third, the phase of the clock can be reset by external stimuli such as lightning, humidity, or temperature so as to be synchronized to the external phase (synchronization).

KaiC, a core protein of the circadian clock in cyanobacteria, undergoes rhythmic structural changes over approximately 24 h in the presence of KaiA and KaiB (Kai oscillator). This slow dynamics spanning a wide range of both temporal and spatial scales is not well understood, and is central to a fundamental question: What determines the temperature-compensated 24 h period?[1,2] The Kai oscillator reconstitutable *in vitro* is advantageous for studying its dynamic structure through a complementary usage of both X-ray crystallography and solution scattering, its transient response by using physicochemical techniques, and its molecular motion through a collaborative work with computational groups.

Our mission is to explore the frontier in molecular science of the cyanobacterial circadian clock from many perspectives. This Annual Report summarizes our recent activities.

1. Tracking the Ticking of Cyanobacterial Clock Protein KaiC in Solution[3]

The ATPase activity of KaiC *alone* is strongly correlated with the oscillatory period of the Kai oscillator. This correlation suggests that the ATPase activity of KaiC is one of the period-determining factors of the Kai oscillator. Hence, the determination of the structural change of KaiC interlocked with the ATPase activity is of great of importance.

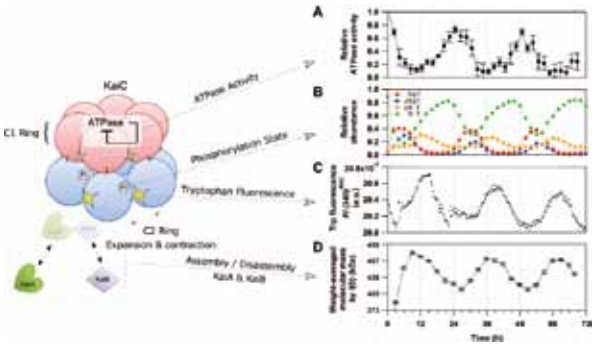

Figure 1. Circadian dynamics of cyanobacterial clock protein KaiC. The C1 and C2 domains in each protomer of KaiC are drawn as red and blue spheres, respectively. Expansion and contraction motions of the C2 ring (B, C) in solution serves as a timing cue for assembly/disassembly of KaiA and KaiB (D), and is interlocked with its C1 ATPase udder a control of negative-feedback regulation (A).

To track the dynamic transition of KaiC in real-time, we recorded the time evolution of intrinsic tryptophan (Trp) fluorescence from KaiC contained in the Kai oscillator. KaiC is a dumbbell-shaped molecule composed of tandemly duplicated N-terminal (C1) and C-terminal (C2) domains. Six protomers are assembled into a hexamer to attain a double-doughnut shape. Two tryptophan (Trp) residues located in the protomer-protomer interface of the C2 domain can serve as a sensitive probe to monitor the potential structural transition of

the C2 ring. The intensity of the Trp fluorescence from KaiC revealed a rhythmic fluctuation with the period of approximately 24 h (Figure 1, panel C). So far as we know, this is the first experimental evidence that demonstrated a dynamic structural transition of the C2 ring of KaiC in solution.

Concomitantly with the Trp-fluorescence dynamics, KaiC underwent a periodic change in its phosphorylation state (Figure 1, panel B). KaiC has the two phosphorylation sites, *i.e.*, Ser431 and Thr432, in the C2 domain, and both residues are phosphorylated and then dephosphorylated in a programmed sequence during the phosphorylation cycle as follows: KaiCS/pT → KaiCpS/pT → KaiCpS/T → KaiCS/T (where 'S' represents Ser431, 'pS' represents phosphorylated Ser431, 'T' represents Thr432, and 'pT' represents phosphorylated Thr432). Interestingly, the Trp fluorescence was maximized at the timing when the KaiCpS/T state was populated (Figure 1, panels B and C). The result suggests the Trp fluorescence is an excellent measure of the phosphor-coupled transition of the C2 ring in KaiC.

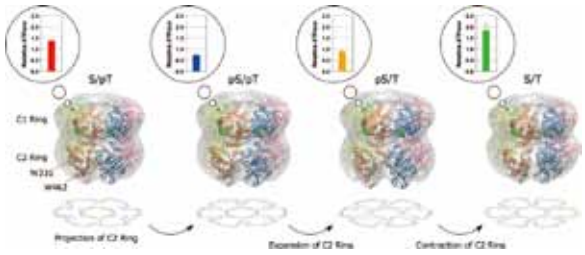

Figure 2. Expansion and contraction motions of C2 ring of KaiC interlocked with ATPase activity.

2. Visualization of Dynamic Structural Changes of KaiC Using Small-Angle X-Ray Solution Scattering Technique[3,4)]

To visualize the C2-ring dynamics confirmed by tracking Trp fluorescence, we measured the small-angle x-ray scattering (SAXS) from KaiC in solution. To obtain the SAXS data of biological samples in solution, one must first record the scattering intensity of the sample (biomacromolecules in solution) and then that of the matching buffer in the separate experiment, and finally find the difference between two intensities. The cuvette used for conventional SAXS experiments has only a single observation chamber in order to ensure the qualitative subtraction of the scattering contributed by the solvent molecules. On the other hand, the use of the single-chamber cuvette makes both the experiment and analysis time-consuming.

To record the SAXS pattern of KaiC both efficiently and qualitatively, we designed and constructed an eight-chamber cuvette (octuplet cuvette), each chamber of which was fabricated so uniformly to ensure the inter-chamber subtraction. The developed cuvette enabled us to acquire SAXS dataset of KaiC roughly 10 times faster without any significant degradation of data quality.

On the basis of the obtained SAXS data, we built low-resolution models of the KaiC hexamer as shown in Figure 2. The overall shape is almost unchanged in the transition from KaiCS/pT to KaiCpS/pT, whereas the radius of the C2 ring is dramatically enlarged in the subsequent transition from KaiCpS/pT to KaiCpS/T. The expanded C2 ring is partly contracted in the transition from KaiCpS/T to KaiCS/T, and is further contracted in the subsequent transition from KaiCS/T to KaiCS/pT. The present model suggests that KaiC ticks through expanding and contracting motions of the C2 ring.

The dynamic motion of the C2 ring uncovered throughout our study is chronobiologically meaningful, we believe, in terms of the elucidation of the key conformational change tightly coupled to the period-determining ATPase of KaiC. Our group is trying to improve spatio-temporal resolution of the experiments so as to draw a more dynamic and detailed picture of KaiC ATPase.

3. Instrumentation for the Molecular Origin of 24 Hour Period in Cyanobacterial Circadian Clock

How can biological-clock systems be so slow and stable? It is important to revisit the biological and structural backgrounds for the slowness and specificity both experimentally and theoretically. For this purpose, much effort has been focused on designing dedicated instrumentations for the molecular origin of the circadian period. We have made considerable improvements of instrument stability, signal-to-noise ratio, time resolution, temperature control, automated high-throughput measurements each for fluorescence tracking system,[3)] auto-sampling device (unpublished work), HPLC (unpublished work), FTIR (unpublished work) and so on. Using the developed device, we recently succeeded in site-specific monitoring of conformational change of KaiC in solution, and also in identifying a core process of generating circadian periodicity in cyanobacterial circadian clock.[5)]

References

1) S. Akiyama, *Cell. Mol. Life Sci.* **69**, 2147–2160 (2012).
2) A. Mukaiyama, T. Kondo and S. Akiyama, *SPring-8 Research Frontiers 2011* 47–48 (2012).
3) Y. Murayama, A. Mukaiyama, K. Imai, Y. Onoue, A. Tsunoda, A. Nohara, T. Ishida, Y. Maéda, T. Kondo and S. Akiyama, *EMBO J.* **30**, 68–78 (2011).
4) S. Akiyama and T. Hikima, *J. Appl. Crystallogr.* **44**, 1294–1296 (2011).
5) Y. Mukaiyama, M. Osako, T. Hikima, T. Kondo and S. Akiyama, submitted.

Theoretical Studies of Chemical Dynamics in Condensed and Biomolecular Systems

Research Center of Integrative Molecular Systems
Division of Trans-Hierarchical Molecular Systems

ISHIZAKI, Akihito
Research Associate Professor

YAMADA, Mariko Secretary

Photosynthesis provides the energy source for essentially all living things on Earth, and its functionality has been one of the most fascinating mysteries of life. Photosynthetic conversion of the energy of sunlight into its chemical form suitable for cellular processes involves a variety of physicochemical mechanisms. The conversion starts with the absorption of a photon of sunlight by one of the light-harvesting pigments, followed by transfer of electronic excitation energy to the reaction center, where charge separation is initiated. At low light intensities, surprisingly, the quantum efficiency of the transfer is near unity. A longstanding question in photosynthesis has been the following: *How does light harvesting deliver such high efficiency in the presence of disordered and fluctuating dissipative environments?* At high light intensities, on the other hand, the reaction center is protected by regulation mechanisms that lead to quenching of excess excitation energy in light harvesting proteins. The precise mechanisms of these initial steps of photosynthesis are not yet fully elucidated from the standpoint of molecular science.

1. An Analytical Continuation Approach for Evaluating Emission Lineshapes of Molecular Aggregates and the Adequacy of Multichromophoric Förster Theory

In large photosynthetic chromophore-protein complexes not all chromophores are coupled strongly, and thus the situation is well described by formation of delocalized states in certain domains of strongly coupled chromophores. In order to describe excitation energy transfer among different domains without performing extensive numerical calculations, one of the most popular techniques is a generalization of Förster theory to multichromophoric aggregates (generalized Förster theory) proposed by Sumi [*J. Phys. Chem. B* **103**, 252 (1999)] and Scholes and Fleming [*J. Phys. Chem. B* **104**, 1854 (2000)].

The aim of this project is twofold. In the first place, by means of analytic continuation and a time convolutionless quantum master equation approach, a theory of emission lineshape of multichromophoric systems or molecular aggregates was proposed.[1)] In the second place, a comprehensive framework that allows for a clear, compact and effective study of the multichromophoric approach in the full general version proposed by Jang, Newton and Silbey [*Phys. Rev. Lett.* **92**, 218301 (2004)] was developed.[1)]

We applied the present theory to simple paradigmatic systems and we showed on one hand the effectiveness of time-convolutionless techniques in deriving lineshape operators and on the other hand we showed how the multichromophoric approach can give significant improvements in the determination of energy transfer rates in particular when the systems under study are not the purely Förster regime. The presented scheme allows for an effective implementation of the multichromophoric Förster approach which may be of use for simulating energy transfer dynamics in large photosynthetic aggregates, for which massive computational resources are

usually required. Furthermore, our method allows for a systematic comparison of multichromophoric Förster and generalized Förster theories and for a clear understanding of their respective limits of validity.

2. Interactions between Quantum Mixing and the Environmental Dynamics Controlling Ultrafast Photoinduced Electron Transfer Reaction

All the photosynthetic reaction centers (RCs) share considerable similarities in the nature and arrangement of the redox cofactors. The primary charge separation in photosystem II (PSII) of green plants was assumed to be similar to purple bacteria. In the mid-1990s, the charge separation in the PSII RC was shown to follow a different mechanism than bacterial RCs. In the 2000s, the primary charge separation in the PSII RC was investigated by independent studies using femtosecond pump-probe spectra of the D1/D2/cyt*b*559 complex isolated from PSII in the visible/mid-IR [Groot, *et al.*, *Proc. Natl. Acad. Sci. USA* **102**, 13087 (2005).] and visible [Holzwarth, *et al.*, *Proc. Natl. Acad. Sci. USA* **132**, 6895 (2006).] spectral regions. Both reports identified the accessory chlorophyll as the primary electron donor and pheophytin as the primary electron acceptor. Time constants of 600–800 fs and 3 ps were extracted for the pheophytin reduction, which yielded values of 200–300 fs and 1 ps as the intrinsic time constant of the primary charge separation. Theoretical analyses of time-dependent emissions from the PSII core complex yielded 100 fs as the intrinsic time constant. [Raszewski and Renger, *J. Am. Chem. Soc.* **130**, 4431 (2008).] Regardless of the controversial differences, all the values for the PSII RC are faster than the time constant of 3 ps measured for the primary electron transfer (ET) starting from the special pair in purple bacterial RCs. An ultrafast primary charge separation pathway was also revealed in a purple bacterial RC (approximately 400 fs), which starts from the accessory bacteriochlorophyll. [van Brederode, *et al.*, *Biochemistry* **36**, 6855 (1997).] The coupling strengths between electron donors and acceptors are usually thought to be tens of cm^{-1}, and the precise mechanisms enabling the subpicosecond charge separation are mostly unknown.

The timescales of most environmental dynamics, such as solvation or protein reorganization involved in photoinduced ET, occur in the subpicosecond and picosecond range. Thus, the reported subpicosecond timescales imply that the ET reaction may take place beyond the nonadiabatic limit; an adiabatic fashion in which the reaction is dominated by vibrational/environmental motions in an adiabatic (free) energy surface that reflects quantum mixing between the initial and final states.

In this project, to explore the potential causes for subpicosecond timescales of the primary charge separation in photosynthetic RCs, we investigated the interactions between environmental dynamics and quantum mixing that affects the ultrafast photoinduced ET dynamics using quantum dynamics simulation. It was shown that the timescales of environmental dynamics change the nature of the ET reaction (*i.e.*, adiabatic or nonadiabatic), dramatically affect the rates and temperature dependences, and enable subpicosecond reactions despite small donor–acceptor coupling.[2)]

References

1) L. Banchi, G. Costagliola, A. Ishizaki and P. Giorda, *J. Chem. Phys.* **138**, 184107 (14 pages) (2013).

2) A. Ishizaki, *Chem. Lett.* **42**, 1406–1408 (2013).

Ultimate Quantum Measurements for Quantum Dynamics

Research Center of Integrative Molecular Systems
Division of Trans-Hierarchical Molecular Systems

SHIKANO, Yutaka
Research Associate Professor

HARDAL, Ali Umit Cemal — Visiting Scientist*
NAKANE, Junko — Secretary

Due to great development on experimental technologies, it is possible to capture quantum dynamics in some physical and chemical systems. On the other hand, all experiments are in principle open and dissipative systems. Up to now, the well-explained experiments are approximated to the equilibrium situation. However, by recent technological development, some experiments reach to a transition from equilibrium to non-equilibrium situations. While there are the well-known tools on the non-equilibrium situations; the linear response theory and the Keldysh Green function method, this analysis cannot basically catch dynamical situations. Our goal is to construct the time-resolved theoretical models included the non-equilibrium situations. However, the quantum measurement theory is needed on measuring quantum dynamics, especially considering the measurement backaction. Our current activities are to resolve how sensitive (quantum) measurement can we carry out in principle, to build up some toy models on quantum dynamic, and to explain photo-luminescence phenomena in nitrogen vacancy center in diamond and in the semiconductor microcavity.

1. Quantum Measurement Sensitivity without Squeezing Technique[1–4)]

As alluded before, our aim is to capture quantum dynamical phenomena. Capturing some phenomena needs to carry out the measurement. The conventional quantum measurement technique has huge measurement backaction. The measurement backaction prevents us chasing quantum dynamics like the classical trajectory. On the other hand, reducing the measurement backaction needs the tiny coupling between the target and probe quantum systems. However, under this situation, the signal in the probe system is also tiny small, that is, it is difficult to capture information. To resolve this problem, the squeezing technique was proposed and was experimentally implemented. However, this technique is practically difficult to be implemented. Our proposal is to use the weak measurement initiated by Aharonov, Albert, and Vaidman without squeezing technique. The profound meaning and interpretation of the weak measurement is seen in the review paper.[3)] The key of this method is to take the post-selection of the target system. Due to this effect, tiny probe signal can be amplified. In the original proposal by Aharonov, Albert, and Vaidman, the amplification factor is infinite by the approximation method. However, the effect measurement backaction is simultaneously amplified. When the probe state is Gaussian to be used in the original proposal, we have analytically shown the upper bound of the amplification factor. We have analytically derived the probe state to maximally amplify the signal by the variational method.[1,2)] By this optimal probe state, the amplification factor has no upper bound. Our result tells us the infinitely

amplified single under the known coupling between the target and the probe. However, in this result, we ignore the physical implementation. As the preliminary result, we demonstrate the single effect for the Laguerre-Gauss modes.[3)]

2. Discrete Time Quantum Walk as Quantum Dynamical Simulator[5–10)]

The discrete time quantum walk is defined as a quantum mechanical analogue of the classical random walk but is not the quantization of the classical random walk. This mathematical description is very simple but leads to many quantum dynamical phenomena. This is a toy model to better understand the quantum dynamics. Also, this has recently been various experimental demonstrations in the ultracold atoms in the optical lattice, trapped ions, and optical systems. Recently, we propose the physical implementation in the solid-state system using the nitrogen-vacancy centers in diamond and superconducting qubit.[10)] We have analytically shown that the one- and two-dimensional discrete time quantum walks can be taken as the quantum dynamical simulator,[8)] which concept is to emulate some classes of the differential equations, for example, the Dirac equation. Our approximation is used from the discrete lattice to continuous line for the large time steps of the discrete time quantum walk. This mathematical treatment is so powerful like the relationship between the cellular automaton and the integrable system.

3. Photoluminescence Phenomenon from Solid-State System[11)]

A method to measure some physical properties by light is widely used in physical, chemical, and biological systems. Therefore, laser science has been developed along with our demands from science and technology. A single photon source is expected as the low power laser source and the quantum communication tool. A nitrogen vacancy center in diamond and a quantum dot in a semiconductor system are the promising candidate of the single photon source. Especially, a nitrogen vacancy center in diamond has been attracted since this is run at room temperature. For an application as the highly controlled photon source, the photoluminescence process in the nitrogen vacancy center in diamond needs to be well understood. This system has the $S = 1$ electronic spin with the hyperfine structure 2.87 GHz. Furthermore, inserting a magnetic field, the different magnetic states are separated due to the Zeeman shift. Since this electronic spin is highly localized, the local magnetic field evaluation is needed. We have shown the method to evaluate the local magnetic field from the conventional confocal microscopy. Also, the nitrogen vacancy center in diamond is a candidate of the quantum memory. Since a lifetime of the nuclear spin of a ^{13}C atom nearly located in the nitrogen vacancy spot is long (~ sec order), the perfect quantum state transfer is needed. However, we have proposed the simple spin transfer scheme under the dissipative situation.[10)] As the next step, we will study the photoluminescence process from the nitrogen vacancy center in diamond.

As the current activities of our group, we are studying the photoluminescence processes of the quantum dots and the exciton-polariton Bose-Einstein condensations in the two dimensional electronic gas of the semiconductor. Experimentally, we measure the photoluminescence by the confocal microscopy. These materials are expected to be used as the classical optical devices; the optical switching, collaborated with the various experimentalists.[11)]

References

1) Y. Susa, Y. Shikano and A. Hosoya, *Phys. Rev. A* **85**. 052110 (2012).
2) Y. Susa, Y. Shikano and A. Hosoya, *Phys. Rev. A* **87**, 046102 (2013).
3) H. Kobayashi, G. Puentes and Y. Shikano, *Phys. Rev. A* **86**, 053805 (2012).
4) Y. Shikano, *Phys. Scr.* **T151**, 014015 (2012).
5) Y. Shikano, T. Wada and J. Horikawa, *Phys. Scr.* **T151**, 014016 (2012).
6) Y. Shikano, *Quant. Infor. Proc.* **11**, 1013 (2012).
7) Y. Shikano, E. Segawa, A. Perez and J. Wang, *J. Comput. Theor. Nanosci.* **10**, 1555 (2013).
8) Y. Shikano, *J. Comput. Theor. Nanosci.* **10**, 1558 (2013).
9) M. Gonulol, A. Ekrem, Y. Shikano and O. E. Mustecaplioglu, *J. Comput. Theor. Nanosci.* **10**, 1596 (2013).
10) A. U. C. Hardal, P. Xue, Y. Shikano, O. E. Mustecaplioglu and B. C. Sanders, *Phys. Rev. A* **88**, 022303 (2013).
11) T. Horikiri, Y. Matsuo, Y. Shikano, A. Loffler, S. Hofling, A. Forchel and Y. Yamamoto, *J. Phys. Soc. Jpn.* **82**, 084709 (2013).

* IMS International Internship Program

Studies of Field-Effect-Transistor Based on Highly-Correlated Molecular Materials

Research Center of Integrative Molecular Systems
Division of Functional Molecular Systems

YAMAMOTO, Hiroshi
Professor

SUDA, Masayuki
Assistant Professor

URUICHI, Mikio
Technical Associate

LE GOFF, Florian — Visiting Scientist*
SHIMIZU, Atsuko — Secretary

Field effect transistors (FETs) with organic channel materials are under intense studies because of the possibilities of application in flexible, printable, and large-area electronic devices. Despite single-component neutral molecules like pentacene and ruburene are mainly investigated to pursuit high performance (*ex.* high mobility *etc.*) organic FETs, few studies are known for FETs based on compound-type organic semiconductors. We have been exploiting FET devices with charge-transfer salts of organic molecules, namely cation-radical salts of electron-donating molecules (donors) such as BEDT-TTF and anion-radical salts of electron accepting molecules (acceptors) such as $Ni(dmit)_2$. Among these materials, our focus concentrates in Mott-insulators in which Coulomb interaction among carriers blocks metallic transport. In this highly correlated situation of charge carriers, Mott insulator stays in a fragile semiconducting state, where carrier injection, chemical and/or physical pressure (or strain), and thermal fluctuation can drive it into a metallic state by phase transition (*i.e.* Mott transition: Figure 1). One can expect an abrupt change of the conductivity of device due to phase transition that is induced by very small external stimuli. More specifically, it is anticipated that the Mott-insulating state can be switched to a metallic state by a field effect, since the carrier density (band-filling) of a FET interface can be finely modulated by an electrostatic field from the gate electrode. Indeed, our previous work showed such an insulator-to-metal transition in terms of the band structure, and these results provide not only a possibility of application use of organic Mott-FET but also a significant insight into the mechanism of Mott transition itself. We are now expanding our research target both to the superconducting transition of Mott-FET and to its room-temperature operation.
(BEDT-TTF = bis(ethylenedithio)tetrathiafulvalene,
dmit = 1,3-dithiole-2-thione-4,5-dithiolate)

1. Field-Induced Superconductivity in an Organic Mott-FET

κ-(BEDT-TTF)$Cu[N(CN)_2]Br$ (κ-Br) is an organic super-

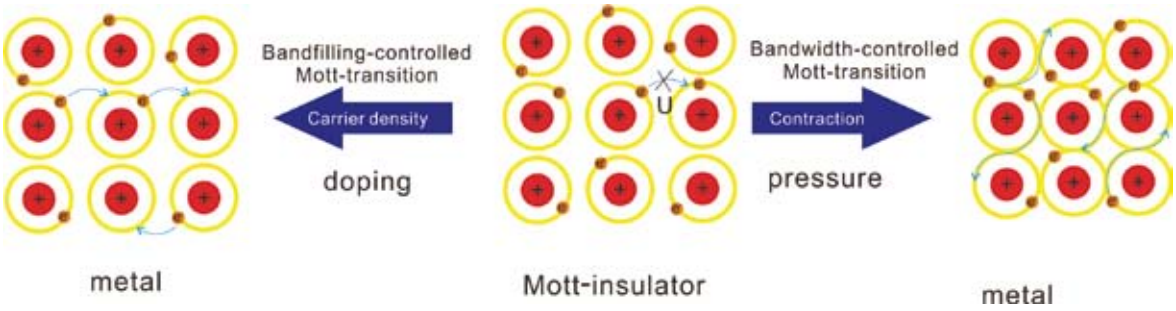

Figure 1. Concept of a Mott-insulator (center) along with its bandfilling-controlled (left) and bandwidth-controlled (right) Mott transitions. When the band is half-filled and band energy is small, the carriers are localized because of on-site Coulomb interaction (*U*). This situation is broken down either by changing the carrier concentration or by compressing the lattice. In many cases, the Mott transitions are associated with superconductivity at the boundary between metallic and insulating phases.

conductor whose electronic state is Mott-insulating at room-temperature but turns into metallic at low temperature through a crossover around 50–100 K, possibly because of an increase of bandwidth upon thermal contraction. In our previous works, a tensile strain altered its ground state into a Mott-insulating state, when its thin (100–300 nm) crystal is laminated on top of SiO_2/Si^{++} substrate and cooled down to low temperature. Although the electronic state at low temperature became completely insulating in this experiment because of the very small thermal expansion coefficient of Si substrate (2 ppm/K), one can anticipate from the *T–P* (temperature *vs.* pressure) phase diagram that mixed electronic state between superconducting and Mott-insulating states can be realized when the tensile strain is much weaker. To achieve such a mixed state (or, percolate-superconducting state) in the device, where phase-separation occurs between superconducting and Mott-insulating states, we have chosen Nb-doped $SrTiO_3$ as a back-gate substrate because of its larger thermal expansion coefficient (*ca.* 10 ppm/K) than Si. An aluminum oxide layer was grown by atomic layer deposition technique to form a gate dielectric on the substrate. After lamination of κ-Br on the substrate, the Mott-FET device which showed a weakly insulating behavior at low temperature was fabricated (Figure 2).

Upon applying a positive gate voltage, the resistivity went down and weakly metallic behavior was observed at $V_G > 2$ V. By further increasing the gate voltage up to 8 V, the device showed a sudden drop of resistivity around 5 K, which can be attributed to superconductivity. Taking into account of bistable I–V characteristics observed in the low resistance region, the above transition can be understood as a percolation transition of superconducting islands that is induced by the electrostatic doping of electrons. The transition temperature increased as the gate voltage rose and saturated around $V_G = 11$ V. The above result is the first example of field-induced superconductivity in organic materials, and can be utilized for uncovering a phase diagram of organic Mott system in the simultaneous control of band filling and band width.[1)]

2. Operation of Organic Mott-FET at Higher Temperature

In order to operate the organic Mott-FET at higher temperature, hopefully at room temperature, it is necessary to realize much larger Mott gap energy and thinner crystal thickness. For this purpose, we are examining several strategies in parallel.

κ-(BEDT-TTF)Cu[N(CN)$_2$]Cl (κ-Cl) is a Mott-insulator with larger Mott gap than κ-Br and is therefore suitable for examining the influence of an increase in Mott-gap energy on the device performance. For example, it has higher resistance than κ-Br and exhibit better ON/OFF ratio. In addition, it always shows ambipolar behavior, probably because of its clean surface. This situation allows us to analyze the critical exponents of filling-controlled Mott transition, which will give us important information about ON/OFF efficiency of the device (Figure 3).[2)] Because it is also possible to control the Mott gap energy by applying a mechanical strain, κ-Cl device provides an ideal platform to expand Mott-FET strategy to higher temperature.

Another candidate of the channel material for Mott-FET that can be used at room temperature is (BEDT-TTF)(TCNQ). We are exploiting this material both in a crystalline and amorphous form to find a better FET setup for simple but highly efficient device operatable at room temperature. (TCNQ = tetracyanoquinonedimethane)

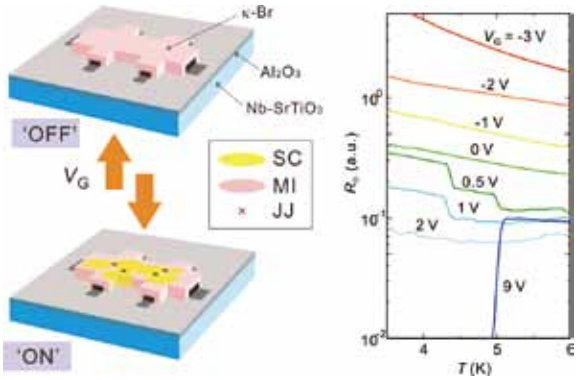

Figure 2. The device structure and temperature dependency of device resistance under various gate voltages. The device comprises κ-Br thin-layer single crystal and $Al_2O_3/SrTiO_3$ substrate. By applying a positive gate voltage, the resistance of the device starts decreasing, while a negative gate voltage results in an increase of the resistance. Although superconducting (SC) and Mott-insulating (MI) phases are separated in the device, the four-terminal resistance drops to zero when the Josephson junction (JJ) network forms a pathway to shunt the voltage terminals. This kind of percolation transition is clearly observed in the right panel, where the resistance drops at 5 K with a gate voltage of 9 V.

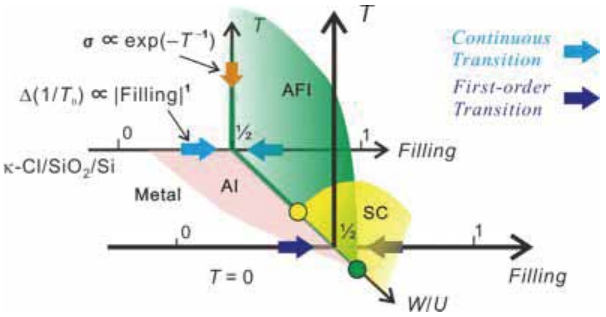

Figure 3. Universal phase diagram based on the experimental results obtained by organic Mott-FETs.

References

1) H. M. Yamamoto, M. Nakano, M. Suda, Y. Iwasa, M. Kawasaki and R. Kato, *Nat. Commun.* **4**, 2379 (7 pages) (2013).
2) H. M. Yamamoto, J. Ueno and R. Kato, E*ur. Phys. J. Special Topics* **222**, 1057–1063 (2013).

* IMS International Internship Program

Synthetic Inorganic and Organometallic Chemistry of Transition Metals

Research Center of Integrative Molecular Systems
Division of Functional Molecular Systems

YAMAMOTO, Koji
Assistant Professor

MURAHASHI, Tetsuro
Professor

HORIUCHI, Shinnosuke	IMS Fellow	KIMURA, Seita	Graduate Student†
KHOURY ATHIEH, Bruno	Visiting Scientist*	ISHIKAWA, Yuki	Graduate Student‡
TACHIBANA, Yuki	Graduate Student†	MASAI, Kohei	Graduate Student
		KAWAMATA, Shiori	Research Fellow
		TANIWAKE, Mayuko	Secretary
		NOGAWA, Kyoko	Secretary

Our research focuses on synthesis and structural elucidation of a new class of transition metal complexes. This research leads to development of fundamental concepts of transition metal chemistry as well as applications to catalysis and materials science. Novel synthetic methods are developed to realize transition metal complexes having unique bonding nature. The newly synthesized transition metal complexes are further converted to more reactive forms, and their reaction mechanisms are elucidated. The aspects gained by this research are applied to the understanding and development of molecular catalysis. Furthermore, unique properties of low-dimensional metal-organic hybrid molecules are investigated and developed in our group.

1. Chemistry of Multinuclear Sandwich Complexes

The molecular sandwich framework is one of the fundamental structures in transition metal chemistry. It had been believed that the structural concept can be applied only to mono- and dinuclear complexes. Our group revealed that the multinuclear sandwich complexes containing a one-dimensional metal chain or a two-dimensional metal sheet exist stably.[1,2] These findings expand the scope of the structural concept of sandwich compounds (Figure 1).

For the two-dimensional metal sheet sandwich complexes, our group has shown that six-, seven-, eight-, and nine-membered carbocycles, as well as polycyclic arenes behave as the excellent binders for metal sheets. These metal sheet sandwich complexes are stable even in solution. Thus, a reactive form of such metal sheet sandwich complexes may provide a new opportunity to develop sandwich type late transition metal catalysts.

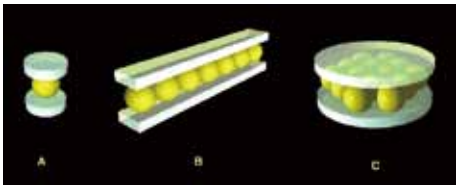

Figure 1. Schematic representation of sandwich compounds: (**A**) mononuclear metallocenes, (**B**) one-dimensional metal chain sandwich complexes, (**C**) two-dimensional metal sheet sandwich complexes. Our group revealed the existence of categories **B** and **C**.

Conversion of Trinuclear Sandwich Complexes to Trinuclear Half-Sandwich Complexes[5]

Our group recently showed that triangular trimetal sandwich complexes are isolable. It is now known that a variety of cyclic unsaturated hydrocarbons such as arene, cycloheptatrienyl, cycloheptatriene, and cyclooctatetraene work as excellent μ_3-face-capping binder for a Pd_3 moiety.[2–4] We found that the tripalladium sandwich complexes of [2.2]paracyclophane, cycloheptatriene, and cyclooctatetraene can be converted to trinuclear half-sandwich complexes upon treatment with 1,10-phenanthroline (phen). During the reaction, one of the facially-capping ligands is replaced with three phen ligands. Interestingly, the Pd_3 moiety underwent trinuclear addition to the remaining carbocyclic ligand to form unusual coordination modes. For the [2.2]paracyclophane ligand, a $Pd^0 \rightarrow Pd^{II}$ dative bonded moiety and a Pd^{II} moiety coordinated to an arene ring synfacially in a η^3:η^3 manner (eq. 1). The cycloheptatriene ligand was added by a Pd_3 moiety, where a Pd^I–Pd^I moiety and a Pd^{II} moiety is bound synfacially to the triene face (eq. 2). On the other hand, the Pd_3 moiety added to a cyclooctatetraene to form a cyclooctatetraenetetrayl tripalladium complex, where formally tetraanionic cyclooctatetraene ligand

coordinates to three Pd^{II} centers through a μ_3:η^1:η^3:η^1:η^3 coordination mode (eq. 3). The tripalladium addition product of cyclooctatetraene further converted to a dihydropentalenediyl complex via intramolecular reductive C–C coupling (eq. 4).

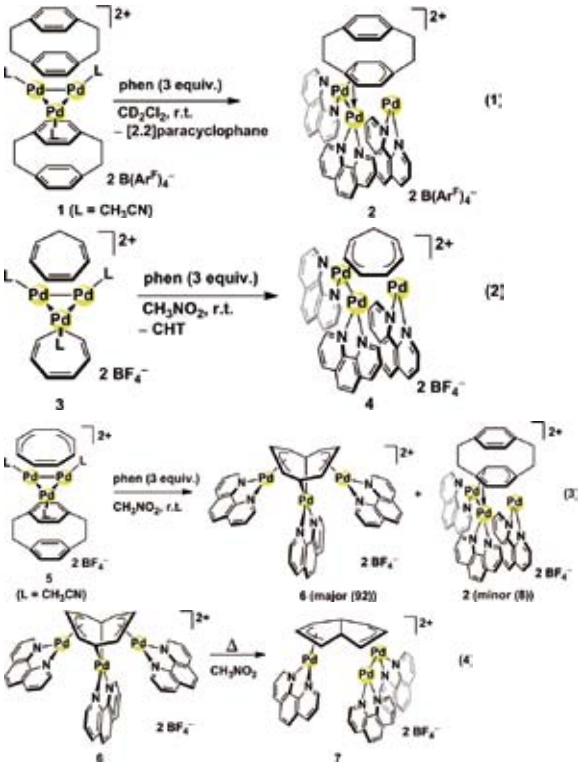

2. Reaction Mechanism of Highly Reactive Pd–Pd Complexes

Our group has shown that a homoleptic dinuclear Pd–Pd complexes of nitriles such as $[Pd_2(CH_3CN)_6][BF_4]_2$ are isolable.[6] These homoleptic solvento-Pd_2 complexes are highly substitutionally labile, and allow us to investigate reaction mechanism of the Pd–Pd complexes in details. For example, our group has shown that a Pd–Pd moiety adds to various unsaturated hydrocarbons including arenes in a syn addition manner.[7]

π-Coordination Pyrrole and Indole on a Pd–Pd Bond[8]

We found that pyrrole and indole form stable π-complexes. Thus, the reaction of $[Pd_2(CH_3CN)_6][BF_4]_2$ with pyrrole or indole gave the dinuclear sandwich complexes (eqs 5 and 6). These results provided the first evidence of the π-coordination of azoles having no chelating functionality to a Pd center. Particularly interesting is the coordination mode of indole which used its six-membered ring in the μ-η^2:η^2-coordination. Usually, the carbons at 2- and 3-positions are reactive sites in indole transformations. The bridging coordination mode of indole using six-membered ring carbons at 4-, 5-, 6-, and 7-positions is understood by a qualitative MO consideration: The π-orbital array at 4-, 5-, 6-, and 7-positions is isolobal with that of the 1,3-butadiene, which becomes an excellent bridging ligand on a Pd–Pd bond due to the efficient orbital overlap of diene-type HOMO or LUMO with (dσ–dσ)* or (dσ–dσ).

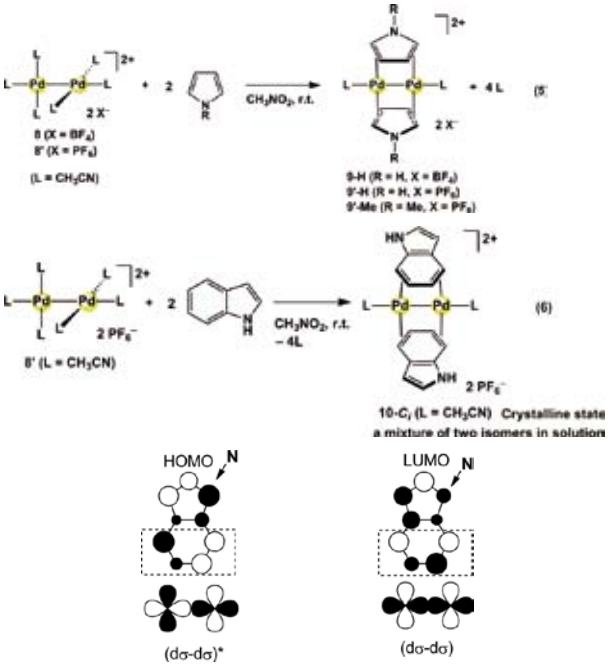

Scheme 1. Schematic representation of the HOMO and the LUMO of indole, and (dσ–dσ)* and (dσ–dσ) of a Pd−Pd moiety.

References

1) For the first report on the metal chain sandwich complexes: T. Murahashi, *et al.*, *J. Am. Chem. Soc.* **121**, 10660–10661 (1999).
2) For the first report on the metal sheet sandwich complexes: T. Murahashi, *et al.*, *Science* **313**, 1104–1107 (2006).
3) T. Murahashi *et al.*, *Angew. Chem., Int. Ed.* **46**, 5440–5443 (2007).
4) T. Murahashi *et al.*, *J. Am. Chem. Soc.* **130**, 8586–8587 (2008).
5) T. Murahashi, K. Takase, K. Usui, S. Kimura, M. Fujimoto, T. Uemura, S. Ogoshi and K. Yamamoto, *Dalton Trans.* **42**, 10626–10632 (2013).
6) (a) T. Murahashi, *et al.*, *Chem. Commun.* 1689–1690 (2000). (b) T. Murahashi *et al.*, *J. Am. Chem. Soc.* **128**, 4377–4388 (2006).
7) T. Murahashi *et al.*, *J. Am. Chem. Soc.* **133**, 14908–14911 (2011).
8) T. Murahashi, S. Kimura, K. Takase, S. Ogoshi and K. Yamamoto, *Chem. Commun.* **49**, 4310–4312 (2013). This paper was published in the special issue "Emerging Investigators 2013."

* IMS International Internship Program

† carrying out graduate research on Cooperative Education Program of IMS with Osaka University

‡ carrying out graduate research on Cooperative Education Program of IMS with Rikkyo University

Development of Organic Semiconductors for Molecular Thin-Film Devices

Research Center of Integrative Molecular Systems
Division of Functional Molecular Systems

SUZUKI, Toshiyasu
Associate Professor

SAKAMOTO, Youichi
Assistant Professor

KURODA, Yasuhiro — Post-Doctoral Fellow
WATANABE, Yoko — Secretary

Organic light-emitting diodes (OLEDs) and organic field-effect transistors (OFETs) based on π-conjugated oligomers have been extensively studied as molecular thin-film devices. Organic semiconductors with low injection barriers and high mobilities are required for highly efficient OLEDs and OFETs. Radical cations or anions of an organic semiconductor have to be generated easily at the interface with an electrode (or a dielectric), and holes or electrons must move fast in the semiconducting layer. Compared with organic p-type semiconductors, organic n-type semiconductors for practical use are few and rather difficult to develop. We found that perfluorinated aromatic compounds are efficient n-type semiconductors for OLEDs and OFETs.

1. Optical Properties of Fully and Partially Fluorinated Rubrene in Films and Solution[1)]

We present the optical properties of fully ($C_{42}F_{28}$, **PF-RUB**) and half-fluorinated ($C_{42}F_{14}H_{14}$, **F14–RUB**) rubrene, both in thin films and as monomers in solution and compare them to hydrogenated rubrene ($C_{42}H_{28}$, **RUB**). All three compounds show similar optical absorption bands and photoluminescence line shapes. The results are interpreted with density functional calculations of the orbital energies and time-dependent density functional theory for the HOMO–LUMO transition. Red shifts induced by the surrounding solvent or organic thin films remain much smaller than for polyacenes, in keeping with previous observations for rubrene and existing models for the solvatochromic shifts.

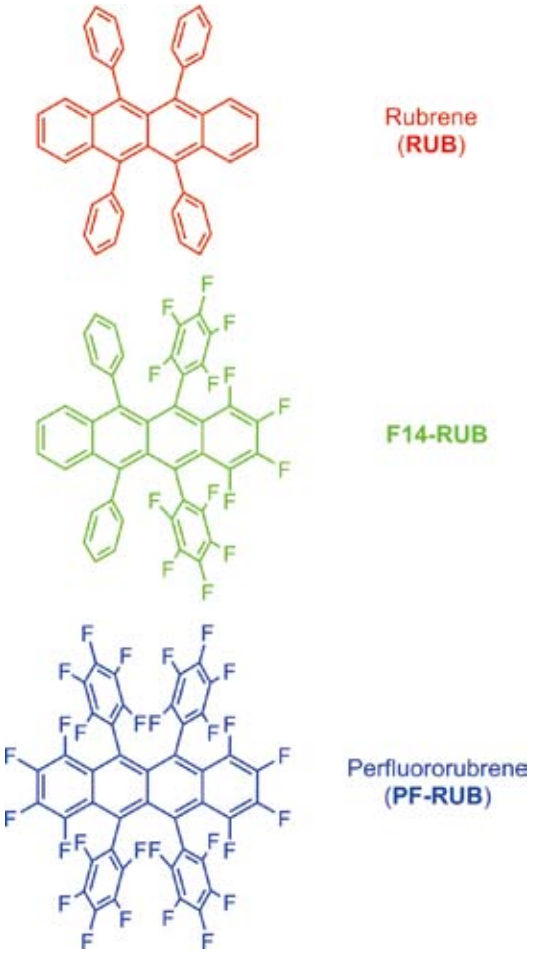

Figure 1. Structures of **RUB**, **F14-RUB**, and **PF-RUB**.

2. Selective Synthesis of [6]-, [8]-, and [10] Cycloparaphenylenes[2)]

The selective synthesis of [6]-, [8]-, and [10]cycloparaphenylenes (CPPs) was achieved by a new synthetic route involving Ni(0)-mediated coupling of bis(*para*-haloaryl)dinuclear arylplatinum complexes and the reductive elimination of the complexes. Importantly, the highly strained [6]CPP was prepared in good overall yield.

3. Experimental Reorganization Energies of Pentacene and Perfluoropentacene: Effects of Perfluorination[3)]

Electron–phonon coupling of the highest occupied molecular orbital (HOMO) state is studied by high-resolution ultraviolet photoelectron spectroscopy (UPS) for pentacene (PEN) and perfluoropentacene (PFP) monolayers on graphite. The reorganization energy and related coupling constants associated with the interaction between holes and molecular vibrations are obtained experimentally using a single mode analysis (SMA) of the observed vibronic-satellite intensities of the monolayers. The results are compared with those estimated by multimode analyses of UPS spectra and those derived by means of theoretical approaches, indicating that the purely experimental method with SMA is useful for studying the reorganization energy and the hopping mobility of organic systems. Furthermore, we found that the reorganization energy of PFP is significantly greater than that of PEN, which is ascribed to the extended HOMO distribution of PFP by perfluorination of PEN. The comparison with the results derived from gas-phase UPS measurements is also discussed.

References

1) F. Anger, R. Scholz, E. Adamski, K. Broch, A. Gerlach, Y. Sakamoto, T. Suzuki and F. Schreiber, *Appl. Phys. Lett.* **102**, 013308 (2013).
2) E. Kayahara, T. Iwamoto, T. Suzuki and S. Yamago, *Chem. Lett.* **42**, 621–623 (2013).
3) S. Kera, S. Hosoumi, K. Sato, H. Fukagawa, S. Nagamatsu, Y. Sakamoto, T. Suzuki, H. Huang, W. Chen, A. T. S. Wee, V. Coropceanu and N. Ueno, *J. Phys. Chem. C* **117**, 22428–22437 (2013).

Building Photosynthesis by Artificial Molecules

Research Center of Integrative Molecular Systems
Division of Functional Molecular Systems

NAGATA, Toshi
Associate Professor (–March, 2013)*

SAKURAI, Rie	IMS Fellow	WANATABE, Yoko	Secretary
YUSA, Masaaki	Graduate Student		
MIURA, Takahiro	Technical Fellow		

The purpose of this project is to build nanomolecular machinery for photosynthesis by use of artificial molecules. The world's most successful molecular machinery for photosynthesis is that of green plants—the two photosystems and related protein complexes. These are composed almost exclusively from organic molecules, plus a small amount of metal elements playing important roles. Inspired by these natural systems, we are trying to build up multimolecular systems that are capable of light-to-chemical energy conversion. At present, our interest is mainly focused on constructing necessary molecular parts and examining their redox and photochemical behavior.

1. Synthesis and Dynamic Behavior of Tweezer-Like Molecules with Opposite Electric Charges

The biological photosynthetic devices have mostly static structures that are optimized for efficient energy transfer and charge separation. After the photoinduced charge separation, however, many chemical transformations are necessary to complete the light-to-chemical energy conversion. For this particular purpose, it is rather beneficial to introduce "dynamic" structural features, because chemical transformation is often accompanied by substantial structural change of the substrates.

We aimed at introducing dynamic behavior on photosynthetic model compounds. The ultimate goal should be control of chemical transformation by way of photoinduced electron transfer. Presently, we focus on the synthesis of molecules that potentially respond to local electric field resulting in structural change.

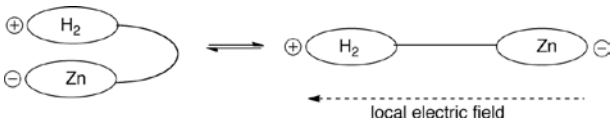

Figure 1. The design of the tweezer molecule.

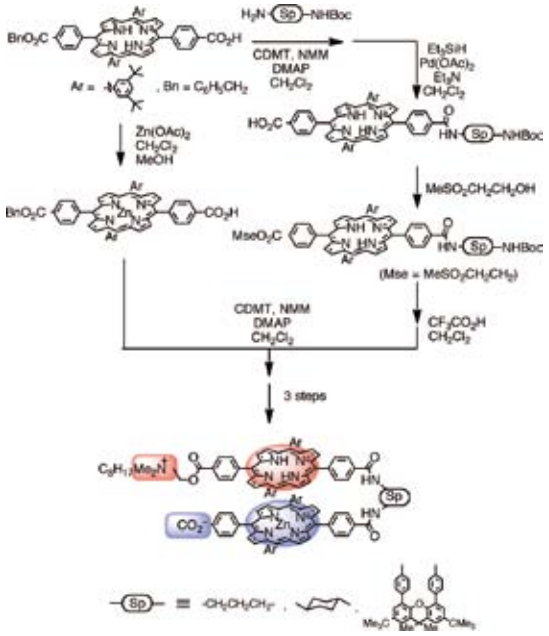

Figure 2. Synthesis of the tweezer molecule.

The design of the target molecule is shown in Figure 1. The molecule has a tweezer-like structure, with a free-base porphyrin and a zinc porphyrin at both ends. The shape of the

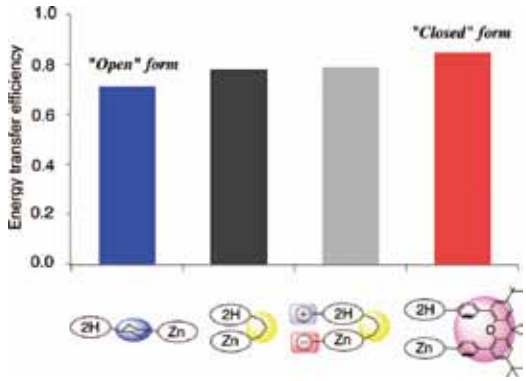

Figure 3. The fluorescence energy transfer efficiencies for the tweezer molecules and reference molecules.

molecule can be estimated from the degree of the fluorescence energy transfer from the zinc porphyrin to the free-base porphyrin. Moreover, there are introduced two opposite charges on both ends.

The synthesis of the tweezer molecule is shown in Figure 2. Three different spacers were used: Trimethylene (flexible), cyclohexane-1,4-diyl (fixed at "open" conformation), and xanthene-1,8-diyl (fixed at "closed" conformation). The equilibrium conformations of these molecules were estimated by fluorescence energy transfer experiments (Figure 3). The trimethylene-bridged molecules were found to have intermediate conformation between "open" and "closed" forms. Contrary to our expectation, the conformations of the tweezer molecules did not change when two opposite charges were introduced at both ends. In fact, molecular dynamic simulations revealed that the aryl substituents on the porphyrin rings caused substantial steric repulsion that precludes approach of the two charges at the ends. Simulations also revealed that if the charges were introduced at the 10-positions (instead of the 15-position as in the present molecules), the charges can approach each other in spite of the steric repulsion of the aryl substituents.

2. Synthesis of a Ternary Binucleating Ligand with 1,2,4-Triazole Bridge and Its Metal Complexes

Multinuclear transition metal complexes are promising components for artificial photosynthesis, because of their ability to perform multielectron redox reactions. One challenging issue is to use 3d transition metals for this purpose. The 4d and 5d transition metals (Ru and Ir in particular) are frequently used in the area of artificial photosynthesis, however they are expensive and better to be replaced with cheaper 3d metals. Our group have been tackling this problem by use of multidentate organic ligands.[1–3] Herein we report the synthesis of new "ternary" binucleating ligands consisting of

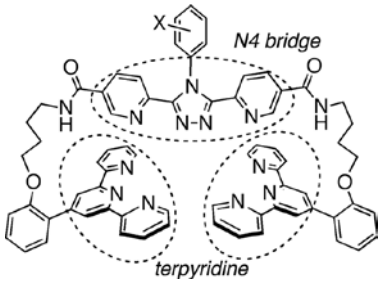

Figure 4. The new ternary binucleating ligand with 1,2,4-triazole bridge.

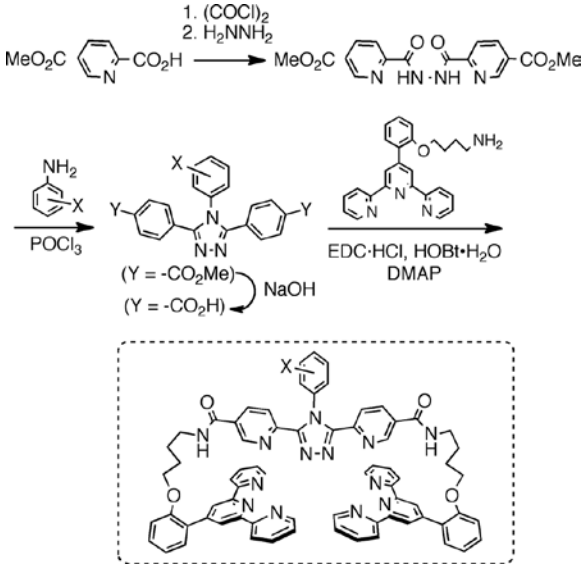

Figure 5. Synthesis of the ternary binucleating ligand.

two terpyridines and one "N4 bridge," 3,5-bis(2-pyridyl)-1,2,4-triazole (Figure 4).

Synthesis of the ligand is shown in Figure 5. Treatment of the ligand with $Co(OAc)_2$ and $Ni(OAc)_2$ afforded metal complexes with formula $[LM_2(OAc)]^{3+}$ (L = ligand, M = Co or Ni). Unlike the ternary binucleating ligands with phthalazine-containing N4 bridges (which we previously reported,[3] complexes with μ_2, η^1-bridging anions (like OH^- or Cl^-) were not observed. Such difference can be ascribed to the presence of the 5-membered ring in the present ligand, which causes larger metal-to-metal distances in comparison with the 6-membered ring in the phthalazine system. This reasoning was also supported by the preliminary X-ray results of the $[LCo_2(OAc)]^{3+}$ complex.

References

1) H. Kon and T. Nagata, *Inorg. Chem.* **48**, 8593–8602 (2009).
2) H. Kon and T. Nagata, *Chem. –Eur. J.* **18**, 1781–1788 (2012).
3) H. Kon and T. Nagata, *Dalton Trans.* **42**, 5697–5705 (2013).

* Present Position; Professor, Department of Applied Chemistry, Faculty of Science and Technology, Meijo University. Address: 1-501 Shiogamaguchi, Tenpaku, Nagoya 468-8502, Japan

Chemistry of Bowl-Shaped Aromatic Compounds and Metal Nanocluster Catalysts

Research Center of Integrative Molecular Systems
Division of Functional Molecular Systems

SAKURAI, Hidehiro
Associate Professor

HIGASHIBAYASHI, Shuhei
Assistant Professor

SUGIISHI, Tsuyuka	IMS Fellow	MANNA, Sudipta Kumar	Visiting Scientist
MORITA, Yuki	Post-Doctoral Fellow	PONGPIPATT, Paweena	Visiting Scientist
KUMAR, Selva	Post-Doctoral Fellow	SINGH, Priyanka	Visiting Scientist
PANDIT, Palash	Post-Doctoral Fellow	AGRAWAL, Meghdeep	Visiting Scientist
MAITY, Prasenjit	Post-Doctoral Fellow	THONGPAEN, Jompol	Visiting Scientist
DHITAL, Raghu Nath	Post-Doctoral Fellow	ONOGI, Satoru	Graduate Student
KAMONSATIKUL, Choavarit	Visiting Scientist	KAEWMATI, Patcharin	Graduate Student
JINASAN, Atchaleeya	Visiting Scientist	KARANJIT, Sangita	Graduate Student
TSAI, I-Chang	Visiting Scientist	SHRESTHA, Binod Babu	Graduate Student
		HAESUWANNAKIJ, Setsiri	Graduate Student
		OKABE, Yuki	Graduate Student
		SASAKI, Tokiyo	Secretary
		HAZAMA, Kozue	Secretary

Bowl-shaped π-conjugated compounds including partial structures of the fullerenes, which are called “buckybowls,” are of importance not only as model compounds of fullerenes but also as their own chemical and physical properties. For example, in solution they show the characteristic dynamic behavior such as bowl-to-bowl inversion. On the other hand, they sometimes favor stacking structure in a concave-convex fashion in the solid state, giving excellent electron conductivity. Furthermore, some buckybowls are conceivable to possess the bowl-chirality if the racemization process, as equal as bowl-to-bowl inversion, is slow enough to be isolated. Very few buckybowls has been achieved for preparation mainly due to their strained structure, and no report on the preparation of chiral bowls has appeared. In this project, we develop the rational route to the various buckybowls with perfect chirality control using the organic synthesis approach.

We also investigate to develop novel catalytic properties of metal nanoclusters. We focus on the following projects: Preparation of size-selective gold nanoclusters supported by hydrophilic polymers and its application to aerobic oxidation catalysts: Synthetic application using metal nanocluster catalyst: Development of designer metal nanocluster catalyst using the highly-functionalized protective polymers.

1. Stereoelectronic Effect of Curved Aromatic Structure Favouring the Unexpected *Endo* Conformation of Benzylic Substituted Sumanene[1)]

Since the discovery of fullerene and carbon nanotubes, curved aromatic compounds including bowl-shaped buckybowls have elicited much attention in science and industry. One principal question in these curved aromatic compounds is the difference between the concave face and the convex face. The curvature affects the nature between the two faces, resulting in differences of the through-space and through-bond effects. The latter would appear as a stereoelectronic effect between the curved aromatic structure and a connected functional group. In general, the stereoelectronic effect is reflected in the conformational stability and chemical reactivity of a molecule. Therefore, it is important to understand such conformations or chemical reactivities as a consequence of stereoelectronic effects. The interpretation of the stereoelectronic effect of curved aromatic compounds would lead to understanding the difference in nature between the two faces. However, no example of stereoelectronic effects of curved aromatic compounds have been found and studied to date. We have found a first example of the stereoelectronic effect of a curved aromatic structure, which dominates the *endo/exo*-R conformational stability of benzylic substituted sumanenes (**1**) (Figure 1).

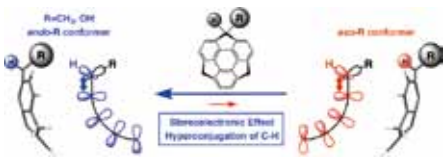

Figure 1. Schematic diagram of the stereoelectronic effect and through-space effects between the bowl and the C-H/C-R of benzylic substituted sumanene.

2. Low-Temperature Carbon–Chlorine Bond Activation by Bimetallic Gold/Palladium Alloy Nanoclusters: An Application to Ullmann Coupling[2)]

In the past decade, nanoclusters (NCs) of bimetallic alloys have attracted considerable research interest because of their unique catalytic properties, which differ substantially from those of single-phase monometallic counterparts. Among the various bimetallic NCs that have been fabricated to date, gold/palladium alloy NCs are particularly fascinating because of their high catalytic activities.

Because of the relatively high dissociation energy of C–Cl bond in comparison with C–Br or C–I, it is difficult to activate chloroarenes by undergoing oxidative addition on Pd without ligation by nucleophilic ligands. Here we demonstrate a new method for activation of C–Cl bonds at low temperature as a result of bimetallic Au/Pd synergy and we report the successful examples of the Ullmann coupling of chloroarenes under ambient conditions. Ullmann coupling, which was first reported in 1901, is a conventional method for the synthesis of symmetrical biaryls. Initially, aryl iodides were used in coupling reactions that were promoted by excess amount of copper at high temperatures. Recent developments in the Ullmann coupling reaction has permitted the use of aryl bromides or chlorides as reactants in the presence of a co-reductant such as Zn powder, formic acid, and dihydrogen under mild conditions. Such reactions can be catalyzed by many types of homogenous or heterogeneous transition-metal catalysts, such as Ni, Pd or Au. However, to the best of our knowledge, there are no reports of any successful examples of Ullmann coupling reactions of chloroarenes under ambient conditions. It is because of relative difficulty in the activation a C–Cl bond, which needs to occur twice within a single catalytic cycle, and because all C–M intermediates need to resist hydrogenation by external co-reductant.

The activity increased markedly for a bimetallic catalyst containing 50% of Pd, giving the coupling product in 98% yield with 100% conversion. The coupling reaction occurred smoothly even when the reaction temperature was decreased to 35 °C or to 27 °C (room temperature) quantitatively for 6 h and 24 h, respectively. To the best of our knowledge, this is the first example of Ullmann coupling of chloroarenes under ambient conditions.

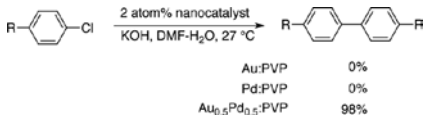

An essential step, which determines the characteristics difference in the catalytic activities of Au, Au/Pd, and Pd NCs is the oxidative addition of chloroarene followed by the spill over of Cl, and we therefore intensively studied only this step at present. Our previous report demonstrated that Au_{20}^-, a negatively charged homogeneous Au NCs, is a suitable model for simulating reaction on the surface of Au:PVP. We therefore examined the model systems Au_{20}^-, $Au_{16}Pd_4^-$, $Au_{10}Pd_{10}^-$, and Pd_{20} to compare the reaction pathway for oxidative additions on Au, Pd, and Au/Pd alloy clusters. Fundamental consideration of these models and the computational details are given in supporting information. The calculations were performed by the Gaussian09 suite of programs. The energy diagram of the oxidative addition of chlorobenzene (**1b**) on Au_{20}^- and $Au_{10}Pd_{10}^-$ is shown in Figure 2 where the energies are shown by taking those of adsorption complexes being the same for these clusters.

In the case of the Au_{20}^- system, **1b** is adsorbed on the facet site and a local minimum is obtained for the dissociative chemisorption (Int_B1). However, the calculated activation energy barrier for this (C–Cl) dissociative chemisorption is very high at 137.9 kJ/mol. In $Au_{10}Pd_{10}^-$ bimetallic cluster which simulates $Au_{0.5}Pd_{0.5}$ alloy, we found two types of intermediates for chemisorption. The adsorption was calculated to proceed with low activation energy barrier of 63.1 kJ/mol to give adsorption intermediate (Int_A2) in which both the phenyl group and the Cl atom are attached to the same Pd site. The other intermediate for dissociative chemisorption (Int_B2) is also stable as the adsorbed complex (Ads) or Int_A2. The calculated activation energy barrier from Int_A2 is 56.0 kJ/mol. The reaction pathway, which directly provides Int_B2 from the adsorption complex is also possible and has a moderate energy barrier of 52.6 kJ/mol. Note that an intermediate corresponding to Int_A2 was not obtained in the case of Au_{20}^- system. These results clearly show that the inclusion of Pd has an effect of stabilizing the dissociative adsorption and reducing activation energy, which is not possible in pure Au cluster.

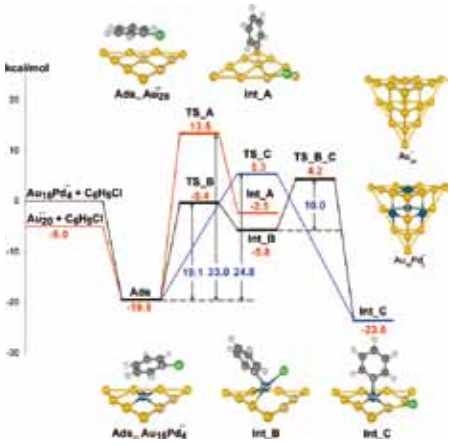

Figure 2. Energy profile diagram of oxidative addition of chlorobenzene on Au_{20}^- and $Au_{10}Pd_{10}^-$ NCs.

References

1) S. Higashibayashi, S. Onogi, H. K. Srivastava, G. N. Sastry, Y.-T. Wu and H. Sakurai, *Angew. Chem., Int. Ed.* **52**, 7314–7316 (2013).
2) R. N. Dhital, C. Kamonsatikul, E. Somsook, K. Bobuatong, M. Ehara, S. Karanjit and H. Sakurai, *J. Am. Chem. Soc.* **134**, 20250–20253 (2012).

Awards

HIGASHIBAYASHI, Shuhei; Insentive Award in Synthetic Organic Chemistry (2012).
HIGASHIBAYASHI, Shuhei; Sumitomo Chemical Award in Synthetic Organic Chemistry (2012).
HAESUWANNAKIJ, Setsiri; Best Poster Presentation, PERCH-CIC Congress VIII (2013).